

Synthesis of ruthenium and manganese carbonyl complexes: a search for new carbon monoxide releasing molecules (CORMs)



seit 1558

Dissertation
zur Erlangung des akademischen Grades doctor rerum naturalium
(Dr. rer. nat.)

vorgelegt dem Rat der Chemisch-Geowissenschaftlichen Fakultät der
Friedrich-Schiller Universität Jena

von : M.Sc. Vaneza Paola Lorett Velásquez
geboren am 07.11.1982 in Cartagena de Indias, Kolumbien

Gutachter:

1. Prof. Dr. Matthias Westerhausen, Friedrich-Schiller-Universität Jena
2. Jun.-Prof. Dr. Alexander Schiller, Friedrich-Schiller-Universität Jena

Tag der öffentlichen Verteidigung: 27. September 2013

Acknowledgements

Without the human, scientific and financial support this thesis would have not been possible. I want to start by giving credit to my family, because this Thesis is theirs as it is mine. My parents: Ena del Carmen, and Juan Francisco, They have always believed in me, giving me support in all my decisions and encouraging me with their example to face life in all the situations. Special mention deserve also my husband Cristian Ignacio, I cannot start to imagine what it would have been like without him: his patience and support, whether from Argentina or during his visits, made me stay focused. The hard last lap would just not have happened without him. Your comfort and presence simply makes everything easier. I am very grateful as well to the rest of my big family: brothers and sisters Thank you guys, for being always there! Even though in the last years the distance did not allow us to share many moments together, you put a smile in my face with each of your words, anecdotes and successes in life. cousins, uncles, grandparents, etc.

My most sincerely gratitude to my supervisor, **Prof. Dr. Matthias Westerhausen**, who gave me the opportunity to join his group also for letting me work at this excellent theme. I have learned many things from you. Also deserve special mention **Dr. Helmar Görls**, for his patience and the kindly help

with the measurements of crystal structures. I am really grateful with **Dr. Jens Langer** for his support and wise advices along my PhD studies. Also I want to thank the AG Westerhausen for the great time: Dr Reinald Fischer, Dr. Helmar Görls, Dr. Kristina Dubnack Dr Sven Kriek, Dr, Jens Langer, Dr. Wolfgang Poppitz, Dr Astrid Malassa, Carolin Göbert, Stephan Härling, Jörg Hildebrandt, Kay Hinze, Maurice Klopffleisch, Matthias Köhler, Class Loh, Ralf Mede, Christoph Müller, Silvio Preußner, Björn Schowtka, David Schrader, Fadi Younis, Steffen Ziemann, Christine Agthe, Martina Gase, Monika Heineck, Denny Renner, Sigrid Schönau and Regina Suxdorf

It is time to thank the cooperation partners. This thesis would have not been feasible without the nice interaction between chemical experiments and Biophysical experiments. All my gratitude to the groups of **Prof. Dr. Heinemann**. Specially, I will like to mention here Dr. Guido Geßner for the work concerning Myoglobin assay.

Very special mention deserves also my friends in Jena city specially Cintia, Lorena, Kevin, Veronica, Kiara, Sarahi, Beatriz, Daniel, Maritza, Paul, Jorge, Diana, Ricardo, Pilar, Antonio, Emilio, Paola, Javier, Martha, Laura, Hans. Thank you all for the great experiences that we have lived together. I will never forget you.

Finally, I will like to thank the financial support during the thesis. I acknowledge the economical support of the Deutsche Akademischer Austausch Dienst DAAD also the Deutsche Forschungsgemeinschaft DFG project FOR 1738.

Contents

List of figures	viii
List of tables	xi
List of publications	xiii
List of abbreviations	xiv
1. Introduction	16
1.1 Carbon monoxide as active agent (signaling molecule)	16
1.1.1 CO endogenous production	17
1.1.2 Biologic effects of CO	18
1.2 Carbon monoxide-releasing molecules (CORMs)	19
1.2.1 Development of a first generation of CORMs	20
1.2.2 Development of photo-CORMs	21
2. Results and discussion	24
2.1 Ruthenium-based carbonyl complexes	24
2.1.1 Synthesis and characterization of $[\text{Ru}(\text{CO})_2(\text{H}_2\text{NC}_2\text{H}_4\text{S})_2]$ and $[\text{Ru}(\text{CO})_2(\text{H}_2\text{NC}_6\text{H}_4\text{S})_2]$	24
2.1.2 Molecular Structures of $[\text{Ru}(\text{CO})_2(\text{H}_2\text{NC}_2\text{H}_4\text{S})_2]$ (1) and $[\text{Ru}(\text{CO})_2(\text{SC}_6\text{H}_4\text{NH}_2)_2]$ (2)	28
2.1.3 Synthesis and characterization of $[\text{Ru}_2(\text{CO})_5(\text{adamantyl-APE})]$ (APE= 1,2-bis(μ -alkylamido)-1,2-bis(2-pyridyl)ethane)	33
2.1.4 Molecular structure of $[\text{Ru}_2(\text{CO})_5(\text{adamantyl-APE})]\cdot\text{THF}$ (3) and $[\text{Ru}_2(\text{CO})_5(\text{adamantyl-APE})]\cdot\text{CH}_2\text{Cl}_2$ (3B)	36

2.1.5 CO release properties of ruthenium based complexes and comparison with CORM-S1	42
2.2 Manganese-based carbonyl complexes	44
2.2.1 Oxidation of [Mn ₂ (CO) ₁₀] by organic disulfides	44
2.2.1.1 Synthesis and characterization of [Mn(CO) ₄ (μ-SC ₆ H ₄ -4-R)] ₂	45
2.2.1.2 Molecular structures of [Mn(CO) ₄ (μ-SC ₆ H ₅)] ₂ (4), [Mn(CO) ₄ (μ-SC ₆ H ₄ -4-CH ₃)] ₂ (5), [Mn(CO) ₄ (μ-SC ₆ H ₄ -4-OMe)] ₂ (6), [Mn(CO) ₄ (μ-SC ₆ H ₄ -4-Cl)] ₂ (7) and [Mn(CO) ₃ (SC ₆ H ₃ Me-o-SC ₆ H ₄ Me)] ₂ (8)	51
2.2.2 Salt metathesis reactions of [BrMn(CO) ₅] with potassium aryl thiolates	61
2.2.2.1 Synthesis and characterization of [Mn(CO) ₄ (μ-SR)] _n (n=2, 3) and [Mn(CO) ₃ (μ-SR)] _n (n=4)	61
2.2.2.2 Molecular structure of [Mn(CO) ₃ (μ-SC ₆ H ₄ -4-CH ₃)] ₄ , (9) [Mn(CO) ₄ (SC ₆ H ₂ -2,4,6-CH ₃)] ₃ , (10) [Mn(CO) ₄ (SC ₆ H ₄ -4-CF ₃)] ₂ (11) and [Mn(CO) ₃ (SC ₆ H ₄ -4-CF ₃)] ₄ (12)	67
2.2.2.3 Molecular structure of solvent-separated [Mn ₂ (CO) ₆ (μ-SC ₆ H ₄ -4-CF ₃)] ₃ [Mn ₄ (DMF) ₃ (CO) ₉ (μ-SC ₆ H ₄ -4-CF ₃)] ₄ (13)	80
2.2.3 Substitution reactions between [BrMn(CO) ₅] and thiols	
2.2.3.1 Synthesis and characterization of [Mn(CO) ₃ (μ-SC ₆ H ₄ -4-R)] ₄ with R = H, CH ₃ , OMe, Cl	86
2.2.3.2 Molecular structure of [Mn(CO) ₃ (μ-SC ₆ H ₄ -4-CH ₃)] ₄ (9B)	89
2.2.3.3 Molecular structure of [Mn ₆ (CO) ₁₈ (μ-SC ₆ H ₄ -4-Cl) ₈ {Mn ₂ (μ-Br) ₂ (THF)}] (17)	93
2.2.4 CO release properties of manganese based complexes and comparison with CORM-1	98
3 Summary and Outlook	105
4. Zusammenfassung und Aussichten	110
5. Experimental	116
5.1 Physical measurements	116
5.2 Crystal structure determinations	117
5.3 Syntheses	117
5.3.1 Syntheses of ruthenium complexes	118
5.3.2 Synthesis of manganese complexes	121
5.4 Quantification of CO release (Myoglobin assay)	130

Appendix	131
A.1 Crystallographic Details	131
Bibliography	147
Selbständigkeitserklärung	152
Curriculum Vitae	153

List of figures

Fig. 1	Catalytic reaction of Heme-oxygenase.	18
Fig. 2	Reaction products between $[\text{RuCl}_2(\text{CO})_3]_2$ and DMSO.	20
Fig. 3	Main CORMs a), b), c) and d) CORMs first generation. e) and f) photo CORMs up to now (tpm = tris(pyrazolyl)methane).	23
Fig. 4	Synthesis of $[\text{Ru}(\text{CO})_2(\text{H}_2\text{NC}_2\text{H}_4\text{S})_2]$ (1) and $[\text{Ru}(\text{CO})_2(\text{SC}_6\text{H}_4\text{NH}_2)_2]$ (2).	25
Fig. 5	IR spectra of the carbonyl region of 2 (left), 2 ·DMF (right) and 2 ·DMF with partial loss of DMF (center) [41].	27
Fig. 6	Molecular structures of $[\text{Ru}(\text{CO})_2(\text{SC}_2\text{H}_4\text{NH}_2)_2]$ (1) (top) and its interaction with $[\text{Ru}(\text{CO})_2(\text{SC}_2\text{H}_4\text{NH}_2)_2]\cdot\text{THF}$ (bottom). Thermal ellipsoids are drawn at the 50% probability level. Hydrogen atoms are shown with arbitrary radii.	29
Fig. 7	Molecular structure of $[\text{Ru}(\text{CO})_2(\text{SC}_6\text{H}_4\text{NH}_2)_2]$ (2) (top) and its interaction with co-crystallized·DMF (bottom). Thermal ellipsoids are drawn at the 50% probability level. Hydrogen atoms are drawn with arbitrary radii.	32
Fig. 8	Synthesis of $[\text{Ru}_2(\text{CO})_5(\text{adamantyl-APE})]$ (3).	35
Fig. 9	Molecular structure of the dinuclear $[\text{Ru}_2(\text{CO})_5(\text{adamantyl-APE})]\cdot\text{THF}$ (3). Thermal ellipsoids are drawn at the 50% probability level. Hydrogen atoms and THF solvent are omitted for clarity. The disordering of the bis(2-pyridyl) ethane backbone is not depicted.	37
Fig. 10	Molecular structure of the dinuclear $[\text{Ru}_2(\text{CO})_5(\text{adamantyl-APE})]\cdot\text{CH}_2\text{Cl}_2$ (3B) (top) and its interaction with co-crystallized· CH_2Cl_2 (bottom). Thermal ellipsoids are drawn at the 50% probability level. Hydrogen atoms are omitted for clarity.	41

- Fig. 11** Absorption spectra for complexes **1** and **2** in a myoglobin assay. (Spectrum without myoglobin (blau), myoglobin alone (red), myoglobin with the compounds after irradiation (black) and myoglobin saturated with CO (green)). 44
- Fig. 12** Synthesis of manganese carbonyl complexes $[\text{Mn}(\text{CO})_4(\mu\text{-SC}_6\text{H}_5\text{-4-R})]_2$ (**4-7**). 45
- Fig. 13** ^1H NMR spectra in $[\text{D}_8]$ THF, 400 MHz shown the AA'BB' spin system for the aromatic ring protons. Left: Complex $[\text{Mn}(\text{CO})_4(\mu\text{-SC}_6\text{H}_4\text{-4-OMe})]_2$ (**6**). Right: Complex $[\text{Mn}(\text{CO})_4(\mu\text{-SC}_6\text{H}_4\text{-4-Cl})]_2$ (**7**). 51
- Fig. 14** Representation of the structural motif of $[\text{Mn}(\text{CO})_4(\mu\text{-SC}_6\text{H}_5)]_2$ (**4**). 52
- Fig. 15** Molecular structure of $[\text{Mn}(\text{CO})_4(\mu\text{-SC}_6\text{H}_4\text{-4-CH}_3)]_2$ (**5**). Thermal ellipsoids of non-hydrogen atoms are drawn at the 50% probability level. 54
- Fig. 16** Molecular Structure of $[\text{Mn}(\text{CO})_4(\text{SC}_6\text{H}_4\text{-4-OMe})]_2$ (**6**). Thermal ellipsoids of non-hydrogen atoms are drawn at 50% probability level. 56
- Fig. 17** Molecular structure of $[\text{Mn}(\text{CO})_4(\text{SC}_6\text{H}_4\text{-4-Cl})]_2$ (**7**) Thermal ellipsoids of non-hydrogen atoms are drawn at 50% probability level. 58
- Fig. 18** Molecular structure of $[\text{Mn}(\text{CO})_3(\text{SC}_6\text{H}_3\text{Me-}o\text{-SC}_6\text{H}_4\text{Me})]_2$ (**8**) Thermal ellipsoids of non-hydrogen atoms are drawn at 50% probability level. 60
- Fig. 19** Synthesis of potassium thiophenolates starting from potassium bis(trimethylsilyl)amide and subsequent synthesis of manganese complexes. 63
- Fig. 20** Selected regions of the ^1H NMR spectrum of $[\text{Mn}(\text{CO})_4\{\mu\text{-SC}_6\text{H}_2\text{-2,4,6-(CH}_3)_3\}]_3$ **10** in $[\text{D}_8]$ THF. 66
- Fig. 21** Molecular structure of complex $[\text{Mn}(\text{CO})_3(\mu\text{-SC}_6\text{H}_4\text{-4-CH}_3)]_4$ (**9**). Thermal ellipsoids are drawn at the 50% probability level. Hydrogen atoms are omitted for clarity. Top: View of the molecular structure of **9**. Bottom: View of the two independent molecular structures of $[\text{Mn}(\text{CO})_3(\mu\text{-SC}_6\text{H}_4\text{-4-CH}_3)]_4$ (right) and $[\text{Mn}(\text{CO})_4(\mu\text{-SC}_6\text{H}_4\text{-4-CH}_3)]_2$ (left). 69
- Fig. 22** Crystal Structure of $[\text{Mn}(\text{CO})_4(\text{SC}_6\text{H}_2\text{-2,4,6-(CH}_3)_3)]_3$ (**10**) (top). Thermal ellipsoids are drawn at the 50% probability level. Hydrogen atoms are omitted for clarity. Bottom: Representation of the trinuclear core unit of **10**. The atoms are drawn with arbitrary radii. 73
- Fig. 23** Crystal Structure of $[\text{Mn}(\text{CO})_4(\text{SC}_6\text{H}_4\text{-4-CF}_3)]_2$ (**11**). Thermal ellipsoids of non-hydrogen atoms are drawn at the 50% probability level. 76
- Fig. 24** Crystal Structure of $[\text{Mn}(\text{CO})_3(\text{SC}_6\text{H}_4\text{-}p\text{-CF}_3)]_4$ (**12**). Thermal ellipsoids are drawn at the 50% probability level. Hydrogen atoms are omitted for

	clarity. Symmetry equivalent atoms are labeled with the suffix A.	78
Fig. 25	View of the molecular structure of complex $[\text{Mn}_2(\text{CO})_6(\mu\text{-SC}_6\text{H}_4\text{-4-CF}_3)_3][\text{Mn}_4(\text{DMF})_3(\text{CO})_9(\mu\text{-SC}_6\text{H}_4\text{-4-CF}_3)_4]$ (13). Hydrogen atoms are omitted for clarity. The atoms are drawn with arbitrary radii.	83
Fig. 26	Synthesis of manganese carbonyl complexes $[\text{Mn}(\text{CO})_3(\mu\text{-SC}_6\text{H}_4\text{-4-R})]_4$	87
Fig. 27	Molecular structure of $[\text{Mn}(\text{CO})_3(\mu\text{-SC}_6\text{H}_4\text{-4-CH}_3)]_4$ (9B). Thermal ellipsoids are drawn at the 50% probability level. Hydrogen atoms are omitted for clarity	91
Fig. 28	View of the molecular structure of $[\text{Mn}_6(\text{CO})_{18}(\mu\text{-SC}_6\text{H}_4\text{-4-Cl})_8\{\text{Mn}_2(\mu\text{-Br})_2(\text{THF})\}]$ (17). The disordering of the structure is depicted. Thermal ellipsoids are drawn at the 50% probability level. Hydrogen atoms are omitted for clarity (top). Representation of the molecular structure with resolved disorder (bottom)	96
Fig. 29	^1H NMR (400 MHz) spectra of 4 in $[\text{D}_6]\text{DMSO}$. Left: a sample recently prepared. Right: a sample after 2 days	99
Fig. 30	Manganese-based complexes selected for the investigation of CO release properties	99
Fig. 31	Absorption spectrum in the range of 380-460 nm for solutions of $5\ \mu\text{M}$ of CORM-1 and $10\ \mu\text{M}$ deoxymyoglobin upon 5 min irradiation	102
Fig. 32	Absorption spectra demonstrating the conversion of deoxy-myoglobin (Mb, start spectrum) to carbon mono. xide myoglobin (MbCO) for complexes 4 , 5 , 7 upon light irradiation, also monitoring the influence of sodium dithionite	104
Fig. 33	Schematic representation of the dinuclear core unit in the manganese complexes	107

List of tables

Table 1. Selected bond length and angles of complex $[\text{Ru}(\text{CO})_2(\text{SC}_2\text{H}_4\text{NH}_2)_2]$ (1)	30
Table 2. Selected bond length and angles of $[\text{Ru}(\text{CO})_2(\text{SC}_6\text{H}_4\text{NH}_2)_2]$ (2)	33
Table 3. Selected bond lengths and angles of $[\text{Ru}_2(\text{CO})_5(\text{adamantyl-APE})] \cdot \text{THF}$ (3)	38
Table 4. Selected bond lengths and angle of $[\text{Ru}_2(\text{CO})_5(\text{adamantyl-APE})] \cdot \text{CH}_2\text{Cl}_2$ (3A)	40
Table 5. Selected bond lengths and angles of $[\text{Ru}_2(\text{CO})_5(\text{adamantyl-APE})] \cdot \text{CH}_2\text{Cl}_2$ (3B)	42
Table 6. Selected bond lengths and angles for $[\text{Mn}(\text{CO})_4(\mu\text{-SC}_6\text{H}_4\text{-4-CH}_3)]_2$ (5)	54
Table 7. Selected bond lengths and angles of $[\text{Mn}(\text{CO})_4(\text{SC}_6\text{H}_4\text{-4-OMe})]_2$ (6)	56
Table 8. Selected bond lengths and angles of $[\text{Mn}(\text{CO})_4(\text{SC}_6\text{H}_4\text{-4-Cl})]_2$ (7)	58
Table 9. Selected bond lengths and angles of $[\text{Mn}(\text{CO})_3(\text{SC}_6\text{H}_3\text{Me-}o\text{-SC}_6\text{H}_4\text{Me})]_2$ (8)	60
Table 10. Selected bond lengths and angles of $[\text{Mn}(\text{CO})_3(\mu\text{-SC}_6\text{H}_4\text{-4-CH}_3)]_4$ (9)	70
Table 11. Selected bond lengths and angles of $[\text{Mn}(\text{CO})_4(\mu\text{-SC}_6\text{H}_2\text{-2,4,6-(CH}_3)_3)]_3$ (10)	74

Table 12. Selected bond lengths and angles of $[\text{Mn}(\text{CO})_4(\mu\text{-SC}_6\text{H}_4\text{-4-CF}_3)]_2$ (11)	76
Table 13. Selected bond lengths and angles of $[\text{Mn}(\text{CO})_3(\mu\text{-SC}_6\text{H}_4\text{-4-CF}_3)]_4$ (12)	79
Table 14. Selected bond lengths and angles of $[\text{Mn}_2(\text{CO})_6(\mu\text{-SC}_6\text{H}_4\text{-4-CF}_3)_3][\text{Mn}_4(\text{DMF})_3(\text{CO})_9(\mu\text{-SC}_6\text{H}_4\text{-4-CF}_3)_4]$ (13)	84
Table 15. ^1H NMR data for the aromatic ring protons of $[\text{Mn}(\text{CO})_3(\mu\text{-SC}_6\text{H}_4\text{-4-R})]_4$ ($[\text{D}_8 \text{ THF}]$, 400 MHz, ppm)	89
Table 16. Selected bond lengths and angles of $[\text{Mn}(\text{CO})_3(\mu\text{-SC}_6\text{H}_4\text{-4-CH}_3)]_4$ 9B	92
Table 17. Selected bond lengths and angles of $[\text{Mn}_6(\text{CO})_{18}(\mu\text{-SC}_6\text{H}_4\text{-4-Cl})_6\{\text{Mn}_2(\mu\text{-Br})_2(\text{THF})_2\}]$ (17)	97
Table 18. Stretching modes $\nu(\text{CO})$ [cm^{-1}] and bond distances [\AA] of the dinuclear complexes 4 , 5 , 6 , 7 and CORM 1	100

List of Publications

Scientific Articles

1. Derivatives of Photosensitive CORM-S1 - CO Complexes of Iron and Ruthenium with the $(OC)_2M(S-C-C-NH_2)_2$ Fragment. Lorett-Velásquez V.P., Jazzazi T.M.A., Malassa A., Görls H., Gessner G., Heinemann S.H., Westerhausen M. Eur. J. Inorg. Chem. 2012, 1072-1078

Presentations at conferences

1. Vaneza Lorett and Ralf Mede

Oral Presentation: Synthesis of new manganese carbonyls complexes as CO-releasing molecules 13th HHDP Workshop and 2nd HHDP Retreat at (Oppurg - Germany, December 13-14 2012)

2. Vaneza Lorett

Oral Presentation: Developing drug molecules of therapy with carbon monoxide 1st Retreat of FOR 1738 (Siegmundsburg-Germany June 27 29 2012)

3. Vaneza Lorett

Oral Presentation: Synthesis of manganese complexes for the search of new CORMs
First CORMeeting (Jena-Germany March 21 2012)

List of abbreviations

A	Absorbance
Å	Angstrom
Ad	Adamantyl
APE	1,2-bis(amido)-1,2-bis(pyridyl) ethane
BKCa	Big-conductance Ca, voltage-activated K channels
br	broad
cGPM	Cyclic guanosine monophosphate
CO	Carbon monoxide
COHb	Carbon monoxid hemoglobin
CORMs	Carbon monoxid releasing molecules
d	doublet
DAB	1,4-diaza-1,3-butadiene
DMF	Dimethylformamide
DMSO	Dimethyl sulfoxide
EI	electron impact
ESI	electrospray ionization
FAB	fast atom bombardement
HO	Heme oxygenase
Hz	Hertz
IR	Infrared
LED	light-emitting diode

m	multiplett (NMR); medium (IR)
<i>m</i>	<i>meta</i>
m/z	Mass-to-charge ratio
M ⁺	Mol peak
Mb	deoxymyoglobin
MHz	megahertz
MS	mass spectrometry
NADP	Nicotinamide adenine dinucleotide phosphate
NMR	Nuclear magnetic resonance
<i>p</i>	<i>para</i>
ppm	parts-per-million
PQG	protein kinase G
1-Adamantyl-Pyca	2-pyridylmethyl-N-adamantyl imine
R	aromatic rest
r.t.	Room temperature
s	singlet (NMR); strong (IR)
t	triplett
T	thiophene
THF	tetrahydrofuran
Tpm	tris(1-pyrazolyl)methane
UV	ultraviolet
ν	wavenumber
vs	very strong
w	weak
δ	chemical shift
λ	wavelength

1 Introduction

The motivation of the present thesis centers on two main parts. In the first one, fundamental aspects of biological applications of carbon monoxide, among them carbon monoxid releasing molecules (CORMs) are discussed. The second section presents a review on the development of CORMs and shows attractive candidates for therapeutical treatment, emphasizing on the CO-releasing properties.

1.1 Carbon monoxide as active agent (signaling molecule)

The carbon monoxide (CO) is the diatomic oxide of carbon. It is a colorless and odorless toxic gas. Due to its covalent triple bond, it is a chemically stable molecule. Under standard conditions its water solubility is low (aprox. 3.54mL/100mL ~44.3 ppm by mass). Its ability to react with water or oxygen requires high activation energies. Typically CO is produced by the incomplete combustion of organic materials [1]. The production rate of CO in a normal human being is on average 20 $\mu\text{mol/h}$ [2]. As a toxin, pathological levels of CO can induce both acute and chronic health hazards. The affinity of CO to hemoglobin, resulting in the formation of carbonmonoxid hemoglobin (COHb),

is about 210 to 250 times higher than that for oxygen. The CO molecule has a relatively high stability in contrast to its congener NO which is a free radical [3]. The binding affinity and specificity of CO for the HEME proteins are high, joining the HEME ferro cores (i.e. with reduced iron atoms) unlike NO that binds to HEMO ferri cores (i.e. with oxidized iron atoms). This fact enables CO to interact with hemoproteins and hence to regulate or modify their total properties. The CO is constantly being oxidized to CO₂, removed and exhaled in our body, so one could say that there is a constant metastability between produced and catabolized CO [3].

1.1.1 CO endogenous production

The main endogenous source of CO is heme oxygenase, which exists in constitutive (HO-2 and HO-3) and inducible (HO-1) isoforms. The HO enzymes are essential for the metabolism of heme (also technically called ferroprotoporphyrin IX), which works as the prosthetic group of various proteins including many enzymes of oxidoreductase nature. The HO transforms HEME group heme by oxidation the into a biliverdin pigment (biliverdin IX α), which is subsequently converted into bilirubin (bilirubin IX α) through the biliverdin enzyme [4].

The classical catalytic reaction of HO produces: Biliverdin, CO, Iron(II) ions, metabolic water and Oxidase Coenzyme NADP (figure 1). In addition to a main route there are several alternatives for CO biosynthesis such as auto-oxidation

and enzymatic oxidation of phenols, photooxidation of organic compounds and lipid peroxidation [1, 5, 6].

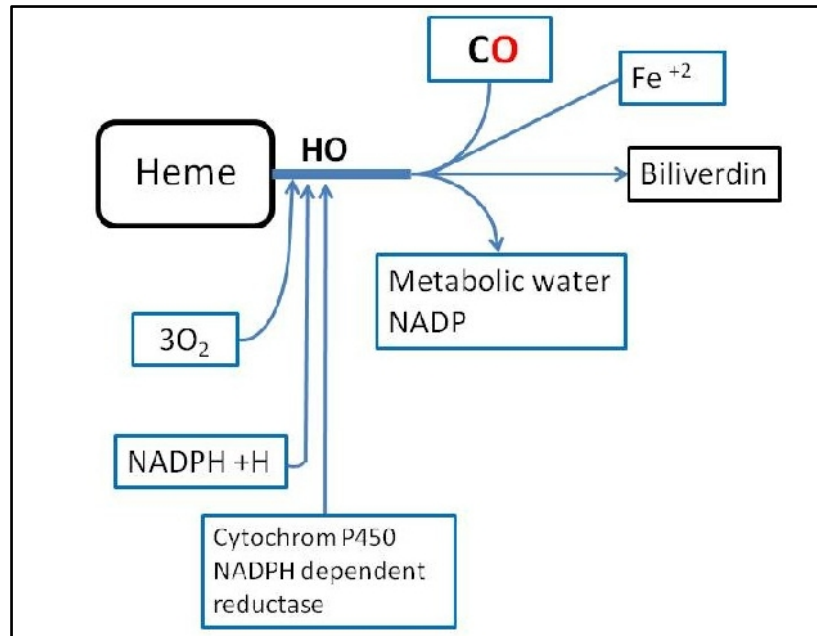


Figure 1: Catalytic reaction of Heme-oxygenase.

1.1.2 Biologic effects of CO

The activity of CO in biological substrates is based on four facts.

- CO acts as first and second messenger in cellular communication [3].
- The induction of HO-1 and the production of CO exhibit anti-inflammatory, anti-apoptotic, antiproliferative and cytoprotective effects [3].
- Activation of soluble guanylyl cyclase increases the biosynthesis of cyclic guanosine monophosphate (cGMP) which in turn binds to and activates the protein kinase G (PQG). The PQG phosphorylates various substrates so that they have a buffering effect against calcium [3].

- The direct interaction of CO with some ion channels and especially with those of high conductance for potassium called BKCa (Big conductance KCa channels). Activation of these channels is due to a specific interaction of α subunit with the CO, unlike the β subunit that is recognized by NO, to which it binds. In addition, the heme and HO-2 can bind directly to these channels and regulate their function. The four above mentioned facts are the basis of several physiological functions of the HO-CO system [3].

1.2 Carbon monoxide-releasing molecules (CORMs)

The studies of carbon monoxide as a therapeutic agent began in the early 1990s and consisted predominantly in the use of CO gas. Pre-clinically CO gas administration proved beneficial in animal models of various human diseases, as well as has already been tested in human clinical trials [2, 7]. However, the inherent toxic nature of CO gas limits its therapeutic application by inhalation. For this reason, the challenge for the researchers and practitioners in the field has been within the last decade, the development of safe and convenient methods for the delivery of therapeutic amounts of CO. These methods comprise the development of carbon monoxide-releasing molecules (CORMs) that can release CO *in vivo* in a controlled manner represents the best option for the delivery of CO in diseased tissues and organs [7]. Due to the fact that carbon monoxide is a widely used π acceptor ligand in organometallic complexes, the application of metal carbonyl complexes as synthetic CORMs might offer a way to controlled and tissue-selective CO liberation.

1.2.1 Development of a first generation of CORMs

The first report on CO releasing molecules was done by Motterlini *et al.* in early 2002. In its publication they reported the use of metal carbonyls as CORMs, the already commercialized metal carbonyl compounds $[\text{Mn}_2(\text{CO})_{10}]$ (CORM-1), $[\text{Fe}(\text{CO})_5]$ and $[\text{Ru}_2(\text{CO})_6\text{Cl}_4]$ (CORM-2). CORM-1 and $[\text{Fe}(\text{CO})_5]$ are insoluble in water and require photolysis to release CO, furthermore $[\text{Fe}(\text{CO})_5]$ is highly toxic. However, despite the fact that CORM-2 is also insoluble in water it can be used as a solution in DMSO, releasing CO spontaneously yielding a mixture of $[\text{Ru}(\text{DMSO})(\text{CO})_3\text{Cl}_2]$ (**2**) and $[\text{Ru}(\text{DMSO})_2(\text{CO})_2\text{Cl}_2]$ (**3**). Subsequently, **3** is isomerized (figure 2). The initial results showed that all three compounds cause vasodilatation [8]. A number of publications have reported the biological use of CORM-2, and covered a wide range of properties such as: reno-protective, anti-inflammatory, anti-carcinogenic, pro-angiogenic, anti-apoptotic and inhibitor of cell proliferation [9-18]. The complex $[\text{Ru}(\text{CO})_3\text{Cl}(\text{glycinate})]$ (CORM-3) was the first water-soluble CORM to be synthesized and tested in biological systems.

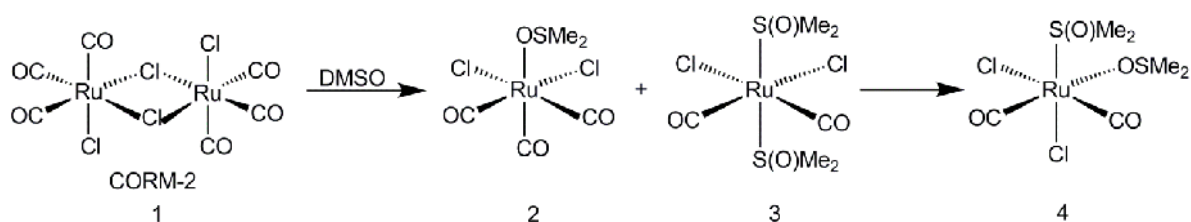


Figure 2: Reaction products between $[\text{RuCl}_2(\text{CO})_3]_2$ and DMSO.

It was nicely shown that the release of CO from CORM-3 depends strongly on the medium in which the compound is stored. The initial study showed that it has low toxicity, is a vasodilator and greatly increases the survival of mice following heart transplants. However, it should be kept in mind that CORM-3

rapidly releases CO ($t_{1/2} < 1$ min at 37°C , $\text{pH} = 7.4$) once in contact with biological fluids and cellular components [19]. Research subsequently demonstrated vasodilator, reno-protective, cardioprotective, anti-inflammatory, anti-ischemic effects, and inhibition of platelet aggregation [20-27].

A fourth compound was identified, the sodium boranocarbonate $\text{Na}_2[\text{H}_3\text{BCO}_2]$ (CORM-A1) which is a highly water-soluble compound that spontaneously liberates CO in aqueous solutions. In contrast to the above mentioned compounds, CORM-A1 does not contain a transition metal carbonyl but a carboxylic group that is converted into CO during hydrolysis. At $\text{pH} 7.4$, $[\text{H}_3\text{BCO}_2]^{2-}$ releases CO relatively fast at 37°C with a half life of $t_{1/2} = 21$ min [28]. CORM-A1 is a vasodilator, reno-protective, anti-ischemic and anti-apoptotic compound [20, 28-30]. CORM-1, CORM-2, CORM-3 and CORM-A1 represent the first generation of CO-releasing molecules that provide the first basis for research and development of new compounds [28].

1.2.2 Development of photo-CORMs

Recently, photolysis has been employed for some metal carbonyls which are called "photoCORM" as a mechanisms for CO release effect [2, 31]. In this group of compounds light is used as the external trigger that allows to define location and timing of CO release. The advantage of a photo-activated carbon monoxide releasing moiety is that it is a very promising way to approach a more controlled and specific CO delivery and a temporal control of their biological activity [34, 37, 38]. To achieve photoinduced delivery of carbon monoxide to biological systems, one needs the photo-CORMs that are stable in the dark in

aqueous solution and release one or more equivalents of carbon monoxide upon irradiation with visible light. During this process the metal-coligand fragment should ideally stay intact and finally the CO thus released diffuses into its biological target structure while the metal-coligand moiety will likely bind a solvent molecule to complete its coordination sphere [34].

Such photo-CO-RMs, which have been recently reviewed, include $[\text{Mn}(\text{CO})_3(\text{tpm})]\text{PF}_6$. (tpm = tris(1-pyrazolyl)methane) [32] and *cis*- $[\text{Fe}(\text{CO})_2(\text{H}_2\text{NCH}_2\text{CH}_2\text{S})_2]$, (CORM-S1) [33]. Photoactivation of water soluble $[\text{Mn}(\text{CO})_3(\text{tpm})]^+$ shows photoinitiated cytotoxicity against the human colon cancer cell line HT29, with a reduction in cell biomass. However, this observed cytotoxicity is likely to derive from the metal containing scaffold that results after the release of 2 equivalents of CO ligands rather than from CO alone [32, 34]. Subsequently, the tpm ligand has been modified with conjugated peptides [35]. Another strategy employed was the grafting on the surface of SiO_2 nanoparticles designed to deliver CO to solid tumors [36]. CORM-S1 was shown to be stable after 15 min in the dark, but to release CO upon irradiation with 470 nm light and under physiological conditions, leading to an activation of the previously mentioned potassium channels by CO [33].

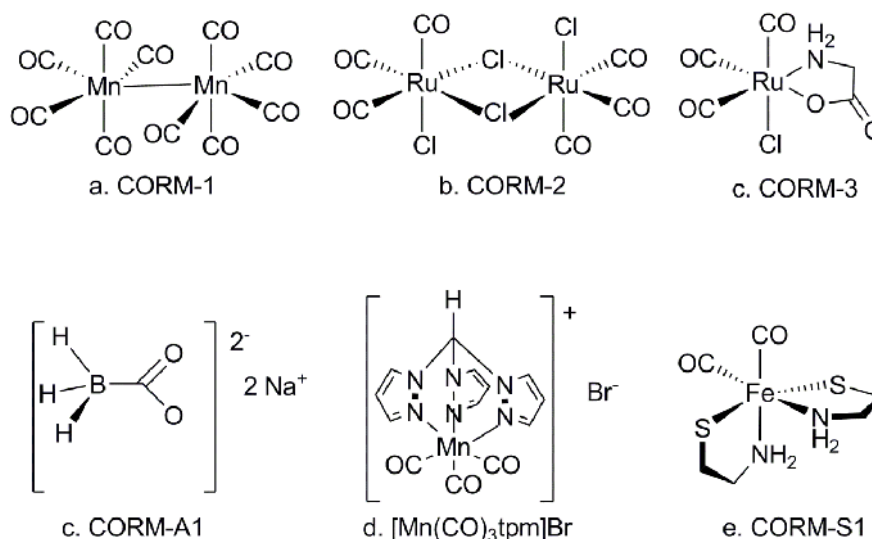


Figure 3: Main CORMs **a)**, **b)**, **c)** and **d)** CORMs first generation. **e)** and **f)** photo-CORMs up to now (tpm = tris(pyrazolyl)methane).

The aim of this doctoral thesis is the synthesis of ruthenium and manganese carbonyl complexes and their application as new CORMs. A detailed study of the structure and characterization of all the metal carbonyl complexes by NMR and IR spectroscopy as well as X-ray diffraction studies is reported. A particular emphasis on the investigation of the mechanisms of CO release from complexes via photoactivation is accomplished as well.

2 Results and discussion

2.1 Ruthenium-based carbonyl complexes

In this section the synthesis and characterization of two ruthenium carbonyl complexes with the general formula $[\text{Ru}(\text{CO})_2(\text{S}^{\wedge}\text{N})_2]$ with ($\text{S}^{\wedge}\text{N}$) representing a bidentate amino thiolate ligand and one $[\text{Ru}_2(\text{CO})_5(\text{R-APE})]$ complex with R-APE being an 1,2-bis(amido)-1,2-bis(pyridyl) ethane ligand are discussed.

2.1.1 Synthesis and characterization of $[\text{Ru}(\text{CO})_2(\text{H}_2\text{NC}_2\text{H}_4\text{S})_2]$ (**1**) and $[\text{Ru}(\text{CO})_2(\text{H}_2\text{NC}_6\text{H}_4\text{S})_2]$ (**2**)

The compounds **1** and **2** were synthesized by the oxidative addition of cysteamine or 2-aminothiophenol to $[\text{Ru}_3(\text{CO})_{12}]$ in a 1:6 ratio, respectively as depicted in figure 4. Ruthenium is oxidized to ruthenium(II) in this process under release of six CO molecules. Moreover, the thiol group of the ligand is deprotonated, counterbalancing the positive charge of the ruthenium(II) centers and the deprotonated ligands coordinate as bidentate Lewis bases.

The reaction of cysteamine with $[\text{Ru}_3(\text{CO})_{12}]$ in THF yields 72% of **1**. As it is shown in figure 4, the synthesis was performed in a similar manner as in the case of the iron analog CORM-S1 [33]. This homologous Fe-based derivative was independently prepared from iron(II)-sulfate, triethylamine and the thiol with a yield of 19.5% [39]. The preparation of **2** in heptane (see figure 4) succeeded with a yield of 94%. A compound with the constitution of $[\text{Ru}(\text{CO})_2(\text{H}_2\text{NC}_6\text{H}_4\text{S})_2]$ was obtained with a yield of 30% by passing CO through ruthenium trichloride in ethanol and subsequent addition of 2-aminothiophenol [40]. The oxidative addition represents an advantageous because gaseous byproducts are easily removed and there will be no formation of salt-like byproducts [41], and hence, the yield of the reaction is significantly higher.

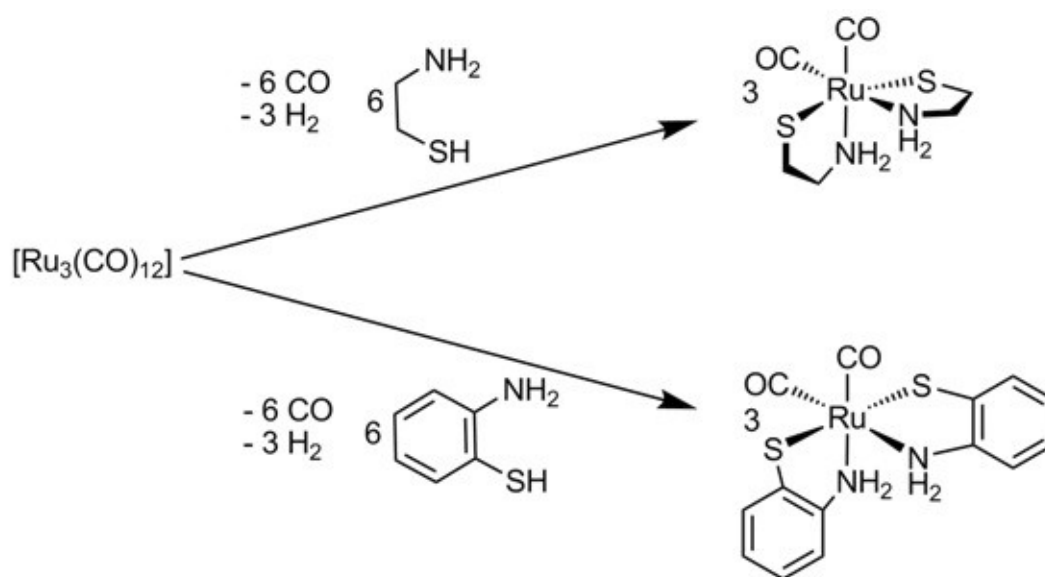


Figure 4: Synthesis of $[\text{Ru}(\text{CO})_2(\text{H}_2\text{NC}_2\text{H}_4\text{S})_2]$ (**1**) and $[\text{Ru}(\text{CO})_2(\text{SC}_6\text{H}_4\text{NH}_2)_2]$ (**2**).

Both complexes were characterized by IR, ^1H NMR, and ^{13}C NMR spectroscopy, mass spectrometry, X-Ray structural analysis and elemental analysis. The crystals of complex **1** were grown from a THF solution and molecules of the solvent co-crystallize in a 1:1 ratio. The mononuclear ruthenium complex $[\text{Ru}(\text{CO})_2(\text{SC}_6\text{H}_4\text{NH}_2)_2]$ (**2**) co-crystallizes with DMF. Unlike complex **1**, in **2** the solvent is chelated by the two amino groups.

In the IR spectra of both complexes, two absorption bands for the CO moieties were observed. For complex **1**, these bands appear at 2023 and 1950 cm^{-1} and correspond to the asymmetric and symmetric C-O stretching vibrations, respectively. Especially complex **2** showed a very interesting behavior, the bands of DMF-free **2** were observed at 2044 and 1989 cm^{-1} , Kingston and coworkers [40] observed these carbonyl bands at 2035 and 1970 cm^{-1} . However, formation of a DMF adduct led to two bands at 2044 and 1963 cm^{-1} . A THF adduct has been reported for an iron(II) complex with the same amino thiolate ligand [39, 41]. The presence of DMF in **2** shifted the symmetric stretching vibrations to a lower wavenumber by 30 cm^{-1} , storage at room temperature led to partial loss of DMF (figure 5).

The ^1H NMR spectra of both complexes showed that the amine protons of **1** resonate at 3.81 and 5.00 ppm and of **2** at 5.75 and 6.83 ppm showing that the protons at the nitrogen atoms are chemical different; the explanation of this occurrence is due to the fixed geometry of the bidentate chelating ligands. In ^{13}C NMR spectra of complex **1**, the chemical shifts of the carbonyl ligands are 201.3 ppm while in **2** the carbonyl signals appear at 189.3 ppm. Fast atom

bombardment (FAB) mass spectrum of **1** shows the molecular ion $[M + H]^+$ at m/z (%) = 310 (80) and signals at 282 (60) and 254 (75), which can be attributed to the fragments $[M + H - CO]$ and $[M + H - 2CO]$, respectively, confirming the presence of the carbonyl ligands.

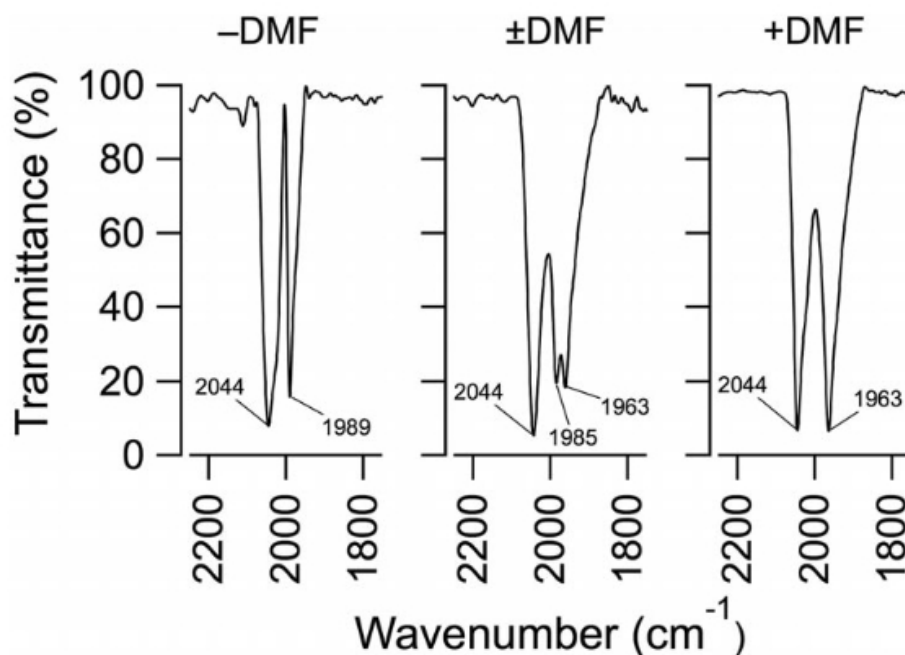


Figure 5: IR spectra of the carbonyl region of **2** (left), **2**·DMF (right) and **2**·DMF with partial loss of DMF (center) [41].

The electrospray ionization (ESI) mass spectrum of complex **2** shows a signal at m/z (%) = 405 (80) assigned to the molecular ion $[M]^+$, verifying the high stability of the complex in solution. As in complex **1**, two signals were detected at 377 (100) $[M - CO]^+$ and 349 (55) $[M - 2CO]^+$, respectively, which can be assigned to the loss of carbonyl ligands.

2.1.2 Molecular Structures of $[\text{Ru}(\text{CO})_2(\text{H}_2\text{NC}_2\text{H}_4\text{S})_2]$ (**1**) and $[\text{Ru}(\text{CO})_2(\text{SC}_6\text{H}_4\text{NH}_2)_2]$ (**2**)

$[\text{Ru}(\text{CO})_2(\text{H}_2\text{NC}_2\text{H}_4\text{S})_2]$ (**1**)

The complex $[\text{Ru}(\text{CO})_2(\text{H}_2\text{NC}_2\text{H}_4\text{S})_2]$ (**1**) crystallized in the space group $P2_1/n$. The structure of the molecule is shown in figure 6, where also the molecular structure with THF is displayed. Selected bond length and angles are listed in table 1. The THF molecule is bonded via an $\text{O}\cdots\text{H}-\text{N}$ hydrogen bridge to the amino group. This ruthenium(II) complex contains two carbonyl and two anionic ligands derived from cysteamine via deprotonation of the thiol functionality. The CO ligands occupy *cis* positions within the octahedral environment of the ruthenium atom, the amino groups of the cysteamine ligands are arranged in a way that the sulfur atoms are in *trans* and the nitrogen atoms in *cis* positions to each other. The *trans*-arrangement of the anionic thiolate units reduces intramolecular electrostatic repulsion.

The coordination sphere of the homologous iron derivative $[\text{Fe}(\text{CO})_2(\text{SCH}_2\text{CH}_2\text{NH}_2)_2]$ CORM-S1 [33, 41] is very similar and the metal atoms have only a weak influence on the structural data. The Ru-S and Ru-N bonds with average value of 2.412 and 2.170 Å, respectively, are longer than the corresponding Fe-S (2.306 Å) and Fe-N bonds (2.040 Å) [31, 39]. The Ru-CO distances show values of 1.861 and 1.871 Å and are significantly elongated compared to CORM-S1 with average Fe-CO values of 1.768 Å. The octahedral coordination sphere of the ruthenium atom is distorted due to small endocyclic

S1-Ru-N1 and S2-Ru-N2 angles of approximately 83.8°. A consequence of this finding is the widening of the S-Ru-C angles with an average value of 94.2°.

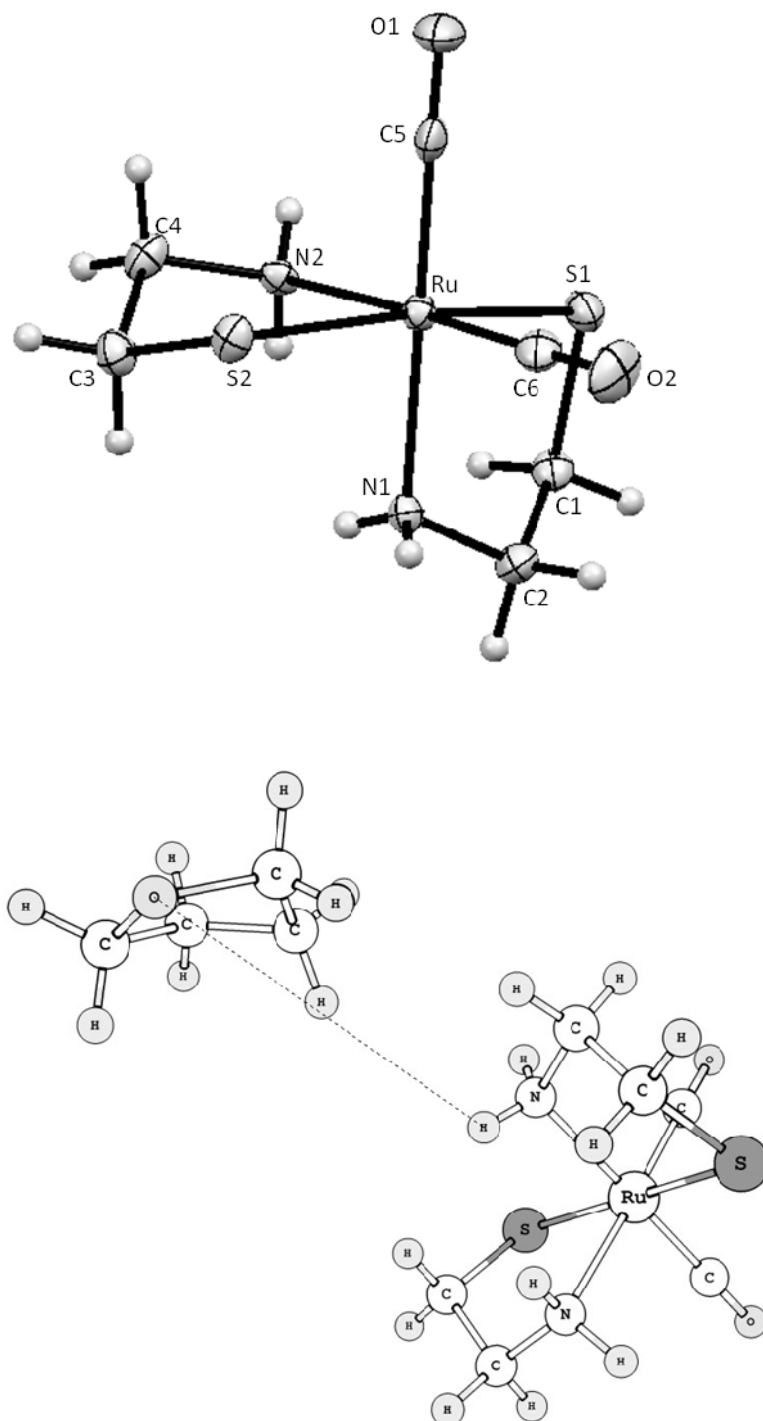


Figure 6: Molecular structures of $[\text{Ru}(\text{CO})_2(\text{SC}_2\text{H}_4\text{NH}_2)_2]$ (**1**) (top) and its interaction with $[\text{Ru}(\text{CO})_2(\text{SC}_2\text{H}_4\text{NH}_2)_2] \cdot \text{THF}$ (bottom). Thermal ellipsoids are drawn at the 50% probability level. Hydrogen atoms are shown with arbitrary radii.

Table 1. Selected bond length and angles of complex [Ru(CO)₂(SC₂H₄NH₂)₂] (**1**)

Bond length [Å]		Angles [°]	
Ru-S1	2.417(2)	S1-Ru-S2	167.88(5)
Ru-S2	2.407(1)	S1-Ru-N1	83.57(13)
Ru-N1	2.168(4)	S1-Ru-N2	86.16(12)
Ru-N2	2.172(4)	S1-Ru-C5	97.48(17)
Ru-C5	1.861(6)	S1-Ru-C6	94.90(17)
Ru-C6	1.871(6)	S2-Ru-N1	88.82(13)
S1-C1	1.822(6)	S2-Ru-N2	84.04(12)
S2-C3	1.822(6)	S2-Ru-C5	89.99(17)
N1-C2	1.4956(7)	S2-Ru-C6	94.73(17)
N2-C4	1.507(7)	N1-Ru-N2	87.13(17)
C5-O1	1.143(7)	N1-Ru-C5	178.63(2)
C6-O2	1.146(7)	N1-Ru-C6	91.53(2)
		N2-Ru-C5	92.07(2)
		N2-Ru-C6	178.2(2)
		C5-Ru-C6	89.24(2)

[Ru(CO)₂(SC₆H₄NH₂)₂] (2**)**

The complex [Ru(CO)₂(SC₆H₄NH₂)₂] (**2**) crystallizes in the monoclinic space group $P2_1/n$. The molecular structure and labeling is depicted in figure 7. Selected bond lengths and angles are listed in table 2. The coordination sphere of the metal center is very similar to **1** with *cis* arranged carbonyl ligands and amino functionalities, while the thiolates are located in *trans* position. The bond lengths and angles are also in accordance with those found for **1**. Therefore the influence of the ligand on these structural parameters is negligible.

The endocyclic angles S1-Ru-N1 (83.82°) and S2-Ru-N2 (83.36°) enforce derivations from the ideal octahedral environment, which coordination are consistent with the observed distortion of the octahedral coordination sphere of

complex **1**. The *trans* angles S1-Ru-S2 (168.54°), N1-Ru-C14 (177.45°) and N2-Ru-C13 (178.72°) also indicate the slight distortions from the octahedral geometry. The coordination spheres of **2** and [Fe(CO)₂(SC₆H₄NH₂)₂] (CORM-S2) [41] are very similar. The mean Ru-S (2.394 Å) and Ru-N (2.152 Å) distances are longer than the corresponding Fe-S (2.293 Å) and Fe-N (2.039 Å). Moreover, the bond lengths of Ru-CO are approx. 9 pm larger than the Fe-CO distances of CORMS-2. The endocyclic angles S1-Ru-N1 and S2-Ru-N2 are slightly narrower than the angles observed in CORM-S2.

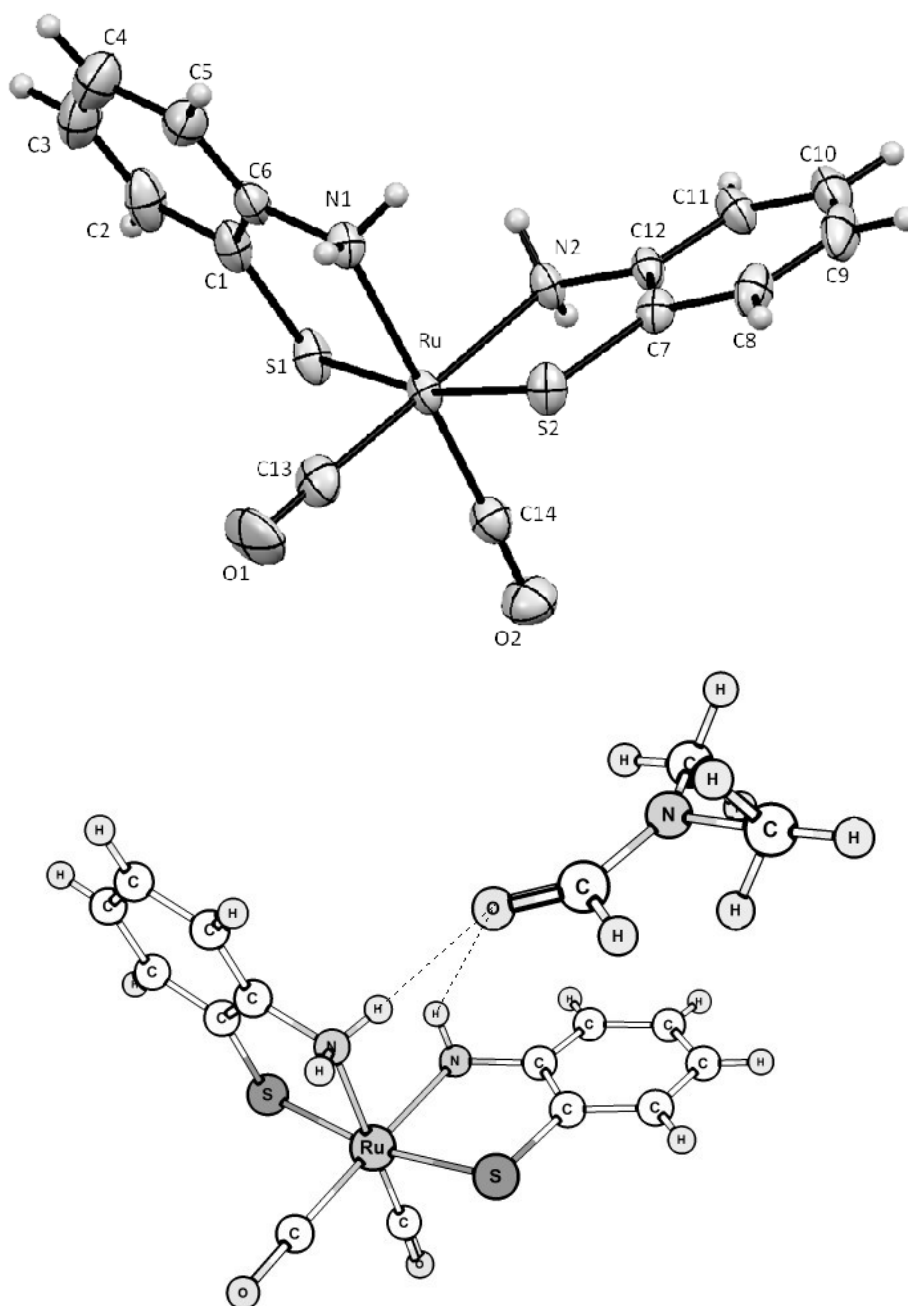


Figure 7: Molecular structure of $[\text{Ru}(\text{CO})_2(\text{SC}_6\text{H}_4\text{NH}_2)_2]$ (**2**) (top) and its interaction with co-crystallized DMF (bottom). Thermal ellipsoids are drawn at the 50% probability level. Hydrogen atoms are drawn with arbitrary radii.

Table 2. Selected bond length and angles of [Ru(CO)₂(SC₆H₄NH₂)₂] (**2**)

Bond lengths [Å]		Angles [°]	
Ru-S1	2.394(1)	S1-Ru-S2	168.54(5)
Ru-S2	2.393(1)	S1-Ru-N1	83.82(10)
Ru-N1	2.149(4)	S1-Ru-N2	89.01(10)
Ru-N2	2.155(4)	S1-Ru-C13	92.18(15)
Ru-C13	1.867(5)	S1-Ru-C14	94.33(17)
Ru-C14	1.876(5)	S2-Ru-N1	87.37(11)
S1-C1	1.767(5)	S2-Ru-N2	83.36(10)
S2-C7	1.759(5)	S2-Ru-C13	95.53(15)
N1-C6	1.461(5)	S2-Ru-C14	94.24(17)
N2-C12	1.456(6)	N1-Ru-N2	87.94(16)
C13-O1	1.142(6)	N1-Ru-C13	92.66(19)
C14-O2	1.143(6)	N1-Ru-C14	177.45(19)
		N2-Ru-C13	178.72(18)
		N2-Ru-C14	90.27(19)
		C13-Ru-C14	89.17(2)

2.1.3 Synthesis and characterization of [Ru₂(CO)₅(adamantyl-APE)] (**3**) (APE= 1,2-bis(μ-alkylamido)-1,2-bis(2-pyridyl)ethane)

In a first step, the novel ligand 2-pyridyl-methy-N-adamantylimine (**1-adamantyl-Pyca**) was prepared by nucleophilic substitution, starting from 2-pyridyl carbaldehyde and 1-adamantylamine according to standard methods [43, 44]. This ligand provides one bidentate N^N binding pocket with the pyridine nitrogen atom and the imine nitrogen atom as potential donors.

The IR spectrum of the ligand exhibits a characteristic strong band at 1641 cm⁻¹ which can be attributed to the stretching vibrations of the imine. The ¹H NMR spectra of the ligand is clearly divided in two parts; the down-field part shows the resonances of the pyridyl and the imine protons N=C(H), the latter appears

as a singlet at 8.32 ppm and is clearly in accordance with values observed in related pyridylmethylideneamine [45]. The up-field sub spectrum shows a multiple peaks between 1.7 and 1.8 ppm and a singlet at 2.10 ppm, originating from the adamantyl protons. Moreover, the ^{13}C NMR spectrum shows the resonance of the imine carbon at 156 ppm. Electron ionization (EI) mass spectrum contains a signal at m/z (%) = 240 (60) which can be attributed to the molecular ion $[\text{M}]^+$.

The synthesis of $[\text{Ru}_2(\text{CO})_5(\text{adamantyl-APE})]$ (**3**) was performed in analogy to related derivatives as reported by Vrieze *et al* [46, 47] (see figure 8). $[\text{Ru}_3(\text{CO})_{12}]$ was refluxed in toluene in the presence of three molar equivalents of the ligand **1-adamantyl-Pyca** and the dinuclear complex **3** was obtained with a yield of 40% of, in which 1-adamantyl-APE consists of two C-C linked **1-adamantyl-Pyca** unit. The C-C coupling reaction takes place at the C atom of the imine moiety. The reaction sequence was investigated by Vrieze *et al* [46, 47], and they proposed as a first step the breakdown of the $[\text{Ru}_3(\text{CO})_{12}]$ cluster into monomeric species stabilized by bidentate R-Pyca ligands, leading to the formation of $[\text{M}(\text{CO})_3(\text{R-Pyca})]$. Restructuring finally leads to dinuclear $[\text{Ru}_2(\text{CO})_5(\text{R-APE})]$ (see figure 8). The complex was characterized by IR, ^1H NMR and ^{13}C NMR spectroscopy, mass spectrometry, X-Ray crystallographic analysis and elemental analysis.

The IR spectra of the $[\text{Ru}_2(\text{CO})_5(\text{adamantyl-APE})]$ (**3**) complex exhibits five characteristic bands in the CO region, four of which appear between 2011, 1976, 1913 and 1911 cm^{-1} and can be attributed to the stretching vibrations of terminal

CO, and one at 1682 cm^{-1} which indicates the presence of a bridging CO group in the compound. The ^1H NMR spectra of **3** shows broad multiple peaks between 1.29 and 1.89 ppm which are assigned to the protons of the adamantyl group. The amido N-C-(H)-C(H)-N protons are found at 4.17 ppm. Vrieze *et al* reported for their complexes $[\text{Ru}_2(\text{CO})_5(\text{R-APE})]$ ($\text{R} = t\text{-Bu}, i\text{-Pr}, c\text{-Hex}$) [47] that these protons appear between 3.76 and 3.94 ppm. Additionally they noted that the carbon-carbon coupling is formed in one enantiomeric pair ((*R,R*) and (*S,S*)) of diastereomers, verified by crystallographic analysis studies at a single crystal. However, the ^1H -NMR data shows only one resonance pattern. The down-field part in the spectrum appears at 7.3-7.8 ppm is due to the pyridyl subunit of the ligand. The ^{13}C -NMR spectrum agrees with the general structure of the complex, showing the carbonyl resonances at 202.4 and 203.6 ppm. These results are consistent with those observed by Vrieze *et al* [47]. The electrospray ionization (ESI) mass spectrum of **3** shows the molecular ion $[\text{M} + 2\text{H}]^+$ at m/z (%) = 824 (25) and an intense signal at 796 (100) which can be attributed to the cation after loss of one CO $[\text{M} + 2\text{H} - \text{CO}]^+$ as well as small signals at 712 (5%) $[\text{M} + 2\text{H} - 4\text{CO}]^+$ and 685 (5%) $[\text{M} + 2\text{H} - 5\text{CO}]^+$.

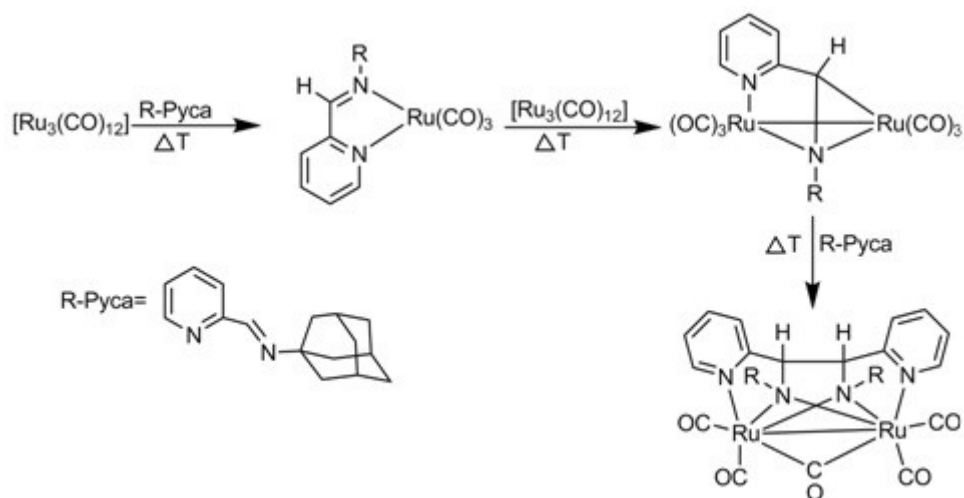


Figure 8: Synthesis of $[\text{Ru}_2(\text{CO})_5(\text{adamantyl-APE})]$ (**3**).

2.1.4 Molecular structures of $[\text{Ru}_2(\text{CO})_5(\text{adamantyl-APE})]\cdot\text{THF}$ (**3**) and $[\text{Ru}_2(\text{CO})_5(\text{adamantyl-APE})]\cdot\text{CH}_2\text{Cl}_2$ (**3B**)

$[\text{Ru}_2(\text{CO})_5(\text{adamantyl-APE})]\cdot\text{THF}$ (3**)**

The dinuclear complex $[\text{Ru}_2(\text{CO})_5(\text{adamantyl-APE})]\cdot\text{THF}$ (**3**) crystallizes in the orthorhombic space group *Pnma*. The molecular structure of the complex from THF together with the labeling scheme is depicted in figure 9. Selected bond lengths and angles are listed in table 3. The complex **3** co-crystallized with one equivalent of tetrahydrofuran. Two ruthenium centers are chelated by the tetradentate ligand (adamantyl-APE). Ruthenium atoms are connected through two central amido bridges, a metal-metal bond and a CO bridge. Furthermore, each ruthenium atom bonds to a pyridine nitrogen atom and two terminal CO ligands in equatorial positions.

In the crystal packing no significant intermolecular contacts occur between the dinuclear complex and the co-crystallized THF molecules. Both ruthenium centers are placed in a pentagonal bipyramidal coordination sphere. The compound exhibits a Ru-Ru bond length of 2.881 Å similar to that observed in the complex $[\text{Ru}_2(\text{CO})_5(i\text{-Pr-APE})]$ [46]. This rather elongated Ru-Ru bond is characteristic for CO bridged dinuclear Ru compounds [48] and is attributed to the electron donating character of the ligand, which results in an increase of the anti-bonding σ^* electron density between the two metal atoms, thus weakening the Ru-Ru bond. The ruthenium atoms and the CO bridge form a slightly asymmetric triangle with Ru-C bond lengths of 2.00 (Ru1) and 2.02 (Ru2) Å, respectively. The terminal ruthenium carbonyl distances Ru-CO exhibit values

of 1.860 Å, similar distances of 1.830 and 1.860 Å were also reported for $[\text{Ru}_2(\text{CO})_5(i\text{PrAPE})]$ [46]. The angle between the planes $\text{Ru}_2\text{N3}$ and $\text{Ru}_2\text{N3A}$ is 83.45°; the other two angles to plane $\text{Ru}_2\text{C22}$ are equal with values of 48.27°. The angles differ slightly for each ruthenium center, within the pentagonal bipyramidal coordination it is indicated a strong distortion that can be also described by the *trans* angles C23-Ru1-N3 (172.1°), C22-Ru1-N1 (164.3°), C24-Ru2-N3 (171.8°) and C22-Ru2-N2 (164.5°). All N-donor-ruthenium distances are rather similar for each ruthenium center ranging between 2.211 and 2.233 Å. A more detailed discussion of distances and angles of the newly formed ligand is not possible. A heavy disorder of this part of the molecule was observed due to co-crystallisation of the *R,R* and *S,S*-form of the molecule which statistically occupy the same position in the crystal lattice. Therefore, the compound was recrystallized from CH_2Cl_2 (see next section).

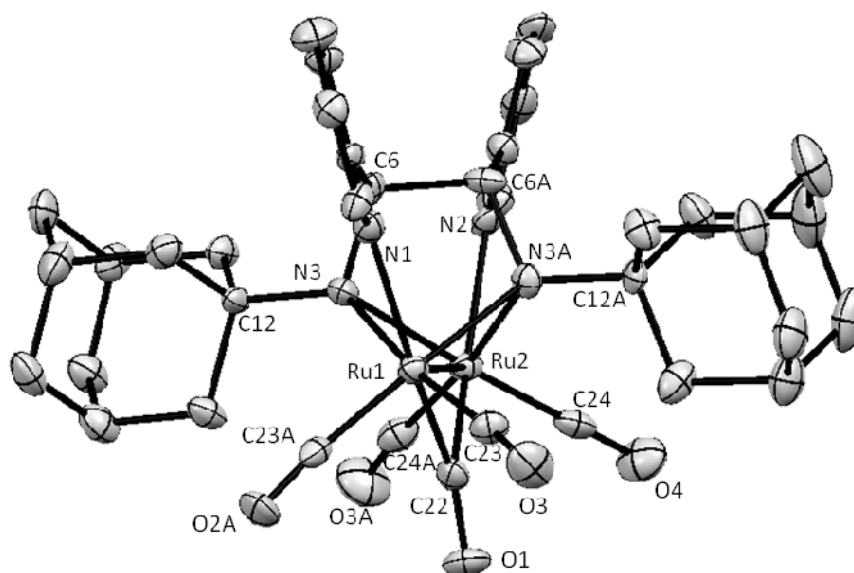


Figure 9: Molecular structure of the dinuclear $[\text{Ru}_2(\text{CO})_5(\text{adamantyl-APE})]\cdot\text{THF}$ (**3**). Thermal ellipsoids are drawn at the 50% probability level. Hydrogen atoms and THF solvent are omitted for clarity. The disordering of the bis(2-pyridyl) ethane backbone is not depicted.

Table 3. Selected bond lengths and angles of [Ru₂(CO)₅(adamantyl-APE)]·THF (**3**)

Bond lengths [Å]			
Ru1-Ru2	2.881(9)	Ru2-C24	1.863(7)
Ru1-C22	2.000(10)	Ru2-N2	2.233(4)
Ru1-C23	1.855(7)	Ru2-N3	2.219(6)
Ru1-N1	2.222(5)	C22-O1	1.235(10)
Ru1-N3	2.211(5)	C23-O2	1.155(9)
Ru2-C22	2.015(8)	C24-O3	1.150(8)
Angles [°]			
N3A-Ru1-N1	85.28(3)	N3A-Ru2-N2	83.49(2)
N3A-Ru1-C23	103.81(3)	N3A-Ru2-C24	103.5(2)
C22-Ru1-C23	91.98(3)	C22-Ru2-C24	92.85(3)
N3-Ru1-N1	81.88(3)	N3-Ru2-N2	84.79(19)
Ru2-Ru1-N1	120.1(2)	Ru1-Ru2-N2	120.6(1)
Ru2-Ru1-C22	44.36(2)	Ru1-Ru2-C22	43.9(3)
N3-Ru1-N3A	69.2(3)	N3-Ru2-N3A	68.9(3)
C23-Ru1-C23A	82.88(5)	C24-Ru2-C24A	83.8(4)
C22-Ru1-N3	83.7(2)	C22-Ru2-N3	83.1(3)
N1-Ru1-C22	164.27(3)	N2-Ru2-C22	164.5(3)
C23-Ru1-N3	172.1(3)	C24-Ru2-N3	171.8(2)
C23A-Ru1-N3A	172.1(3)	C24A-Ru2-N3A	171.8(2)
Ru1-C22-O1	135.6(7)	Ru2-C22-O1	132.69(7)
Ru1-C23-O2	173.85(8)	Ru2-C24-O3	174.86(6)
Ru2-Ru1-N3	49.57(15)	Ru1-Ru2-N3A	49.30(13)
Ru1-C22-Ru2	91.70(4)		

[Ru₂(CO)₅(adamantyl-APE)]·CH₂Cl₂ (3B**)**

Other suitable crystals for X-Ray crystallographic analysis were obtained from dichloromethane at 6°C. The complex [Ru₂(CO)₅(adamantyl-APE)] and the solvent CH₂Cl₂ co-crystallize in the monoclinic space group *P*2₁/*c* as a mixture of two independent chiral molecules (*R,R* and *S,S* enantiomers) in the unit cell, **3A** and **3B** with only slightly different geometries. Due to crystallization in a centric space group, the solid state is formed by a racemate. The molecular structure and labeling scheme of one of the two independent molecules (**3B**) are

depicted in figure 10. Selected bond lengths and angles are summarized in table 4 (**3A**) and table 5 (**3B**). Both dinuclear complexes are highly symmetric.

The two ruthenium centers within each molecule are crystallographically identical. The Ru-Ru bond length in both independent molecules of the complex is 2.891 Å, this distance is only slightly elongated compared to **3**. The bond lengths between ruthenium and the CO bridge are 2.040 and 2.020 Å. In the molecules **A** and **B** of the complex, each terminal Ru-CO distance is slightly different with distances of 1.826 to 1.870 Å. The short distances correspond to **A** while longer bonds are formed in the case of **B**. Furthermore, dichloromethane molecules are weakly bound to the oxygen atoms and causing slightly to the different Ru-C distances. The pyridyl nitrogen atom - ruthenium distances show average values of 2.240 Å. Additional short bonds are formed between the ruthenium centers and the amido nitrogen atoms with distances of Ru1A-N3A (2.166 Å), Ru2A-N4A (2.171 Å), Ru1B-N3B (2.158 Å) and Ru2B-N4B (2.165 Å). As compared to the bond lengths found for **3**, these distances are significantly shortened, probably due to the crystal packing. The carbon-carbon bonds of the adamantyl-APE ligand C6A-C7A (1.574 Å) and C6B-C7B (1.545 Å) are nearly equal. The N4A-C7A bond length of 1.462 Å is shorter compared to the corresponding distances of the other amido moieties of 1.491 Å in N3A-C6A and 1.496 Å for **B**. The N4B-Ru1B-N1B angle of 87.9° is enlarged compared to N4A-Ru1A-N1A (83.4°). The N4A-C7A-C6A angle of 107.4° is slightly enlarged compared to N3A-C6A-C7A (106.2°). These angles are very similar in **B** with average values of 106.5°.

Table 4. Selected bond lengths and angle of [Ru₂(CO)₅(adamantyl-APE)]·CH₂Cl₂ (3A)

Bond lengths [Å]					
Ru1A-Ru-2A	2.890(1)	Ru2A-C34A	2.030 (9)	C35A-O2A	1.156(11)
Ru1A-C34A	2.040(8)	Ru2A-C37A	1.845 (9)	C36A-O3A	1.169(11)
Ru1A-C35A	1.826(11)	Ru2A-C38A	1.867 (9)	C37A-O4A	1.166(10)
Ru1A-C36A	1.862(9)	Ru2A-N2A	2.254 (8)	C38A-O5A	1.136(10)
Ru1A-N1A	2.231(7)	Ru2A-N3A	2.256 (7)		
Ru1A-N3A	2.166(7)	Ru2A-N4A	2.171 (7)		
Ru1A-N4A	2.259(7)	C34A-O1A	1.193 (10)		
Angles [°]					
N4A-Ru1A-N1A	86.4(3)	N4A-Ru2A-N2A	79.0(3)		
N4A-Ru1A-C36A	103.1(1)	N4A-Ru2A-C37A	104.2(3)		
C34A-Ru1A-C35A	94.0(4)	C34A-Ru2A-C38A	93.8(4)		
C34A-Ru1A-C36A	96.6(4)	C34A-Ru2A-C37A	90.7(4)		
C35A-Ru1B-N3A	104.1(3)	C38A-Ru2A-N3A	103.1(3)		
N3A-Ru1A-N1A	80.8(3)	N3A-Ru2A-N2A	87.7(3)		
Ru2A-Ru1A-N1A	119.7(2)	Ru1A-Ru2A-N2A	119.2(2)		
Ru2A-Ru1A-C34A	44.6(3)	Ru1A-Ru2A-C34A	44.9(2)		
N3A-Ru1A-N4A	69.4(3)	N3A-Ru2A-N4A	69.4(2)		
C35A-Ru1A-C36A	83.4(4)	C37A-Ru2A-C38A	83.4(4)		
N1A-Ru1A-C34A	163.3(3)	N2A-Ru2A-C34A	164.0(3)		
C36-Ru1A-N3A	172.5(4)	C38A-Ru2A-N4A	172.4(3)		
C35-Ru1A-N4	173.4(3)	C37A-Ru2A-N3A	169.8(3)		
Ru2A-Ru1A-N3A	50.6(2)	Ru1A-Ru2A-N3A	47.9(2)		
Ru1A-C34A-O1A	134.3(7)	Ru2A-C34A-O1A	135.2(7)		
Ru1A-C35A-O2A	175.8(8)	Ru2A-C37A-O4A	173.8(8)		
Ru1A-C36A-O3A	173.9(9)	Ru2A-C38A-O5A	175.7(8)		
Ru1A-C34A-Ru2A	90.5(4)				

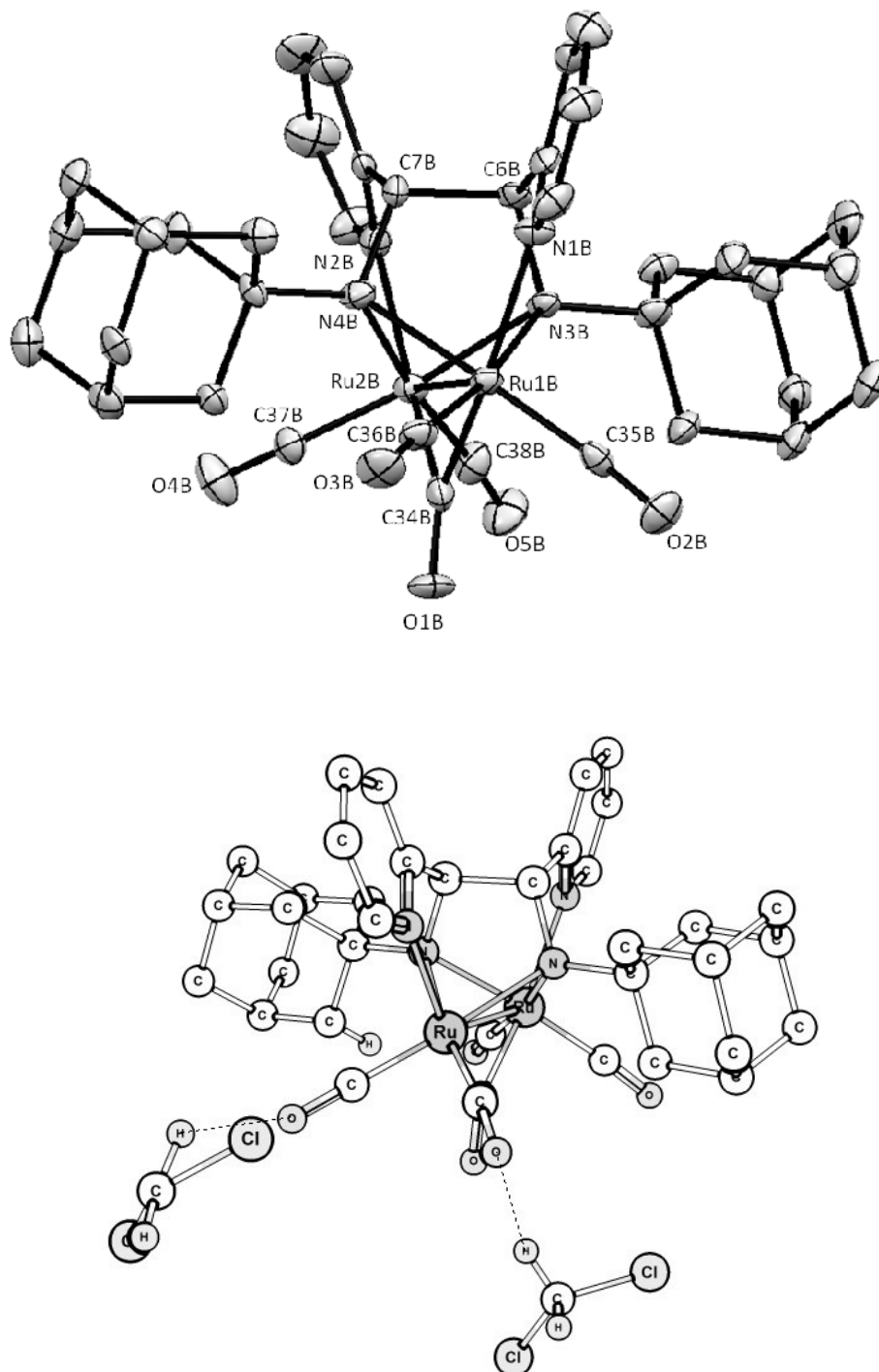


Figure 10: Molecular structure of the dinuclear $[Ru_2(CO)_5(adamantyl-APE)] \cdot CH_2Cl_2$ (**3B**) (top) and its interaction with co-crystallized CH_2Cl_2 (bottom). Thermal ellipsoids are drawn at the 50% probability level. Hydrogen atoms are omitted for clarity.

Table 5. Selected bond lengths and angles of $[\text{Ru}_2(\text{CO})_5(\text{adamantyl-APE})] \cdot \text{CH}_2\text{Cl}_2$ (**3B**)

Bond lengths [\AA]					
Ru1B-Ru-2B	2.891(1)	Ru2B-C34B	2.029(9)	C35B-O2B	1.154(10)
Ru1B-C34B	2.020(9)	Ru2B-C37B	1.852(9)	C36B-O3B	1.156(10)
Ru1B-C35B	1.859(9)	Ru2B-C38B	1.870(9)	C37B-O4B	1.156(11)
Ru1B-C36B	1.870(9)	Ru2B-N2B	2.243(7)	C38B-O5B	1.154(10)
Ru1B-N1B	2.228(7)	Ru2B-N3B	2.243(8)		
Ru1B-N3B	2.158(6)	Ru2B-N4B	2.165(7)		
Ru1B-N4B	2.266(7)	C34B-O1B	1.216(10)		
Angles [$^\circ$]					
N4B-Ru1B-N1B	87.9(3)	N4B -Ru2B- N2B	80.5(2)		
N4B-Ru1B-C36B	102.3(3)	N4B-Ru2B-C37B	102.7(3)		
C34B-Ru1B-C35B	92.3(4)	C34B-Ru2B-C38B	95.7(4)		
C34B-Ru1B-C36B	95.4(4)	C34B-Ru2B-C37B	97.6(4)		
C35B-Ru1B-N3B	104.4(3)	C38B-Ru2B-N3B	103.5(3)		
N3B-Ru1B-N1B	80.2(3)	N3B-Ru2B-N2B	87.5(2)		
Ru2B-Ru1B-N1B	119.8(2)	Ru1B-Ru2B-N2B	120.1(2)		
Ru2B-Ru1B-C34B	44.5(3)	Ru1B-Ru2B-C34B	44.3(2)		
N3B-Ru1B-N4B	69.2(2)	N3B-Ru2B-N4B	69.6(3)		
C35B-Ru1B-C36B	84.2(4)	C37B-Ru2B-C38B	84.2(4)		
N1B-Ru1B-C34B	164.1(3)	N2B-Ru2B-C34B	163.2(3)		
Ru2B-Ru1B-N3B	50.2(2)	Ru1B-Ru2B-N3B	47.7(2)		
Ru1B-C34B-O1B	134.5(7)	Ru2B-C34B-O1B	134.3(7)		
Ru1B-C35B-O2B	175.5(8)	Ru2B-C37B-O4B	174.2(8)		
Ru1B-C36B-O3B	176.4(8)	Ru2B-C38B-O5B	175.5(9)		
Ru1B-C34B-Ru2B	91.1(4)				

2.1.5 CO release properties of ruthenium based complexes and comparison with CORM-S1

The complexes $[\text{Ru}(\text{CO})_2(\text{H}_2\text{NC}_2\text{H}_4\text{S})_2]$ (**1**) and $[\text{Ru}(\text{CO})_2(\text{H}_2\text{NC}_6\text{H}_4\text{S})_2]$ (**2**) were examined with respect to CO release as photo-CORMs during irradiation with visible light in a myoglobin-based spectrophotometric assay [7] in a buffered solution. Even at a concentration of 200 μM no CO liberation was observed upon irradiation. In contrast, the iron complex CORM-S1 demonstrates

attractive properties releasing 2 mol equivalents of CO under the same conditions and only 50 μM of CORM-S1 upon irradiation was sufficient to almost fully convert 100 μM deoxymyoglobin [33, 41]. These experiments confirm the high stability of the ruthenium complexes even when irradiated with visible light ($\lambda > 400$ nm). Thus, ruthenium carbonyl complexes (in comparison to the iron analogous) are systems often more air stable and less labile. This can be attributed to the fact that the metal-centered electronic transitions move to higher energies on going from Fe to Ru. It is thus necessary to maintain more drastic reaction conditions for the liberation of CO. Sellmann *et. al* [42] showed that irradiation of **2** with a mercury lamp in the presence of triphenylphosphane only liberates one CO molecule. However, the use of UV light from a mercury source for the activation of metal complexes in biological system is limited because of its photo-toxicity, which damages cells and tissues. Additionally, these are other complexes know based on iron being photolabile [37, 49, 50]. Figure 11 shows the myoglobin assay for the complexes **1** and **2**. In the case of the dinuclear ruthenium complex **3** which has five CO, it was also not possible to observed light-induced loss of CO. The complexes $[\text{Ru}_2(\text{CO})_5(\text{R-DAB})]$ and $[\text{Ru}_2(\text{CO})_5(\text{R-APE})]$ (R= *i*-Pr, *t*-Bu and *c*-Hex) undergo changes due to thermal decomposition. Thus, refluxing in *n*-heptane for about 8h results in a net loss of a CO molecule and the selective rupture of a carbon-carbon bond [47]. However, these reaction conditions, which are very different from the typical biological environment, have limited applicability because it usually requires the use of temperatures well above 37 °C and organic solvents.

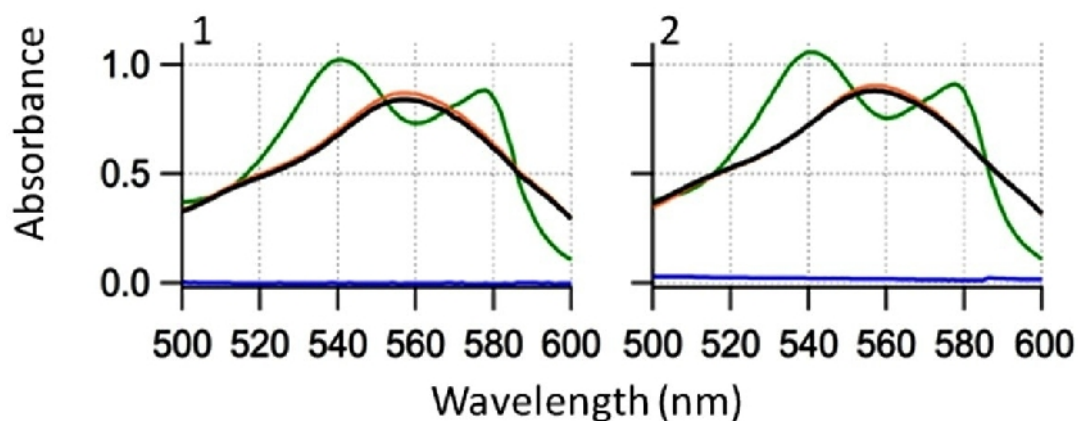


Figure 11: Absorption spectra for complexes **1** and **2** in a myoglobin assay. (Spectrum without myoglobin (blau), myoglobin alone (red), myoglobin with the compounds after irradiation (black) and myoglobin saturated with CO (green)).

2.2 Manganese-based carbonyl complexes

In this section three different synthesis methods were employed for obtaining manganese carbonyl complexes. The reactions yielded dinuclear or tetranuclear products of Mn(I) with a high amount of CO ligands and the CO release during irradiation with visible light occurred in some cases. In subsection 2.2.1 redox reactions between $[\text{Mn}_2(\text{CO})_{10}]$ and diaryl disulfides by photoreaction are described. In 2.2.2 the products are obtained via metathesis reactions using $[\text{BrMn}(\text{CO})_5]$ and potassium thiophenolates, here it was necessary to synthesize the salts. As third synthesis method in subsection 2.2.3 the substitution reactions between $[\text{BrMn}(\text{CO})_5]$ and aryl thiols are presented.

2.2.1 Oxidation of $[\text{Mn}_2(\text{CO})_{10}]$ by organic disulfides

Four manganese carbonyl complexes of the general formula $[\text{Mn}(\text{CO})_4(\mu\text{-SC}_6\text{H}_4\text{-4-R})_2]$ (**4-7**). R= -H, -CH₃, -OMe, -Cl were synthesized by irradiation of a mixture of $[\text{Mn}_2(\text{CO})_{10}]$ and the corresponding diaryl disulfide in heptane (mixture of isomers) at room temperature (see figure 12). A LED of the type NSCU033AT Nichia with a wavelength of 365 nm was used.

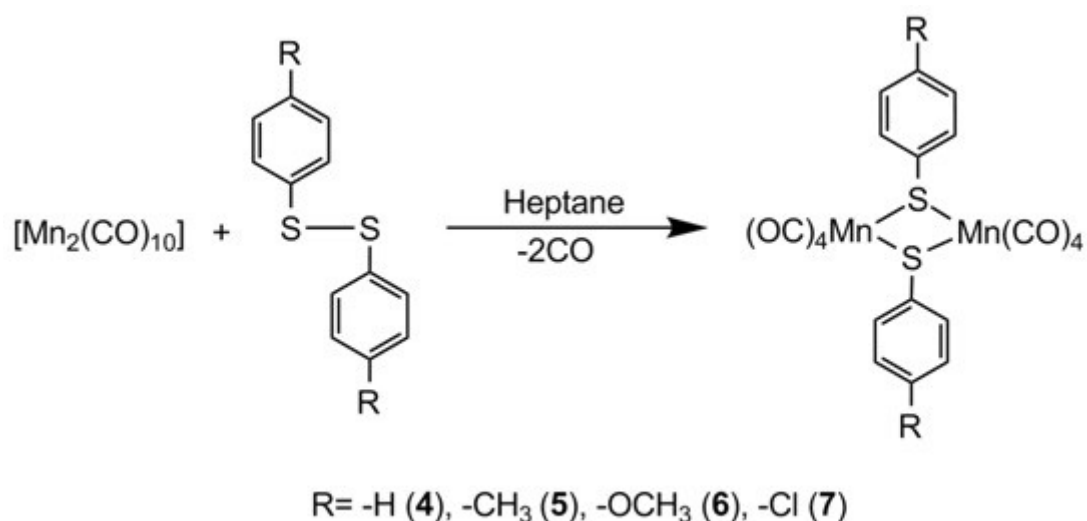


Figure: 12 Synthesis of manganese carbonyl complexes $[\text{Mn}(\text{CO})_4(\mu\text{-SC}_6\text{H}_4\text{-4-R})_2]$ (**4-7**).

2.2.1.1 Synthesis and characterization of $[\text{Mn}(\text{CO})_4(\mu\text{-SC}_6\text{H}_4\text{-4-R})_2]$

The synthesis method was first proposed by Kang-Wook Lee and Theodoro L. Brow in 1987, it involved the photochemical reactions of $[\text{M}_2(\text{CO})_{10}]$ (M=Mn, Re) and RSSR (R= Me, Ph) in *n*-hexane at ambient temperature yielding a mixture of the dinuclear product $[\text{M}_2(\mu\text{-SR})_2(\text{CO})_8]$ and the tetranuclear product $[\text{M}(\text{CO})_3(\mu\text{-SR})]_4$ [51]. This synthetic route is well known from the literature and suggests the cleavage of the Mn-Mn bond in $[\text{Mn}_2(\text{CO})_{10}]$ [52] as well as the

photo-dissociation of the aromatic disulphide [53]. During formation of these products, manganese is oxidized to Mn(I) with the subsequent release of two CO molecules.

The reaction of diphenyl disulfide with $[\text{Mn}_2(\text{CO})_{10}]$ in the molar ratio of 1:6 under irradiation in heptane at room temperature leads to product mixtures containing the dinuclear manganese(I) complex $[\text{Mn}(\text{CO})_4(\mu\text{-SC}_6\text{H}_5)]_2$ (**4**) as the major component. The compound was previously generated by photoreaction [51] and was recently synthesized by hydrogenation of $[(1\text{-phenyl-2,5-dimethylthiophene})\text{Mn}(\text{CO})_3]$ and characterized crystallographically [54].

The IR spectrum of the crude product of the reaction showed six absorption bands for ν_{CO} stretching vibration at 2072, 2013, 1996, 1981, 1945, 1934 cm^{-1} whereas four bands were expected for complex **4**. Therefore, it can be assumed that a mixture of the dinuclear and tetranuclear complexes was isolated. These results are consistent with those reported by Lee and Brown in 1987 [51] and Choi *et al.* in 1999 [54]. Moreover, the spectrum corroborate that a low amount of tetranuclear complex was formed, as the cited authors state.

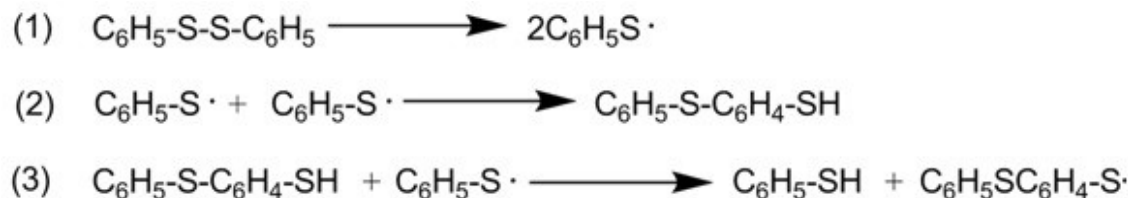
A pure crop of **4** was isolated from the mother liquor after concentration in vacuum. In the ^1H NMR spectrum for the pure complex **4** the corresponding proton signals are observed at 7.23, 7.31 and 7.63 ppm which reflects the three chemically distinct environments for phenyl protons in the molecule. The ^{13}C NMR spectrum showed the carbonyl resonances at 213.4 and 214.8 ppm. The

electron ionization (EI) mass spectrum of **4** shows a signal at m/z (%) = 552 (10) which can be attributed to the molecular ion. Signals of dinuclear fragments are observed at 468 (10) $[M - 3CO]^+$, 440 (30) $[M - 4CO]^+$, 412 (25) $[M - 5CO]^+$, 356 (5) $[M - 7CO]^+$, while the most intense signal was detected at $m/z = 328$ (100) unambiguously assigned to the complex cation without CO ligands $[M - 8CO]^+$. The IR spectrum of **4** showed the absorption bands at 2072, 1996, 1981 and 1945 cm^{-1} .

The photoreaction of $[Mn_2(CO)_{10}]$ with bis(4-methylphenyl) disulfide results in a very unstable pale yellow solid, which could not be identified and an orange solution. The solution in heptane was stored at -20°C and orange crystals were obtained consisting of a mixture of products. The dominant product is the dinuclear manganese(I) complex $[Mn(CO)_4(\mu\text{-}SC_6H_4\text{-}4\text{-}Me)]_2$ (**5**). Recently, the complex was obtained via reaction of the electrophilic complex $[(CO)_3Mn(\mu^5\text{-}T)]$ (T= thiophene or 2,5-dimethylthiophene) with the nucleophilic thiolate $^-(SC_6H_4\text{-}4\text{-}Me)$ [55].

As secondary products dinuclear $[Mn(CO)_3(SC_6H_3Me\text{-}o\text{-}SC_6H_4Me)]_2$ (**8**) and tetranuclear $[Mn(CO)_3(\mu\text{-}SC_6H_4\text{-}4\text{-}Me)]_4$ (**9**) were observed. The newly formed ligand observed in compound **8** was isolated earlier in form of its molybdenum, iron and ruthenium complexes. The corresponding disulfide was synthesized by Killops *et al.* [56] in 1978 via irradiation of a solution of $(MeC_6H_3\text{-}S)_2$ in toluene with UV-light. The mechanism of formation of the closely related phenyl derivative was investigated by Schaafsma *et al.* [53] and a radical chain

mechanism was proposed (scheme 1). A similar mechanism has to be assumed in case of the formation of complex **8**.



Scheme 1: Suggested mechanism for the formation of the radical $\text{C}_6\text{H}_5\text{-o-S-C}_6\text{H}_4\text{-S}\cdot$ [53].

The complexes **5** and **9** were characterized as a mixture by IR, ^1H NMR and ^{13}C NMR spectroscopy. Crystals of **5** suitable for X-Ray crystallography were obtained by cooling a saturated solution of the product mixture in *n*-hexane from ambient temperature to 6°C . In case of compound **8**, the characterization was effected by X-Ray crystallographic analysis. The IR spectrum of the product mixture exhibits six characteristic strong bands in the typical region for CO stretching frequencies at 2075, 2008, 1992, 1982, 1959, 1928 cm^{-1} . The observed number of signals is consistent with a mixture of **5** and **9**, since for the dinuclear compound **5** four signals are expected while the presence of tetranuclear **9** should result in two additional signals. Compound **8** is only present in trace amounts and the IR vibrations of its carbonyl ligands were not observed, possibly due to overlapping with the signals of **5** and **9**.

The ^1H NMR spectrum of the mixture was rather complicated due to the presence of the three compounds **5**, **8** and **9**. For instance, four different signals for the methyl groups were found between 2.28-2.39 ppm as expected. However, only the most intense signal which was observed at 2.30 ppm, can be doubtlessly

assigned to the main product **5**. In the aromatic region of the spectrum, each tolyl group of the complexes **5** and **9** gave rise to the typical pattern of an AA'BB' spin system of a 1,4-substituted benzene derivative. In case of the dinuclear complex **5** the AA' and BB' part are observed at 7.14 and 7.52 ppm, respectively. In the ^{13}C NMR spectrum, the two different CO ligands of **5** are responsible for two signals at 213.6 and 215 ppm.

In order to confirm the above given assignment, the measurements were repeated with pure complex **5** which can be obtained as an orange powder by reduction of the volume of the mother liquor to dryness in vacuo and subsequent washing of the residue with *n*-hexane. The IR spectrum of pure **5** exhibits four characteristic bands in the region for CO stretching frequencies at 2077, 1991, 1957 and 1940 cm^{-1} . The EI mass spectrum shows a signal at m/z (%) = 580 (5) which can be attributed to the molecular ion of **5** $[\text{M} - 2\text{H}]^+$. Furthermore, it is possible to observe important fragments due to the loss of CO such as 523 (10) $[\text{M} - 2\text{H} - 2\text{CO}]^+$, 496 (5) $[\text{M} - 2\text{H} - 3\text{CO}]^+$, 468 (20) $[\text{M} - 2\text{H} - 4\text{CO}]^+$, 440 (10) $[\text{M} - 2\text{H} - 5\text{CO}]^+$ and 356 (100) $[\text{M} - 2\text{H} - 8\text{CO}]^+$. The signals for complexes **8** and **9** will be assigned in the succeeding subsection.

The photoreactions of dimanganese decacarbonyl with bis(4-methoxyphenyl) disulfide and bis(4-chlorophenyl) disulfide, respectively, produced the corresponding dinuclear complexes $[\text{Mn}(\text{CO})_4(\mu\text{-SC}_6\text{H}_4\text{-4-OMe})_2]$ (**6**) and $[\text{Mn}(\text{CO})_4(\mu\text{-SC}_6\text{H}_4\text{-4-Cl})_2]$ (**7**). The crystals of both complexes were grown in the reaction filtrate at 6°C. Bis(4-chlorophenyl) disulfide was prepared by air oxidation of 4-chlorothiophenol under sonication [57], the yield is high with

about 92%, the reaction straight forward and fast (less than 30 minutes) and gave an analytically pure product. The complexes **6** and **7** were characterized by IR, ^1H NMR and ^{13}C NMR spectroscopy, mass spectrometry, X-Ray crystallographic studies and elemental analysis.

The IR spectrum of **6** exhibits only three bands between 2100 and 1900 cm^{-1} which can be attributed to the stretching vibrations of the carbonyl ligands. However, the rather broad band at 1942 cm^{-1} might be the result of two overlapping signals. In contrast, for complex **7** four signals are clearly identified at 2083 , 1991 , 1955 and 1917 cm^{-1} as expected for four terminal carbonyl ligands. The ^1H -NMR spectra of both complexes showed the AA' and BB' part are for the aromatic ring protons at 6.89 and 7.55 ppm for **6**, as well as 7.36 and 7.60 ppm for **7** (see figure 13). Both ^{13}C -NMR spectra show the carbonyl resonances of the CO ligands in the region between 212 and 215 ppm characteristic of these dinuclear structures. In the EI mass spectrum, the molecular ion peaks do not show up clearly for both complexes. The fragmentation of the molecular ion occurs first by successive lost of the eight carbonyls. However, fragments were observed given the loss of CO in the case of **6** at m/z (%) = 500 (10) $[\text{M} - 4\text{CO}]^+$, 472 (5) $[\text{M} - 5\text{CO}]^+$ and 390 (50) $[\text{M} - 8\text{CO}]^+$. For **7** they were detected at m/z = 536 (5) $[\text{M} - 3\text{CO}]^+$, 508 (20) $[\text{M} - 4\text{CO}]^+$, 480 (15) $[\text{M} - 5\text{CO}]^+$, and 396 (100) $[\text{M} - 8\text{CO}]^+$.

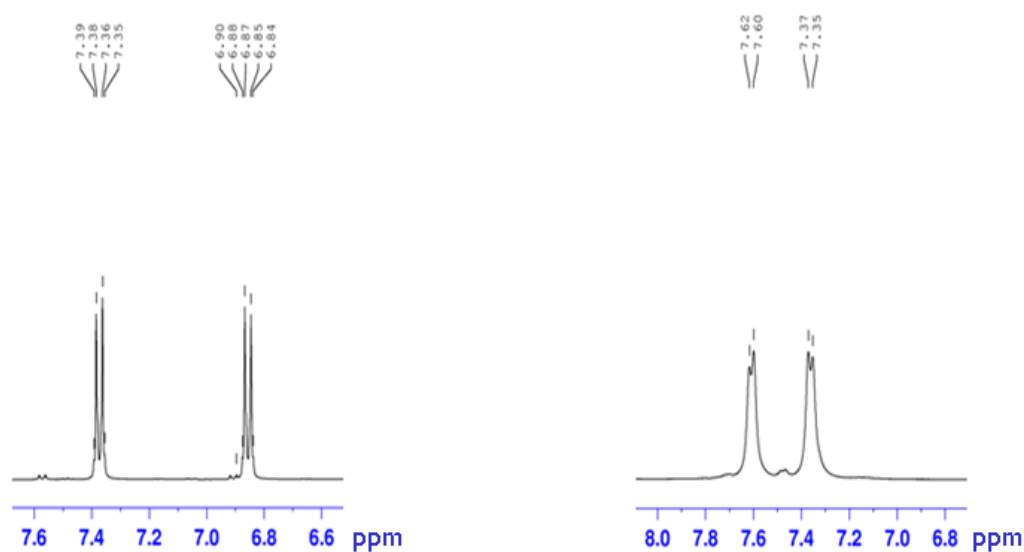


Figure 13: ^1H NMR spectra in $[\text{D}_8]\text{THF}$, 400 MHz shown the AA'BB' spin system for the aromatic ring protons. Left: Complex $[\text{Mn}(\text{CO})_4(\mu\text{-SC}_6\text{H}_4\text{-4-OMe})_2]$ (**6**). Right: Complex $[\text{Mn}(\text{CO})_4(\mu\text{-SC}_6\text{H}_4\text{-4-Cl})_2]$ (**7**).

2.2.1.2 Molecular structures of $[\text{Mn}(\text{CO})_4(\mu\text{-SC}_6\text{H}_5)_2]$ (**4**), $[\text{Mn}(\text{CO})_4(\mu\text{-SC}_6\text{H}_4\text{-4-CH}_3)_2]$ (**5**) $[\text{Mn}(\text{CO})_4(\mu\text{-SC}_6\text{H}_4\text{-4-OMe})_2]$ (**6**), $[\text{Mn}(\text{CO})_4(\mu\text{-SC}_6\text{H}_4\text{-4-Cl})_2]$ (**7**) and $[\text{Mn}(\text{CO})_3(\text{SC}_6\text{H}_3\text{Me-o-SC}_6\text{H}_4\text{Me})_2]$ (**8**)

$[\text{Mn}(\text{CO})_4(\mu\text{-SC}_6\text{H}_5)_2]$ (**4**)

It was reported earlier that the dinuclear complex $\text{Mn}(\text{CO})_4(\mu\text{-SC}_6\text{H}_5)_2$ (**4**) can be isolated in crystalline form from solutions of *n*-hexane. Under these conditions, the compound crystallizes in the triclinic space group $P\bar{1}$ [54]. Another modification of this complex was obtained from heptane (mixture of isomers). Although the same space group $P\bar{1}$ was identified for these crystals, the observed cell parameters (a 7.6194(15), b 17.821(4) and c 18.031(4) Å, α 61.35(3), β 89.77(3) and γ 78.61(3)°) differ significantly from the values

reported by Choi *et al.* [54] (a 7.735(14) b 9.2820(7), c 15.552(2) Å, α 90.709 (8), β 96.634(13) γ 101.727(11)°). Unfortunately, the crystal quality was rather low and a sub-standard dataset was obtained for the new modification. Therefore only a structural motif of **4** was established from the data showing the connectivities between the atoms (see figure 14) but prohibiting detailed discussion of bond lengths and angles.

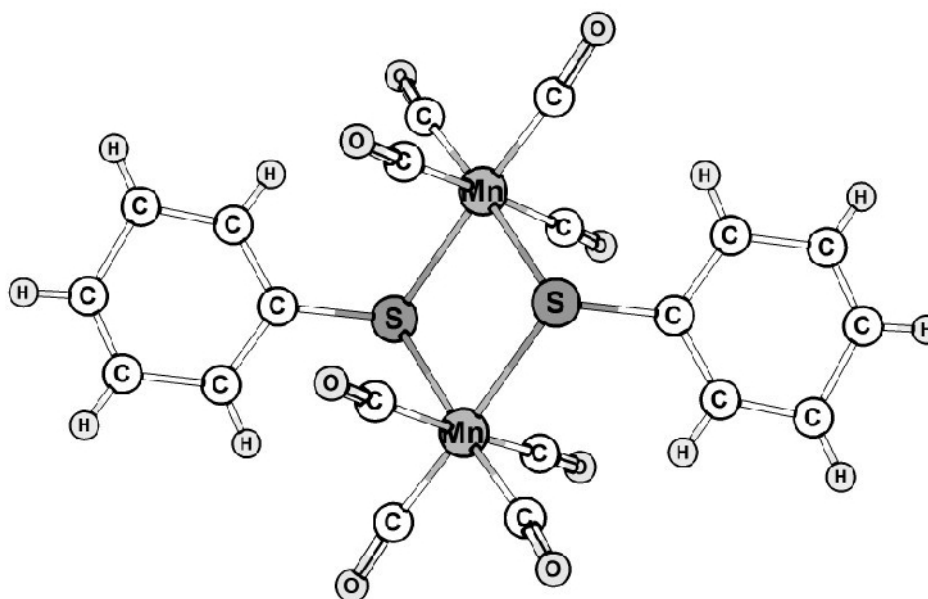


Figure 14: Representation of the structural motif of $[\text{Mn}(\text{CO})_4(\mu\text{-SC}_6\text{H}_5)]_2$ (**4**).

$[\text{Mn}(\text{CO})_4(\mu\text{-SC}_6\text{H}_4\text{-4CH}_3)]_2$ (**5**)

The structure of $[\text{Mn}(\text{CO})_4(\mu\text{-SC}_6\text{H}_4\text{-4CH}_3)]_2$ (**5**) has been published by Chen *et al.* [55]. The monoclinic space group $P2_1/c$ was determined for the orange-yellow crystals obtained from a mixture of hexanes and dichloromethane. However, in this work a second modification of **5** was isolated from *n*-hexane which is discussed below. Under the applied conditions, the dinuclear manganese complex $[\text{Mn}(\text{CO})_4(\mu\text{-SC}_6\text{H}_4\text{-4-CH}_3)]_2$ (**5**) crystallizes in the triclinic space group $P\bar{1}$. The molecular structure and labeling scheme of **5** is depicted in

figure 15. Selected bond distances and angles are summarized in table 6. The core of the compound is formed by two manganese atoms which are bridged by two thiophenolate ligands resulting in a planar Mn_2S_2 core similar to the one observed in the complex $[Mn(CO)_4(\mu-SC_6H_5)]_2$ (**4**). Each Mn atom is octahedrally coordinated by four terminal carbonyl ligands and two 4-methylthiophenolate bridges.

The average Mn-S bond distance of 2.393 Å is slightly shorter than the one observed by Chen *et al.*. The intramolecular Mn...Mn separation is 3.623 Å. The bond lengths Mn1-C16 (1.868 Å), Mn1-C18 (1.874 Å), Mn2-C19 (1.872 Å) and Mn2-C21 (1.874 Å) to the carbonyl ligands which are located in *trans* position to each other are longer than the average Mn-CO distance of 1.822 Å, observed for ligands *trans* to the thiolate anions. In addition, **5** showed rather acute angles S1-Mn1-S2 (81.1°) and S1-Mn2-S2 (80.8°) while the angles Mn1-S1-Mn2 (98.9°) and Mn1-S2-Mn2 (97.9°) are more obtuse. In the other modification, the average S-Mn-S and Mn-S-Mn angles are 82.3 and 97.5°, respectively [55]. The *trans* angles range between 171.5 and 176°, indicating a slight distortion of the ideal octahedral geometry, and are comparable to literature values (171.8 – 176.8°) [55].

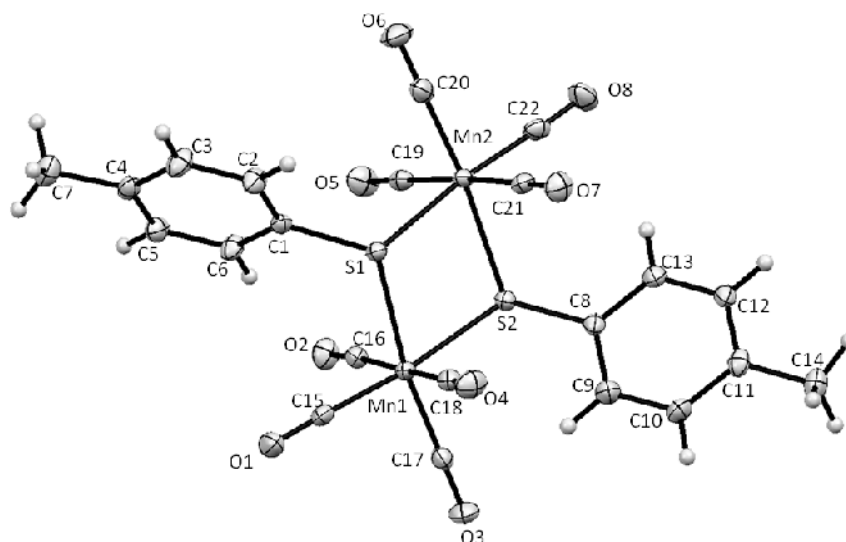


Figure 15: Molecular structure of $[\text{Mn}(\text{CO})_4(\mu\text{-SC}_6\text{H}_4\text{-4-CH}_3)]_2$ (**5**). Thermal ellipsoids of non-hydrogen atoms are drawn at the 50% probability level.

Table 6. Selected bond lengths and angles for $[\text{Mn}(\text{CO})_4(\mu\text{-SC}_6\text{H}_4\text{-4-CH}_3)]_2$ (**5**)

Bond lengths [Å]		Angles [°]	
Mn1-S1	2.385(8)	S1-Mn1-S2	81.12(3)
Mn1-S2	2.394(9)	Mn1-S2-Mn2	97.86(3)
Mn2-S1	2.382(9)	S1-Mn2-S2	80.80(3)
Mn2-S2	2.412(9)	Mn2-S1-Mn1	98.93(3)
Mn1-C18	1.874(3)	S1-Mn1-C16	96.76(10)
Mn1-C16	1.868(3)	C15-Mn1-C16	89.04(14)
Mn1-C15	1.817(3)	C15-Mn1-C17	92.28(14)
Mn1-C17	1.827(3)	C17-Mn1-C18	94.96(14)
Mn2-C19	1.872(3)	S2-Mn1-C18	95.33(10)
Mn2-C21	1.874(3)	S1-Mn2-C19	90.47(10)
Mn2-C20	1.820(3)	C19-Mn2-C20	90.59(14)
Mn2-C22	1.823(4)	C20-Mn2-C22	91.62(15)
C15-O1	1.139(4)	C21-Mn2-C22	90.56(14)
C16-O2	1.129(4)	S2-Mn1-C15	173.28(10)
C17-O3	1.138(4)	S1-Mn1-C17	171.49(10)
C18-O4	1.134(4)	C16-Mn1-C18	176.03(14)
C19-O5	1.133(4)	C19-Mn2-C21	175.54(14)
C20-O6	1.142(4)	S2-Mn2-C20	173.74(11)
C21-O7	1.134(4)	S1-Mn2-C22	173.94(10)
C22-O8	1.141(4)		

[Mn(CO)₄(μ-SC₆H₄-4-OMe)]₂ (6)

The complex [Mn(CO)₄(SC₆H₄-*p*-OMe)]₂ (**6**) crystallizes in the monoclinic space group *P*2₁/*c*. The figure 16 illustrates the view and labels of the complex. Pertinent bond lengths and bond angles are listed in table 7. The central manganese ion is surrounded by four terminal carbonyl groups and the bridging S atoms of the two thiophenolate ligands. Two of the CO ligands are *trans* positioned to each other, while the other two are in *trans* position to the sulfur atoms. The geometric center of the molecule presents a crystallographic inversion center. Consequently, the Mn₂S₂ core is strictly planar and the methoxyphenyl groups attached to the μ-S atoms adopt *anti* positions. These observations are also valid for the manganese compounds [Mn(CO)₄(μ-SC₆H₅)]₂ [54], [Mn(CO)₄(μ-SC₆H₄-4-Me)]₂ [55] and complex **5** as well as for the complexes [Re₂(μ-SR)₂(CO)₈] (R = methoxyphenyl) [58]; (R = CS₂Re(CO)₄) [59].

The intramolecular Mn···Mn separation in the dinuclear complex is 3.616 Å. The two Mn-S bond lengths of 2.388 and 2.400 Å differ slightly and they are comparable to those of 2.389 and 2.400 Å found in the complex [Mn(CO)₄(μ-SC₆H₅)]₂ [54]. Very much alike the other modification of the complex [Mn(CO)₄(μ-SC₆H₄-4-Me)]₂ exhibits Mn-S bond lengths of 2.381 and 2.416 Å [55]. All bond lengths Mn-C to carbonyl ligands of **6** with another carbonyl ligand in *trans* position are significantly longer (average 1.870 Å) than the other, with the carbonyl ligand *trans* positioned to the thiolate (average 1.822 Å). The enclosed ring angles of **6** are Mn-S-Mn (98.08°) and S-Mn-S (81.92°). The *trans*

angles vary from 171.91 to 174.32° indicating a slight distortion from the octahedral geometry.

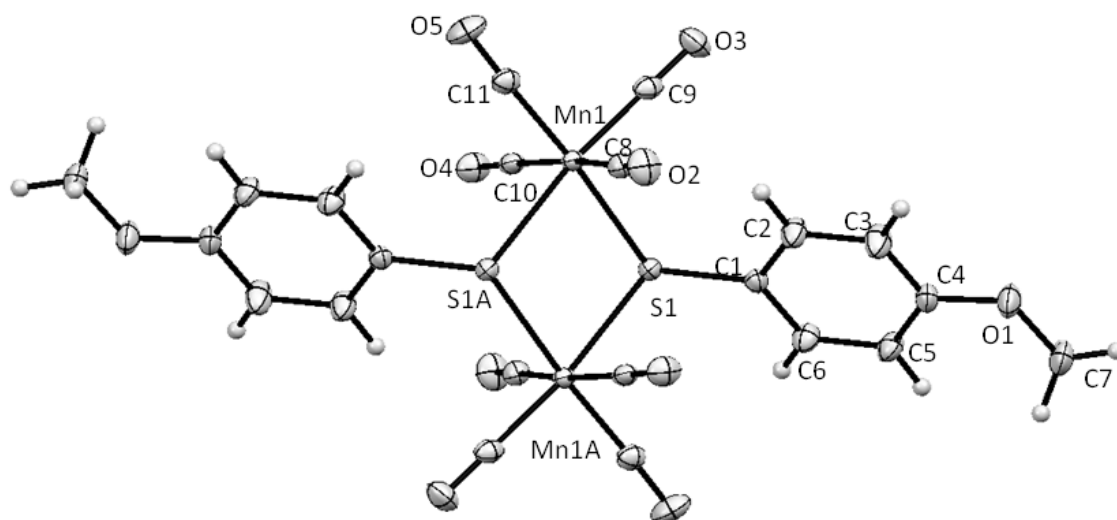


Figure 16: Molecular Structure of $[\text{Mn}(\text{CO})_4(\text{SC}_6\text{H}_4\text{-4-OMe})]_2$ (**6**). Thermal ellipsoids of non-hydrogen atoms are drawn at 50% probability level.

Table 7. Selected bond lengths and angles of $[\text{Mn}(\text{CO})_4(\text{SC}_6\text{H}_4\text{-4-OMe})]_2$ (**6**)

Bond lengths [Å]		Angles [°]	
Mn1-S1	2.388(1)	S1-Mn1-C8	87.36(5)
Mn1-S1A	2.400(1)	S1-Mn1-C9	95.65(6)
Mn1-C8	1.872(2)	S1-Mn1-C10	85.02(6)
Mn1-C9	1.817(2)	S1-Mn1-C11	172.55(6)
Mn1-C10	1.870(2)	S1-Mn1-S1A	81.92(17)
Mn1-C11	1.826(2)	Mn-S-Mn1A	98.08(17)
C8-O2	1.129(2)	C8-Mn1-C9	91.17(8)
C9-O3	1.140(2)	C8-Mn1-C10	171.91(8)
C10-O4	1.134(2)	C8-Mn1-C11	93.09(8)
C11-O5	1.140(2)	C8-Mn1-S1A	83.60(5)
		C9-Mn1-C10	86.87(8)
		C9-Mn1-C11	91.77(8)
		C9-Mn1-S1A	174.32(6)
		C10-Mn1-C11	94.82(8)
		C10-Mn1-S1A	97.99(6)
		C11-Mn1-S1A	90.74(6)

[Mn(CO)₄(SC₆H₄-4-Cl)]₂ (7**)**

The dinuclear manganese complex [Mn(CO)₄(SC₆H₄-4-Cl)]₂ (**7**) crystallizes in the triclinic space group $P\bar{1}$. The molecular structure and the labeling scheme of complex **7** are shown in figure 17. Selected bond lengths and angles are listed in table 8. Figure 17 shown that the molecule exhibit a planar Mn₂S₂ core. Each Mn atom is octahedrally coordinated by four terminal carbonyl ligands and two 4-chlorothiophenolate bridges.

The intramolecular Mn···Mn separation was found to be about 3.620 Å. Comparing **7** with the analogue [Mn(CO)₄(SC₆H₄-*p*-OMe)]₂ **6**, it can be found that the values of Mn-S are slightly elongated (2.392 and 2.410 Å) while in **6** these bond lengths are 2.388 and 2.400 Å. The Mn-C bond lengths depend on the ligand in *trans* position; in case of a *trans* positioned CO longer Mn-C bonds (Mn1-C7 1.870 Å; Mn1-C10 1.876 Å) were observed, whereas Mn-C distances *trans* to a thiolate are clearly shorter (Mn1-C8 1.820 Å; Mn1-C9 1.814 Å). This shortening is caused by the stronger backbonding to the carbonyl ligands which are in *trans* position to the sulfur atoms. The same effect has been observed in the molecular structures of **5**, **6** and in the similar dinuclear sulfido-bridged manganese(I) complexes [54]. The Mn-S-Mn angles in the Mn₂S₂ core are relatively obtuse (97.78° for **7**; 98.08° for **6**), compared with the S-Mn-S angles of 82.219 and 81.916°, respectively. These trends are also observed for the above mentioned manganese compounds [Mn(CO)₄(μ-SC₆H₅)]₂ and [Mn(CO)₄(μ-SC₆H₄-4-Me)]₂. Besides, the related dinuclear iron complexes [Fe(CO)₃(SC₆H₄-4-R)]₂ R= Cl, OMe have been structurally characterized,

showing the formation of a butterfly-type four-membered ring FeS₂Fe with a Fe-Fe bond and six terminal carbonyl ligands. [60]

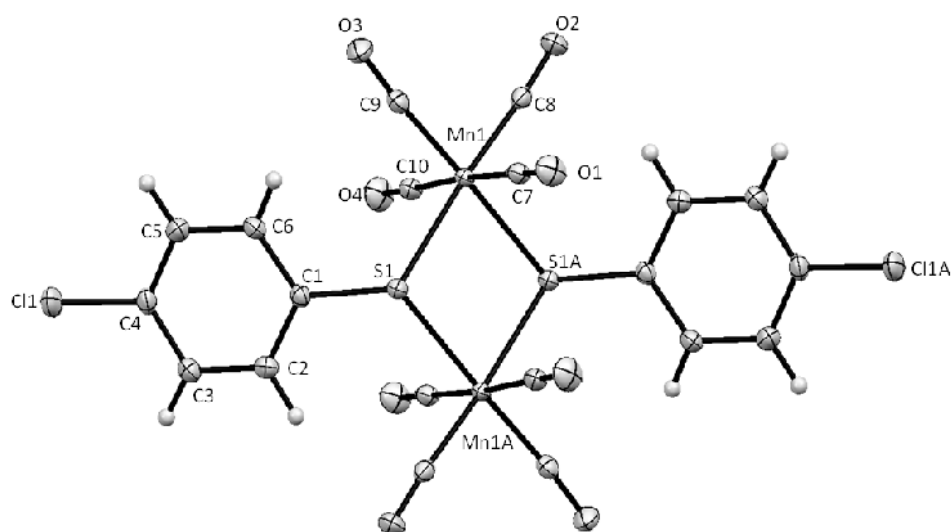


Figure 17: Molecular structure of [Mn(CO)₄(SC₆H₄-4-Cl)]₂ (7) Thermal ellipsoids of non-hydrogen atoms are drawn at 50% probability level.

Table 8. Selected bond lengths and angles of [Mn(CO)₄(SC₆H₄-4-Cl)]₂ (7)

bond lengths [Å]		Angles [°]	
Mn1-S1	2.392(1)	S1-Mn1-C7	86.74(5)
Mn1-S1	2.410(1)	S1-Mn1-C8	178.04(5)
Mn1-C7	1.870(2)	S1-Mn1-C9	94.40(5)
Mn1-C8	1.820(2)	S1-Mn1-C10	90.66(5)
Mn1-C9	1.814(2)	S1-Mn1-S1A	82.22(2)
Mn1-C10	1.876(2)	C7-Mn1-C8	91.98(8)
C7-O1	1.130(2)	C7-Mn1-C9	90.64(7)
C8-O2	1.143(2)	C7-Mn1-C10	175.99(7)
C9-O3	1.145(2)	C7-Mn1-S1	91.26(5)
C10-O4	1.131(2)	C8-Mn1-C9	87.10(7)
		C8-Mn1-C10	90.53(8)
		C8-Mn1-S1	96.33(5)
		C9-Mn1-C10	92.61(7)
		C9-Mn1-S1	176.02(5)
		C10-Mn1-S1	85.36(5)
		Mn1-S1-Mn1A	97.78(2)
		Mn1-C7-O1	178.13(15)
		Mn1-C8-O2	175.49(16)
		Mn1-C9-O3	176.00(15)
		Mn1-C10-O4	179.46(16)

[Mn(CO)₃(μ-SC₆H₃Me-*o*-SC₆H₄Me)]₂ (8**)**

The complex [Mn(CO)₃(SC₆H₃Me-*o*-SC₆H₄Me)]₂ (**8**) crystallizes in the monoclinic space group *C2/c*. The molecular structure as well as the labels of the complex are shown in figure 18. Selected bond lengths and angles for complex **8** are summarized in table 9. Two manganese atoms are coordinated by the sulfur atoms of the aryl thioether ligand and connected through sulfur bridges forming a planar Mn₂S₂ core. Moreover, each manganese atom is coordinated by three terminal carbonyl ligands. The manganese centers are placed in a distorted octahedral coordination environment.

Three coordination sites at each manganese atom are occupied by the sulfide bridges of the thioether ligand with bond lengths of Mn-S1 (2.362 Å) and Mn-S2 (2.325 Å) which differ slightly. These distances are shortened compared with those of 2.393, 2.394 and 2.400 Å found in the sulfide bridges of the complexes **5**, **6** and **7**, respectively. The non-bonding Mn···Mn separation 3.531 Å in **8** is shorter than in **5-7** (see table 6-8). All distances around the manganese centers are slightly shorter compared to those in the complexes **5**, **6** and **7**. Since each carbonyl ligand of **8** is located in *trans* position to a sulfur atom, the average distance between the metal center and the carbon atom of the carbon monoxide ligand of 1.814 Å is rather short due to enhanced back-donation of electron density from the metal center into the antibonding π*-orbitals of the carbonyl ligand. The endocyclic angles of the central Mn₂S₂ ring are Mn1-S1-Mn1A (94.86°) and S1-Mn1-S1A (85.14°). Within the five-membered ring formed by Mn1, S1, C1, C6 and S2 an angle S1-Mn-S2 of 80.8° was observed.

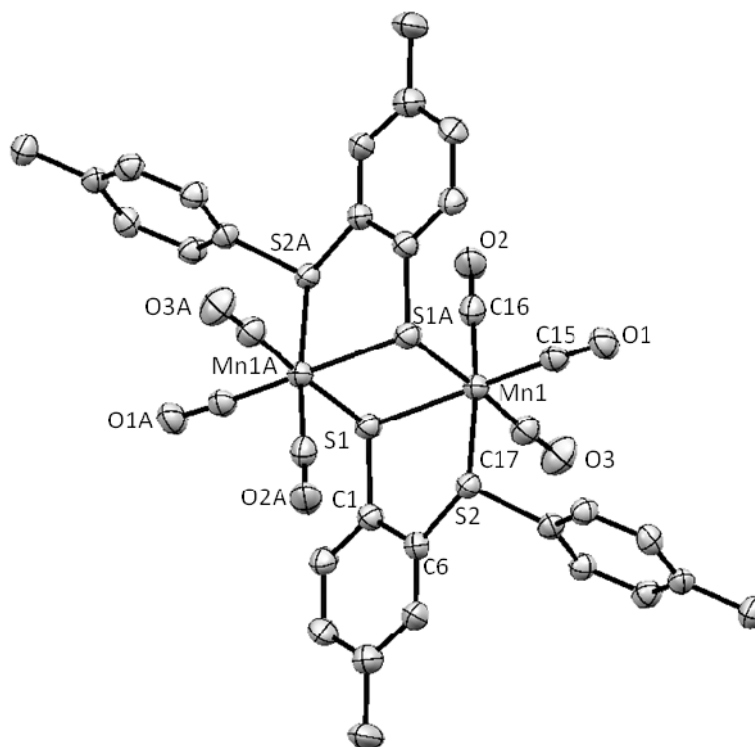


Figure 18: Molecular structure of $[\text{Mn}(\text{CO})_3(\text{SC}_6\text{H}_3\text{Me-}o\text{-SC}_6\text{H}_4\text{Me})]_2$ (**8**) Thermal ellipsoids of non-hydrogen atoms are drawn at 50% probability level.

Table 9. Selected bond lengths and angles of $[\text{Mn}(\text{CO})_3(\text{SC}_6\text{H}_3\text{Me-}o\text{-SC}_6\text{H}_4\text{Me})]_2$ (**8**)

bond lengths [\AA]		Angles [$^\circ$]	
Mn1-S1	2.362(2)	S1-Mn1-S2	83.32(5)
Mn1-S2	2.325(2)	S1-Mn1-C16	91.23(18)
Mn1-S1A	2.432(2)	S1-Mn1-S1A	85.14(5)
Mn1-C15	1.807(6)	S1-Mn1-C15	173.40(18)
Mn1-C16	1.824(6)	S1-Mn1-C17	93.60(2)
Mn1-C17	1.810(7)	S2-Mn1-C17	93.63(19)
C15-O1	1.143(7)	C15-Mn1-C17	91.44(3)
C16-O2	1.136(7)	C15-Mn1-C16	93.14(2)
C17-O3	1.141(7)	S2-Mn1-C15	92.10(17)
		S2-Mn1-C16	174.14(18)
		C17-Mn1-S1	176.88(19)
		S2-Mn1-S1A	83.39(5)
		C15-Mn1-S1A	89.62(18)
		C16-Mn1-C17	88.9(3)
		C16-Mn1-S1A	94.01(19)
		Mn1-S1-Mn1A	94.86(5)

2.2.1 Salt metathesis reactions of $[\text{BrMn}(\text{CO})_5]$ with potassium thiophenolates

In this section, complexes of the formula $[\text{Mn}(\text{CO})_4(\mu\text{-SR})]_n$ ($n = 2, 3$) and $[\text{Mn}(\text{CO})_3(\mu\text{-SR})]_n$ ($n = 4$) were synthesized and characterized, these complexes were a metathetical approach of obtained $[\text{BrMn}(\text{CO})_5]$ with potassium thiophenolates in a 1:1 ratio in THF at room temperature.

2.2.2.1 Synthesis and characterization of $[\text{Mn}(\text{CO})_4(\mu\text{-SR})]_n$ ($n=2, 3$) and $[\text{Mn}(\text{CO})_3(\mu\text{-SR})]_n$ ($n=4$)

Manganese carbonyl complexes with thiolate-bridged ligands have been intensively studied [51, 54, 55, 61-70]. Up to now oligonuclear carbonyl manganese thiolate complexes of the type $[\text{Mn}(\text{CO})_4(\mu\text{-SR})]_2$ and $[\text{Mn}(\text{CO})_3(\mu\text{-SR})]_4$ are known. Additionally, ionic complexes consisting of $[\text{Mn}_2(\text{CO})_6(\mu\text{-SR})_3]^-$ anions and cations like $[\text{Et}_4\text{N}]^+$ or $[\text{Bu}_4\text{N}]^+$ were structurally characterized [54, 55, 61, 62, 70-72]. The tetranuclear carbonyl complexes $[\text{Mn}(\text{CO})_3(\mu\text{-SR})]_4$ were originally formulated as trinuclear species. However, subsequent electron impact mass spectrometry [69, 73], IR studies [74-76] and X-Ray structure analyses [54, 61, 72,] demonstrated that the tetranuclear formulation is correct. Nonetheless, it must be noted that in this work the treatment of $[\text{BrMn}(\text{CO})_5]$ with potassium 2,4,6-trimethyl thiophenolate surprisingly yields a trinuclear complex. Therefore the formation of trinuclear or tetranuclear species may be subject to the nature of the substituent.

Potassium thiophenolates have been synthesized by metalation reactions between potassium bis-trimethylsilyl amide and thiols in toluene at room temperature (see figure 19), which yielded the corresponding products as fine white powders. The yields were high and ranged from 87% up to 97 %. Due to the fact that thiophenols are even more acidic than the corresponding phenols [77] they can easily be deprotonated by highly basic alkali metal amides. The subsequent reaction with $[\text{BrMn}(\text{CO})_5]$ in THF at ambient temperature leads to precipitation of sparingly soluble potassium bromide. Removal of KBr by filtration and of the solvent in a vacuo and subsequent recrystallization of the remaining residue in *n*-hexane gave the desired thiolate modified manganese carbonyl complexes. The initial product of the metathetic reaction, a mononuclear complex of the composition $[\text{Mn}(\text{CO})_5(\text{SR})]$, was not isolated, however, such species were detected in related reactions [66, 70]. Under the applied conditions, this primary product reacts with itself under release of CO to form higher aggregates depending on the substitution pattern of the benzene ring (see Figure 19).

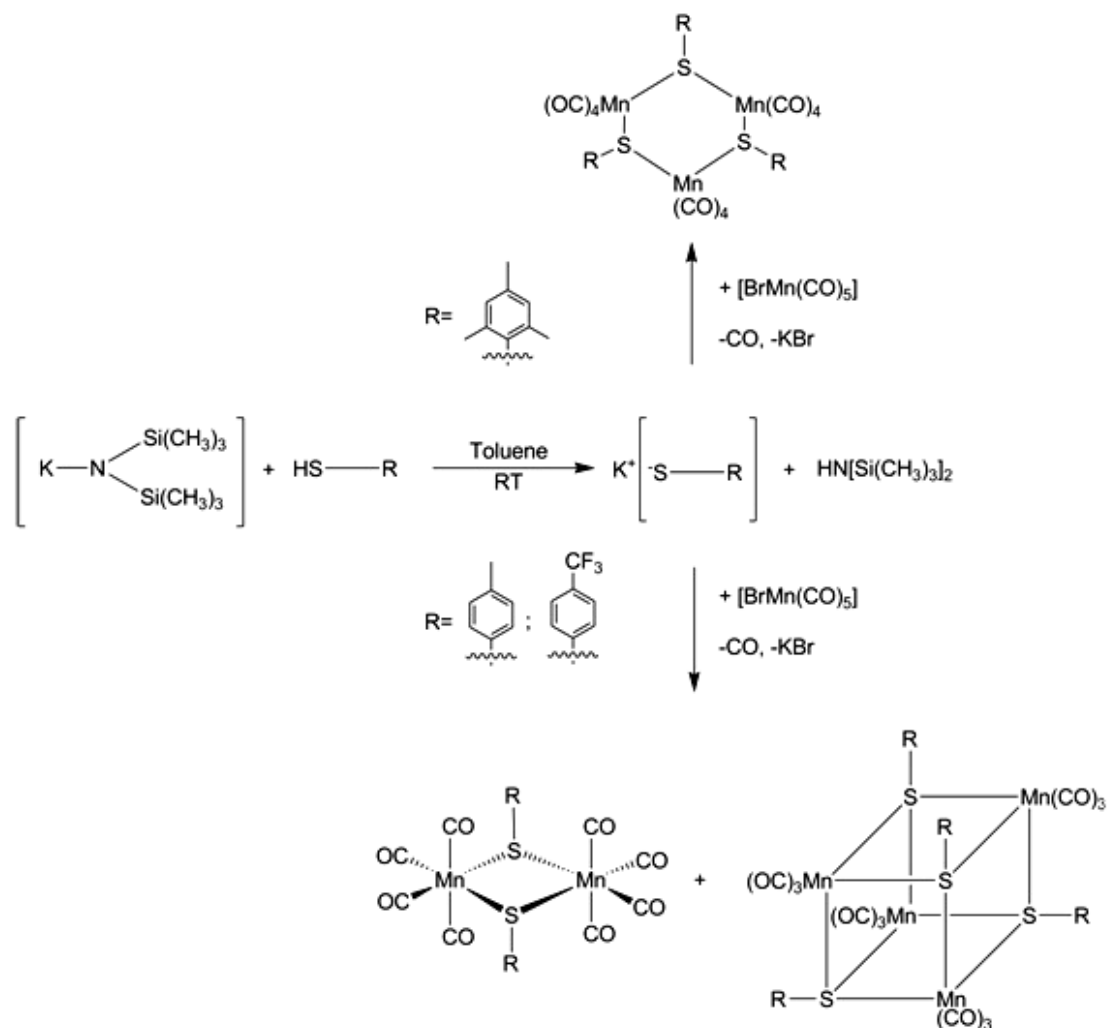


Figure 19: Synthesis of potassium thiophenolates starting from potassium bis(trimethylsilyl)amide and subsequent synthesis of manganese complexes.

The complexes $[\text{Mn}(\text{CO})_4\{\text{SC}_6\text{H}_2\text{-2,4,6-(CH}_3)_3\}]_3$ (**10**), $[\text{Mn}(\text{CO})_4(\mu\text{-SC}_6\text{H}_4\text{-4-CF}_3)_2]$ (**11**) and $[\text{Mn}(\text{CO})_3(\mu\text{-SC}_6\text{H}_4\text{-4-CF}_3)]_4$ (**12**) were synthesized and characterized. Besides, the complex $[\text{Mn}(\text{CO})_3(\mu\text{-SC}_6\text{H}_4\text{-4-CH}_3)]_4$ (**9**) which has been prepared in the previous section is structurally characterized, resolving the assignment of signals in ^1H NMR from the mixture of products previously observed. The crystal structure of **9** is presented.

The ^1H NMR spectra of potassium thiophenolates were measured in $[\text{D}_8]$ THF, the utilization of an ether has a coordinating effect on these systems, where the donor influence induces the formation of either polymeric or ionic species [78]. For the potassium 2,4,6-trimethyl thiophenolate, the protons of the two different methyl groups showed chemical shifts of 2.10 and 2.36 ppm while the aromatic ring protons are low-field-shifted and show resonances at 6.60 ppm. For the potassium 4-trifluoromethyl thiophenolate, the resonance of aromatic ring protons appear at 6.88 and 7.32 ppm while in the spectrum of potassium 4-methyl thiophenolate, the methyl signal was observed at 2.05 ppm and two resonances at 6.48 and 7.12 ppm were assigned to the aryl protons.

The syntheses of the di- and tetranuclear complexes $[\text{Mn}(\text{CO})_4(\mu\text{-SC}_6\text{H}_4\text{-4-CH}_3)]_2$ (**5**) and $[\text{Mn}(\text{CO})_3(\mu\text{-SC}_6\text{H}_4\text{-4-CH}_3)]_4$ (**9**) were performed using potassium 4-methyl thiophenolate as starting material. After recrystallization of the crude product mixture in *n*-hexane, a mixture of two distinct types of red crystals was observed. Both types were suitable for X-Ray crystallography. The first kind of crystals was identified as the dinuclear manganese complex $[\text{Mn}(\text{CO})_4(\mu\text{-SC}_6\text{H}_4\text{-4-CH}_3)]_2$ (**5**) by comparison of the lattice parameters determined earlier (see subsection 2.2.1.2). The other crystals contain both, $[\text{Mn}(\text{CO})_3(\mu\text{-SC}_6\text{H}_4\text{-4-CH}_3)]_4$ (**9**) and **5** in equimolar amounts.

The obtained mixture was further investigated by NMR techniques. The signals of **9** were unambiguously assigned as follows. In the ^1H NMR spectrum, a singlet was found at 2.38 ppm, which was assigned of the methyl group, and two signals at 7.37 and 8.02 ppm correspond to the resonances of the aromatic

protons. A comparison between the signals observed in this spectrum with those of the product mixture of the subsection 2.2.1.1 enables determination of the signals of $[\text{Mn}(\text{CO})_3(\text{SC}_6\text{H}_3\text{Me-}o\text{-SC}_6\text{H}_4\text{Me})]_2$ (**8**), showing chemical shifts of 2.32, 2.36, 7.29, 7.43 and 7.49 ppm.

The metathesis reaction of the potassium 2,4,6-trimethyl thiophenolate with $[\text{BrMn}(\text{CO})_5]$ in the molar ratio of 1:1 led to the formation of the trinuclear manganese complex $[\text{Mn}(\text{CO})_4\{\mu\text{-SC}_6\text{H}_2\text{-}2,4,6\text{-(CH}_3)_3\}]_3$ (**10**) with a yield of 30% as a red crystalline product. The complex was characterized by X-Ray structural analysis, IR, and ^1H NMR spectroscopy as well as mass spectrometry. The IR spectrum of complex **10** exhibits a well separated band at 2080 cm^{-1} as well as broad overlapping bands in the region between 2010 and 1900 cm^{-1} with maxima at 2001 , 1970 , 1952 , and 1922 cm^{-1} , which was attributed to the stretching vibrations of the carbonyl ligands. The ^1H NMR spectrum of **10** in $[\text{D}_8]\text{THF}$ exhibited more than the expected three signals for the 2,4,6 trimethyl thiophenolate ligand. Actually, at least three different sets A-C of signals were observed (see figure 20), showing that the solid state structure (see subsection 2.2.2.2) was not maintained in solution. Furthermore, some of the signals were rather broad indicating fluxional processes which might lead to complexes with varying nuclearity. In the ESI mass spectrum, no signal of the molecular ion $\mathbf{10}^+$ $[\text{M}^+]$ was observed. The most intense signal was detected at m/z (%) = 842 (100) and assigned to the trinuclear fragment $[\text{M} - 4\text{CO}]^+$. In contrast, EI mass spectra of **10** showed exclusively an intense signal at $m/z = 152$ due to the free ligand $[\text{SC}_9\text{H}_{11}]^+$.

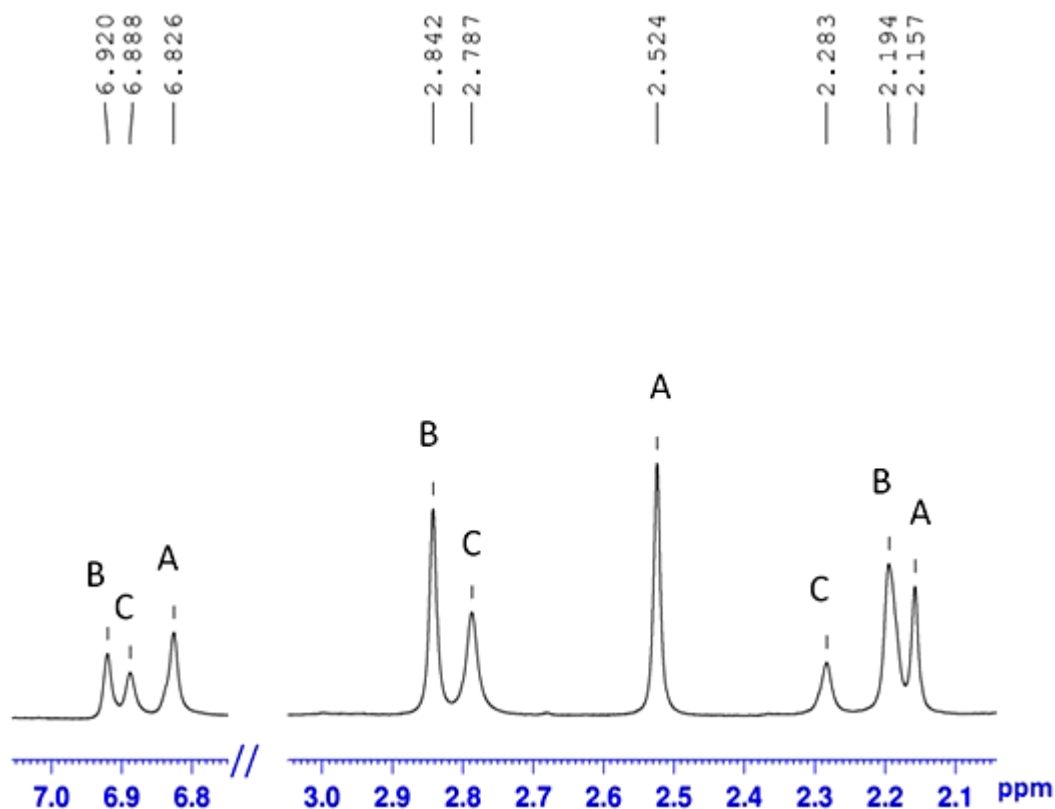


Figure 20: Selected regions of the ^1H NMR spectrum of $[\text{Mn}(\text{CO})_4\{\mu\text{-SC}_6\text{H}_2\text{-2,4,6-(CH}_3)_3\}]_3$ **10** in $[\text{D}_8]$ THF.

The metathesis reaction of potassium 4-trifluoromethyl thiophenolate with $[\text{BrMn}(\text{CO})_5]$ in THF at room temperature led to the formation of the dinuclear complex $[\text{Mn}(\text{CO})_4(\text{SC}_6\text{H}_4\text{-4-CF}_3)]_2$ (**11**) as well as to the tetranuclear derivative $[\text{Mn}(\text{CO})_3(\text{SC}_6\text{H}_4\text{-4-CF}_3)]_4$ (**12**). Crystals suitable for X-Ray crystallography were obtained in both cases by recrystallization in *n*-hexane. The formation of the complexes was also confirmed by IR and NMR spectroscopy.

The IR spectrum of **11** was similar to those of **5**, **6** and **7**, with characteristic bands assigned to stretching vibrations of CO ligands at 2083, 2023, 1994, and 1936 cm^{-1} . The ^1H -NMR spectrum shows two signals at 7.66 and 7.81 ppm assigned to the complex **11**, additional small signals were observed at 8.00 and

8.32 ppm, which were assigned to the tetranuclear complex **12** which was present as a minor impurity. Moreover, the ^{13}C NMR spectrum corroborates this by showing the carbonyl resonances of complex **11** with two signals in the region between 212 and 214 ppm, characteristic for the CO ligands of a dinuclear complex while the signal of tetranuclear **12** was observed over 220 ppm. The ^{19}F NMR spectrum showed a resonance at -63.85 ppm, assigned to the dinuclear complex **11**, and a small signal at -64.13 for the tetranuclear complex **12**.

2.2.2.2 Molecular structures of $[\text{Mn}(\text{CO})_3(\mu\text{-SC}_6\text{H}_4\text{-4-CH}_3)]_4$ (**9**), $[\text{Mn}(\text{CO})_4\{\text{SC}_6\text{H}_2\text{-2,4,6-(CH}_3)_3\}]_3$ (**10**), $[\text{Mn}(\text{CO})_4(\text{SC}_6\text{H}_4\text{-4-CF}_3)]_2$ (**11**), and $[\text{Mn}(\text{CO})_3(\text{SC}_6\text{H}_4\text{-4-CF}_3)]_4$ (**12**)

$[\text{Mn}(\text{CO})_3(\mu\text{-SC}_6\text{H}_4\text{-4-CH}_3)]_4$ (**9**)

The molecular structure of the tetranuclear complex $[\text{Mn}(\text{CO})_3(\mu\text{-SC}_6\text{H}_4\text{-4-CH}_3)]_4$ (**9**) was obtained by X-Ray diffraction experiments performed at a crystal of the composition $[\text{Mn}(\text{CO})_3(\mu\text{-SC}_6\text{H}_4\text{-4-CH}_3)]_4 \cdot [\text{Mn}(\text{CO})_4(\mu\text{-SC}_6\text{H}_4\text{-4-CH}_3)]_2$ (**9·5**). The monoclinic space group $P2_1/c$ was determined for the investigated crystal. The molecular structure of **5** is essentially the same as that one described above (see section 2.2.1.2). The molecular structure of complex **9** as well as the atom labeling scheme is depicted in figure 21. Selected bond lengths and angles are listed in table 10. Four crystallographically identical manganese centers Mn1A, Mn1B, Mn1C, and Mn1D are bridged by four 4-methyl thiophenolate ligands under formation of a Mn_4S_4 heterocubane subunit. The manganese centers possess distorted octahedral coordination spheres; each sulfur atom is

bound to three manganese atoms resulting in μ_3 -bridges. Furthermore, the remaining three facial coordination sites at the manganese atoms are occupied by carbonyl ligands.

The Mn-S bond lengths range from 2.375 to 2.408 Å. Due to the *trans* effect of sulfur in all cases, the Mn-C bond lengths were rather similar and an average value of 1.814 Å was observed. Due to a distortion of the central heterocubane structure, deviating non-bonding Mn···Mn distances in the range of 3.599 to 3.718 Å were found. These distances are shorter than the corresponding Mn···Mn distances in the well-known compound $[\text{Mn}(\text{CO})_3(\mu\text{-SC}_6\text{H}_5)]_4$. A clustering into two distinct groups of distances as reported for the unsubstituted thiophenolate derivative, where two short Mn···Mn distances (3.609 and 3.636 Å) and four long distances (3.767 - 3.775 Å) were observed [61], was not found in case of **9**. The S-Mn-S angles are rather small, around 80° (77.92° - 80.51°), compared to the angles Mn-S-Mn of around 100° (97.80° - 101.89°). The *trans* S-Mn-C angles range from 165.91° to 175.39° indicating a distortion of the octahedral geometry.

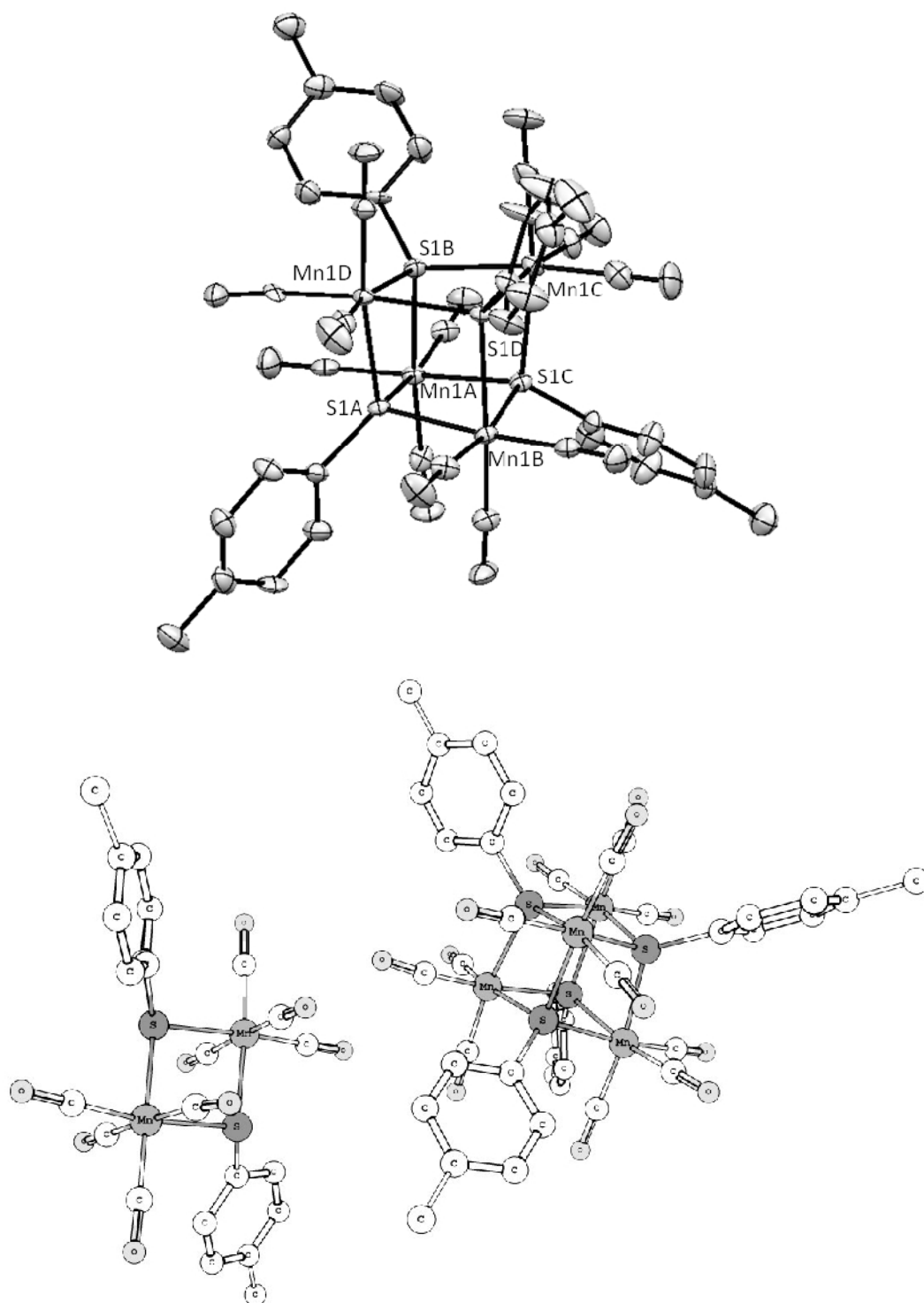


Figure 21: Molecular structure of complex $[\text{Mn}(\text{CO})_3(\mu\text{-SC}_6\text{H}_4\text{-4-CH}_3)]_4$ (**9**). Thermal ellipsoids are drawn at the 50% probability level. Hydrogen atoms are omitted for clarity. Top: View of the molecular structure of **9**. Bottom: View of the two independent molecular structures of $[\text{Mn}(\text{CO})_3(\mu\text{-SC}_6\text{H}_4\text{-4-CH}_3)]_4$ (right) and $[\text{Mn}(\text{CO})_4(\mu\text{-SC}_6\text{H}_4\text{-4-CH}_3)]_2$ (left).

Table 10. Selected bond lengths and angles of $[\text{Mn}(\text{CO})_3(\mu\text{-SC}_6\text{H}_4\text{-4-CH}_3)]_4$ (**9**)

Bond lengths [\AA]			
Mn1A-S1A	2.400(17)	Mn1C-S1B	2.406(17)
Mn1A-S1B	2.377(18)	Mn1C-S1C	2.382(18)
Mn1A-S1C	2.405(17)	Mn1C-S1D	2.392(17)
Mn1A-C8A	1.825(7)	Mn1C-C8C	1.826(7)
Mn1A-C9A	1.819(7)	Mn1C-C9C	1.808(7)
Mn1A-C10A	1.805(7)	Mn1C-C10C	1.825(7)
C8A-O1A	1.138(8)	C8C-O1C	1.135(8)
C9A-O2A	1.144(8)	C9C-O2C	1.151(8)
C10A-O3A	1.151(8)	C10C-O3C	1.135(8)
Mn1B-S1A	2.376(17)	Mn1D-S1A	2.401(17)
Mn1B-S1C	2.408(17)	Mn1D-S1B	2.386(17)
Mn1B-S1D	2.402(17)	Mn1D-S1D	2.375(17)
Mn1B-C8B	1.810(7)	Mn1D-C8D	1.808(6)
Mn1B-C9B	1.815(6)	Mn1D-C9D	1.810(7)
Mn1B-C10	1.814(7)	Mn1D-C10D	1.798(6)
C8B-O1B	1.146(7)	C8D-O1D	1.149(8)
C9B-O2B	1.138(8)	C9D-O2D	1.144(8)
C10B-O3B	1.145(8)	C10D-O3D	1.150(7)
Angles [$^\circ$]			
S1A-Mn1A-S1B	78.11(6)	S1B-Mn1C-S1C	79.37(6)
S1A-Mn1A-S1C	78.00(6)	S1B-Mn1C-S1D	78.20(6)
S1B-Mn1A-S1C	79.51(6)	S1C-Mn1C-S1D	77.92(6)
S1A-Mn1A-C10A	100.50(2)	S1B-Mn1C-C9C	91.34(2)
C8A-Mn1A-C9A	91.75(3)	C9C-Mn1C-C10C	91.06(2)
C8A-Mn1A-C10A	92.81(3)	C8C-Mn1C-C10C	90.68(3)
C9A-Mn1A-C10A	91.43(3)	C8C-Mn1C-S1D	91.64(2)
C8A-Mn1A-S1C	96.58(2)	S1C-Mn1C-C8C	95.58(2)
S1A-Mn1A-C8A	165.91(2)	S1B-Mn1C-C8C	169.36(2)
C9A-Mn1A-S1C	169.74(2)	S1C-Mn1C-C9C	170.59(2)
C10A-Mn1A-S1B	173.64(2)	C10C-Mn1C-S1D	169.67(2)
S1A-Mn1B-S1C	78.41(6)	S1A-Mn1D-S1B	77.93(6)
S1A-Mn1B-S1D	80.47(6)	S1A-Mn1D-S1D	80.51(6)
S1C-Mn1B-S1D	77.25(6)	S1B-Mn1D-S1D	78.94(6)
C8B-Mn1B-S1C	100.75(2)	S1B-Mn1D-C8D	91.96(2)
C8B-Mn1B-C9B	88.58(3)	C8D-Mn1D-C9D	89.61(3)
C8B-Mn1B-C10B	92.30(3)	C8D-Mn1D-C10D	91.94(3)
C9B-Mn1B-C10B	89.45(3)	C9D-Mn1D-C10D	91.05(3)
S1A-Mn1B-C9B	92.08(2)	S1D-Mn1D-C9D	88.79(2)
S1A-Mn1B-C8B	175.39(2)	S1A-Mn1D-C8D	169.22(2)
C9B-Mn1B-S1C	170.31(2)	S1D-Mn1D-C10D	174.05(19)

C10B-Mn1B-S1D	168.61(2)	S1B-Mn1D-C9D	167.71(2)
Mn1A-S1A-Mn1D	100.77(6)	Mn1A-S1C-Mn1B	100.41(6)
Mn1A-S1A-Mn1B	101.46(6)	Mn1B-S1C-Mn1C	101.81(6)
Mn1B-S1A-Mn1D	97.80(6)	Mn1A-S1C-Mn1C	98.81(6)
Mn1A-S1B-Mn1D	101.89(6)	Mn1B-S1D-Mn1C	101.71(6)
Mn1D-S1B-Mn1C	101.89(6)	Mn1B-S1D-Mn1D	97.81(6)
Mn1A-S1B-Mn1C	98.92(6)	Mn1C-S1D-Mn1D	100.90(6)

[Mn(CO)₄{μ-SC₆H₂-2,4,6-(CH₃)₃}₃] (10)

The complex [Mn(CO)₄{μ-SC₆H₂-2,4,6-(CH₃)₃}₃] (10) crystallizes in the triclinic space group $P\bar{1}$. Molecular structure and labeling scheme as well as the central trinuclear core unit are depicted in figure 22. Selected bond lengths and angles are listed in table 11. The complex consists of a central unsymmetrical six-membered ring formed by the three manganese atoms as well as the three μ₂ bridging sulfur atoms of the 2,4,6 trimethyl thiophenolate ligands. The resulting ring showed a boat conformation. Each manganese center possesses a distorted octahedral environment. Beside the two thiolate bridges, four carbonyl ligands occupy the coordination sites at the manganese center. It is noteworthy that, although this type of manganese complexes is rather well investigated, a comparable structure was never described before. However, such manganese structures were suggested, as well as rhenium ones with a metal-metal bond and three terminal carbonyl ligands, resulting also in diamagnetic complexes [79, 80].

All Mn-S bonds in **10** range from 2.403 to 2.446 Å, thus they are notably elongated compared to those of the dinuclear complexes **5**, **6** and **7**. The average value of the non-bonding Mn···Mn separation is 4.460 Å. This separation

between neighboring manganese centers is significantly longer with respect to related dinuclear manganese complexes which show an average distance of 3.600 Å between the manganese ions. The Mn-C bond lengths vary between 1.804 and 1.885 Å. Obviously, the Mn-C bonds of carbonyl ligands *trans* positioned to a sulfur atom are shorter compared to those *trans*-arranged to another ligand. Within the six-membered Mn₃S₃ ring, the Mn-S-Mn angles range from 129.94 to 136.33° and the S-Mn-S angles from 83.55 to 91.70°. The angles between ligands in *trans* position to each other at the manganese center vary from 173.67 to 179.88° indicating only slight distortions of the corresponding octahedral coordination environments.

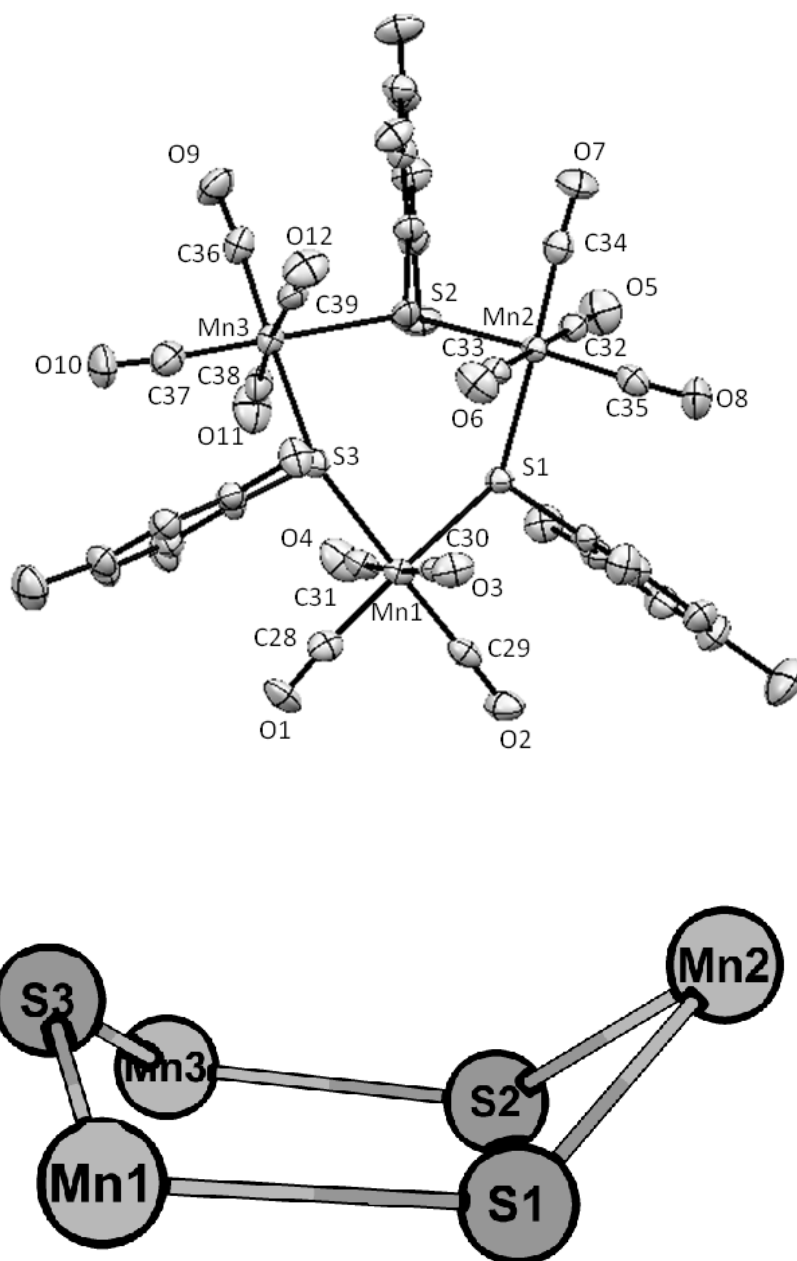


Figure 22: Crystal Structure of $[\text{Mn}(\text{CO})_4(\text{SC}_6\text{H}_2\text{-}2,4,6\text{-(CH}_3)_3)]_3$ (**10**) (top). Thermal ellipsoids are drawn at the 50% probability level. Hydrogen atoms are omitted for clarity. Bottom: Representation of the trinuclear core unit of **10**. The atoms are drawn with arbitrary radii.

Table 11. Selected bond lengths and angles of $[\text{Mn}(\text{CO})_4(\mu\text{-SC}_6\text{H}_2\text{-2,4,6-(CH}_3)_3)]_3$ (**10**)

Bond lengths [Å]		Angles [°]	
Mn1-S1	2.446(11)	Mn1-S1-Mn2	129.94(4)
Mn1-S3	2.436(11)	S1-Mn2-S2	83.55(4)
Mn2-S1	2.425(11)	Mn2-S2-Mn3	136.33(5)
Mn2-S2	2.403(11)	S2-Mn3-S3	87.90(4)
Mn3-S2	2.414(12)	Mn3-S3-Mn1	134.93(4)
Mn3-S3	2.431(11)	S3-Mn1-S1	91.70(4)
Mn1-C30	1.866(4)	C29-Mn1-C28	87.50(18)
Mn1-C31	1.885(4)	C29-Mn1-C30	92.39(17)
Mn1-C28	1.823(4)	C28-Mn1-C30	90.18(17)
Mn1-C29	1.817(4)	C29-Mn1-C31	91.97(18)
Mn2-C32	1.873(4)	S3-Mn1-C29	175.19(13)
Mn2-C33	1.878(4)	C30-Mn1-C31	174.78(17)
Mn2-C34	1.824(4)	S1-Mn1-C28	173.67(13)
Mn2-C35	1.804(4)	S1-Mn1-C31	82.33(13)
Mn3-C38	1.879(4)	S1-Mn2-C33	91.55(12)
Mn3-C39	1.869(4)	S2-Mn2-C33	92.50(13)
Mn3-C36	1.804(4)	S2-Mn2-C34	93.28(14)
Mn3-C367	1.822(5)	C32-Mn2-C34	88.24(18)
C28-O1	1.140(5)	C32-Mn2-C35	88.68(18)
C29-O2	1.140(5)	S1-Mn2-C35	92.16(14)
C30-O3	1.135(5)	C32-Mn2-C33	179.88(19)
C31-O4	1.134(5)	S2-Mn2-C35	174.40(14)
C32-O5	1.126(5)	S1-Mn2-C34	175.48(14)
C33-O6	1.132(5)	S3-Mn3-C38	92.59(14)
C34-O7	1.146(5)	C37-Mn3-C38	93.22(19)
C35-O8	1.145(5)	C36-Mn3-C37	88.49(2)
C36-O9	1.151(5)	C36-Mn3-C39	92.29(18)
C37-O10	1.145(5)	S2-Mn3-C39	89.43(13)
C38-O11	1.133(5)	S2-Mn3-C37	178.36(14)
C39-O12	1.133(5)	C38-Mn3-C39	174.34(18)
		S3-Mn3-C36	177.46(14)

 $[\text{Mn}(\text{CO})_4(\text{SC}_6\text{H}_4\text{-4-CF}_3)]_2$ (11**)**

The complex $[\text{Mn}(\text{CO})_4(\mu\text{-SC}_6\text{H}_2\text{-4-CF}_3)]_2$ (**11**) crystallizes in the monoclinic space group $P2_1/c$. The molecular structure as well as the atom labeling scheme of the dinuclear complex are depicted in figure 23. Selected bond lengths and

angles are listed in table 12. Like in case of the other members of the series under study, the manganese centers and sulfur atoms in **11** form a strictly planar Mn_2S_2 ring. The two aryl substituents show a transoid orientation relative to each other; they were found on opposite sides of the plane defined by the ring atoms Mn1, Mn1A, S1 and S1A.

All observed distances in compound **11** are in typical ranges found for comparable dinuclear manganese(I) complexes. The average Mn-S bond length is 2.402 Å and Mn-C bond lengths vary between 1.820 and 1.877 Å. The intramolecular Mn···Mn separation is 3.608 Å. Furthermore the S-Mn-S1A angle of 82.60° is rather small while the Mn-S-Mn angle is 97.40°. The angles between *trans*-positioned ligands at the manganese center are similar with 173.64° for C9-Mn1-C11, 175.74° for C8-Mn1-S1 and 177.36° for S1-Mn1-C10, indicating only a slight distortion of the octahedral coordination sphere.

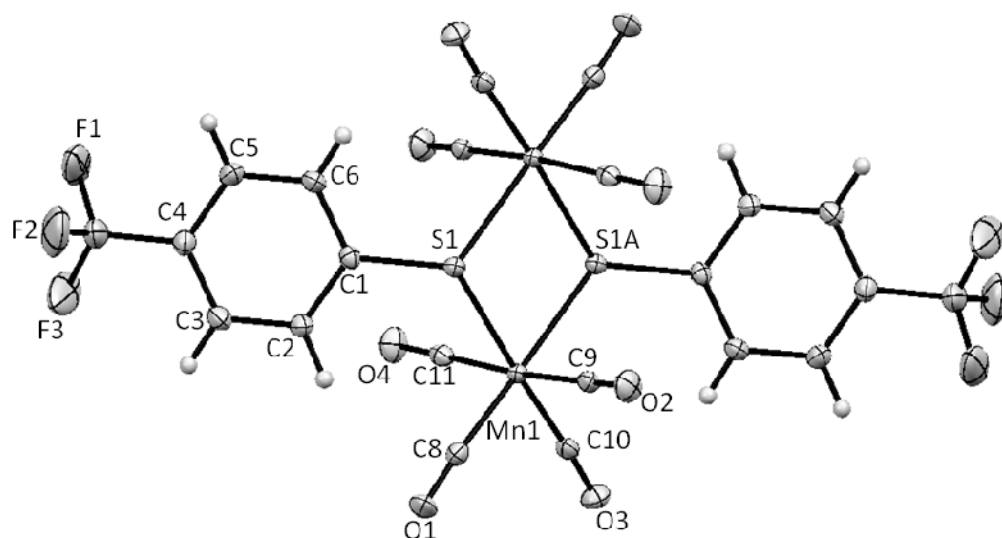


Figure 23: Crystal Structure of $[\text{Mn}(\text{CO})_4(\text{SC}_6\text{H}_4\text{-4-CF}_3)_2]$ (**11**). Thermal ellipsoids of non-hydrogen atoms are drawn at the 50% probability level.

Table 12. Selected bond lengths and angles of $[\text{Mn}(\text{CO})_4(\mu\text{-SC}_6\text{H}_4\text{-4-CF}_3)_2]$ (**11**)

Bond lengths [Å]		Angles [°]	
Mn1-S1	2.402(5)	Mn1-S1-Mn1	97.40(2)
Mn1-S1A	4.008(5)	S1-Mn1-S1A	82.60(2)
Mn1-C8	1.821(2)	S1A-Mn1-C9	88.82(6)
Mn1-C9	1.869(2)	C9-Mn1-C10	92.33(8)
Mn1-C10	1.820(2)	C8-Mn1-C10	88.86(8)
Mn1-C11	1.877(2)	C8-Mn1-C11	96.09(8)
C8-O1	1.145(2)	C11-Mn1-S1	85.68(6)
C9-O2	1.131(2)	S1-Mn1-C8	93.51(6)
C10-O3	1.141(2)	S1-Mn1-C11	90.07(5)
C11-O4	1.133(2)	C8-Mn1-C9	90.22(8)
		S1-Mn1-C10	177.36(6)
		C8-Mn1-S1	175.74(6)
		C9-Mn1-C11	173.64(8)

$[\text{Mn}(\text{CO})_3(\text{SC}_6\text{H}_4\text{-4-CF}_3)_4]$ (**12**)

The complex $[\text{Mn}(\text{CO})_3(\text{SC}_6\text{H}_4\text{-4-CF}_3)_4]$ (**12**) crystallizes in the monoclinic space group $C2/c$. The tetranuclear complex consists of two independent manganese centers Mn1A and Mn1B while the manganese atoms Mn1AA and Mn1BA are symmetry related to these atoms ($A = -x, y, -z + 3/2$). The molecular

structure of complex **12** as well as the atom numbering scheme of the heteroatoms is illustrated in figure 24. Selected bond lengths and angles for this complex are summarized in table 13. The molecular structure of complex **12** contains four manganese atoms placed in distorted octahedral coordination spheres; these are linked by four μ_3 -bridging 4-trifluoromethyl thiophenolate ligands forming a heterocubane structure. Furthermore, the other three facial positions at each manganese center are occupied by the carbonyl ligands.

As expected, the tetranuclear complex **12** is almost identical to complex $[\text{Mn}(\text{CO})_3(\mu\text{-SC}_6\text{H}_4\text{-4-CH}_3)]_4$ (**9**) with very similar bond lengths and angles. The Mn-S bond lengths range from 2.381 to 2.402 Å. Furthermore, the metal-carbon bond lengths around Mn1A are tendentiously shorter than around both Mn1B, ranging between 1.808 and 1.814 Å in the former case and from 1.809 to 1.821 Å in the latter. However, with respect to the standard deviations of those values, these differences are insignificant. Distortion of the heterocubane structure leads to four rather short intramolecular Mn \cdots Mn separations of about 3.659 Å as well as two longer ones of 3.715 Å. Hence, the Mn-S-Mn angles with an average value of 100.26° are significantly enlarged compared to 78.67° for S-Mn-S. The *trans* S-Mn-C angles vary from 168.45 to 174.77° indicating distorted octahedral environments.

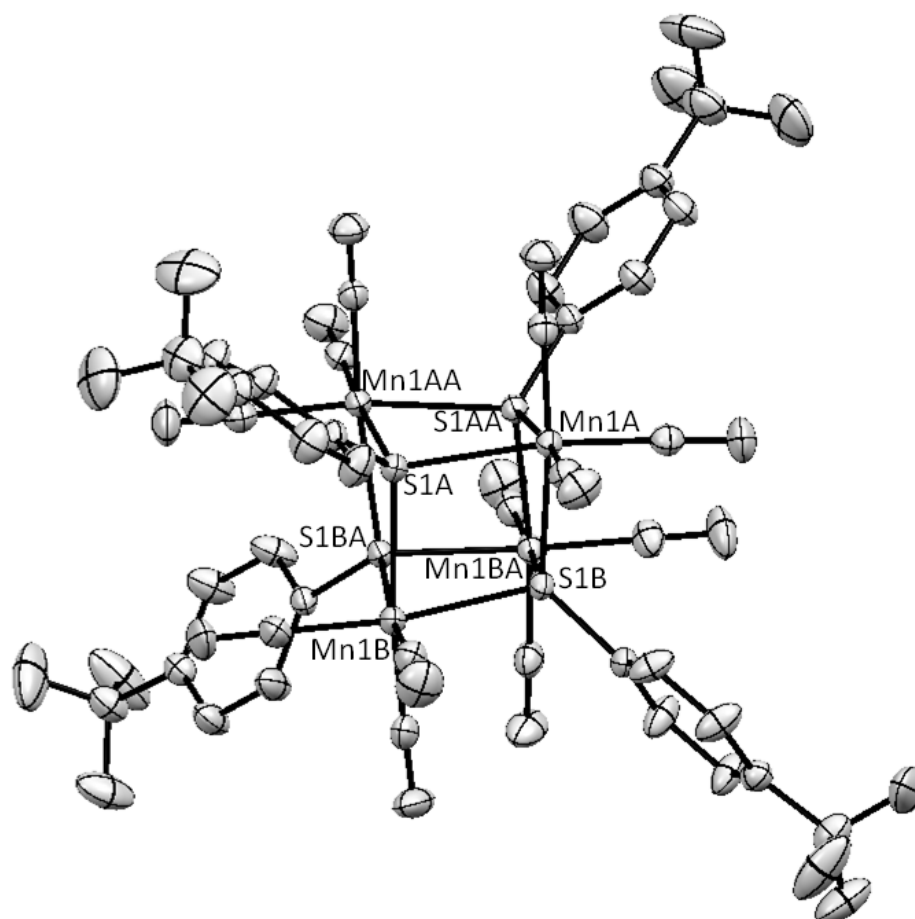


Figure 24: Crystal Structure of $[\text{Mn}(\text{CO})_3(\text{SC}_6\text{H}_4\text{-}p\text{-CF}_3)_4]$ (**12**). Thermal ellipsoids are drawn at the 50% probability level. Hydrogen atoms are omitted for clarity. Symmetry equivalent atoms are labeled with the suffix A.

Table 13. Selected bond lengths and angles of $[\text{Mn}(\text{CO})_3(\mu\text{-SC}_6\text{H}_4\text{-4-CF}_3)]_4$ (**12**)

Bond lengths [\AA]		Angles [$^\circ$]	
Mn1A-S1A	2.398(1)	S1A-Mn1A-S1AA	79.21(2)
Mn1A-S1AA	2.398(1)	S1A-Mn1A-S1BA	77.78(2)
Mn1A-S1BA	2.402(1)	S1AA-Mn1A-S1B	78.94(2)
Mn1A-C8A	1.811(3)	C8A-Mn1A-S1BA	100.30(8)
Mn1A-C9A	1.808(3)	C8A-Mn1A-S1AA	95.68(9)
Mn1A-C10A	1.814(3)	S1A-Mn1A-C9A	91.15(8)
C8A-O1A	1.151(3)	C9A-Mn1A-S1AA	95.87(8)
C9A-O2A	1.148(3)	S1A-Mn1A-C10A	98.13(8)
C10A-O3A	1.138(3)	C10A-Mn1A-S1BA	92.35(8)
Mn1B-S1B	2.381(1)	S1A-Mn1A-C8A	174.77(9)
Mn1B-S1BA	2.398(1)	C9A-Mn1A-S1BA	168.45(8)
Mn1B-S1A	2.398(1)	C10A-Mn1A-S1AA	171.24(8)
Mn1B-C8B	1.809(3)	Mn1A-S1A-Mn1B	101.57(2)
Mn1B-C9B	1.819(3)	Mn1A-S1A-Mn1AA	99.55(2)
Mn1B-C10B	1.821(3)	Mn1B-S1A-Mn1AA	99.39(2)
C8B-O1B	1.143(3)	C10B-Mn1B-S1BA	93.66(9)
C9A-O2A	1.142(4)	S1A-Mn1B-C10B	94.43(9)
C10A-O3A	1.137(4)	S1A-Mn1B-C9B	95.27(9)
		S1B-Mn1B-C9B	96.13(9)
		S1B-Mn1B-C8B	93.03(9)
		C8B-Mn1B-S1BA	97.24(9)
		S1B-Mn1B-C10B	171.12(9)
		S1A-Mn1B-C8B	171.57(9)
		C9B-Mn1B-S1BA	172.10(9)
		S1A-Mn1B-S1B	79.36(2)
		S1A-Mn1B-S1BA	77.85(2)
		S1B-Mn1B-S1BA	78.90(2)
		Mn1B-S1B-Mn1AA	99.75(2)
		Mn1B-S1B-Mn1BA	99.88(2)
		Mn1AA-S1B-Mn1BA	101.44(3)

2.2.2.3 Molecular structure of solvent-separated $[\text{Mn}_4(\text{DMF})_3(\text{CO})_9(\mu\text{-SC}_6\text{H}_4\text{-4-CF}_3)_4][\text{Mn}_2(\text{CO})_6(\mu\text{-SC}_6\text{H}_4\text{-4-CF}_3)_3]$ (**13**)

During the research on $[\text{Mn}(\text{CO})_4(\mu\text{-SC}_6\text{H}_4\text{-4-CF}_3)]_2$ (**11**) and $[\text{Mn}(\text{CO})_3(\mu\text{-SC}_6\text{H}_4\text{-4-CF}_3)]_4$ (**12**) (see section 2.2.2.1), a few crystals of a third complex were isolated in presence of trace amounts of DMF. X-Ray diffraction experiments revealed that this product is an ionic compound of the formula $[\text{Mn}_4(\text{DMF})_3(\text{CO})_9(\mu\text{-SC}_6\text{H}_4\text{-4-CF}_3)_4][\text{Mn}_2(\text{CO})_6(\mu\text{-SC}_6\text{H}_4\text{-4-CF}_3)_3]$ (**13**). Surprisingly, the cation of **13** contains not only manganese ions with the oxidation state +I, but also a single manganese center with the oxidation state +II. Most likely, compound **13** was the result of oxidation of **12** by trace amounts of oxygen, accidentally introduced during preparation and handling. Compound **13** provides the unique opportunity to directly observe the structural effects of such a single site oxidation on structural parameters of tetranuclear complexes like **12**. Compound **13** crystallizes in the triclinic space group $P\bar{1}$. The molecular structure is shown in figure 25. Selected bond lengths and angles are listed in table 14.

In the cation $[\text{Mn}_4(\text{DMF})_3(\text{CO})_9(\mu\text{-SC}_6\text{H}_4\text{-4-CF}_3)_4]^+$ of **13**, each of the four metal ions display a octahedral ligand arrangement. The cation is formally derived from the cluster $[\text{Mn}(\text{CO})_3(\mu\text{-SC}_6\text{H}_4\text{-4-CF}_3)]_4$ (**12**) by substitution of one $\{\text{Mn}(\text{CO})_3\}^+$ moiety by a $\{\text{Mn}(\text{DMF})_3\}^{2+}$ unit because the environments of the Mn1D, Mn1F, and Mn1G atoms in **13** are similar and consist of three carbonyl ligands and three μ_3 -bridging 4-trifluoromethyl thiophenolate ligands while the

environment of the oxidized Mn1E atom is different with three coordinated DMF at the cation.

The Mn-S bond lengths are rather similar for the three manganese(I) centers Mn1D, Mn1F and Mn1G atom ranging between 2.364 and 2.404 Å. The distances can be divided into two groups situated at the lower and upper end of this range. One group of distances is related to the thiolate S1G sulfur atom, which shows only contacts to Mn(I) centers. The resulting bonds Mn1D-S1G, Mn1F-S1G and Mn1G-S1G with an average value of 2.378 Å are slightly shorter than the other group of bonds. This second group involves bonds between Mn(I) centers and the thiolate sulfur atoms S1D, S1E and S1F. These atoms form μ_3 -bridges between one Mn(II) and two Mn(I) centers. The resulting bond lengths to the latter show an average value of 2.397 Å. Similar bond lengths have been observed in the neutral tetranuclear complex $[\text{Mn}(\text{CO})_3(\mu\text{-SC}_6\text{H}_4\text{-4-CF}_3)]_4$ (**12**). Additionally, bonds between Mn(II), Mn1E in cation of **13** and the sulfur atoms S1D, S1E and S1F are elongated with Mn-S bonds ranging from 2.669 to 2.708 Å due to a larger ion radius of the dication which is the result of its high spin d^5 spin state.

Due to its higher charge, the atom MnE has to be considered as a harder Lewis acid than the manganese(I) centers. This interpretation is in agreement with the observed ligands at this metal cation. Here, the oxygen atoms of the DMF molecules as the harder Lewis base is preferred as a donor site compared to over carbon monoxide. In contrast to those, low spin d^6 systems like Mn1D, Mn1F

and Mn1G generally have a greater affinity for π acceptor ligands as for example the carbonyls.

As expected, the Mn-C bond lengths range from 1.790 Å to 1.828 Å; these distances are in excellent agreement with the metal-carbonyl bond lengths found in the neutral manganese(I) complex **12** as well as in $[\text{Mn}(\text{CO})_3(\mu\text{-SC}_6\text{H}_4\text{-4-CH}_3)]_4$ (**9**). Mn(II)-O bond lengths to DMF are averaged with 2.089 Å and are shorter than the related manganese complexes $[\text{L}^{\text{Mn}}\text{MnBr}(\text{DMF})]$ (2.232 Å) and $[\text{L}^{\text{Mn}}\text{Mn}(\text{DMF})_2] \cdot [\text{ClO}_4]$ (2.115/2.256; 2.103/2.112 Å) ($\text{L}^{\text{Mn}} = [5\text{-}\{(\text{CO})_2\text{Mn-}\eta^5\text{-}(\text{H}_4\text{C}_5\text{-CH}_2)\text{Pz-3-}\{\text{CH}_2\text{-N-}(\text{CH}_2\text{Py})_2\}\}]$) [82]. An overall higher distortion of the cube-shaped Mn_4S_4 cage is observed due to the incorporation of a divalent manganese ion.

The intramolecular Mn \cdots Mn separations are composed from three short Mn(I) \cdots Mn(I) distances of 3.621-3.719 Å which are similar to observed values in the neutral tetranuclear complex $[\text{Mn}(\text{CO})_3(\mu\text{-SC}_6\text{H}_4\text{-4-CF}_3)]_4$ (**12**) while the three longer separations refer to the Mn(I) \cdots Mn(II) contacts, (Mn1D \cdots Mn1E, Mn1F \cdots Mn1E) and Mn1G \cdots Mn1E with values of 3.963, 3.954 and 3.921 Å, respectively.

The S-Mn-S angles vary from 71.51 to 82.26 Å. Here, the angles S-Mn1E-S are rather small as it is expected as a result of large Mn1E-S bond lengths. The Mn-S-Mn angles show an average value of 100.9° and the *trans* angles varying from 159.56 to 174.1° indicating that all manganese centers are situated in distorted octahedral environments.

The dinuclear anion $[\text{Mn}_2(\text{CO})_6(\mu\text{-SC}_6\text{H}_4\text{-4-CF}_3)_3]^-$ of **13** exhibits a pseudo-threefold symmetry formed by two six-coordinate Mn centers. Each metal atom is coordinated by three bridging $\mu\text{-SC}_6\text{H}_4\text{-4-CF}_3$ ligands and three terminal CO groups. The $\text{Mn}\cdots\text{Mn}$ separation of 3.215 Å is longer than that found in anionic species like $[\text{Mn}_2(\text{SPh})_3(\text{CO})_6]^-$ (3.185 Å) [62] and $[\text{Mn}_2(\text{SH})_3(\text{CO})_6]^-$ (3.154 Å) [81]. All Mn-S bonds are rather large with distances ranging from 2.376 to 2.397 Å. The Mn-C distances are found between 1.750 and 1.802 Å. The average S-Mn-S bond angle is 79.57° in the Mn_2S_3 metal-thiophenolate dinuclear core, yielding a distorted octahedron for each metal. Furthermore, the *trans* S-Mn-C angles lie between 167.2° and 173.8° confirming the distortion of the octahedral coordination sphere. In addition, the Mn-S-Mn angles were range from 84.26 to 85.07° .

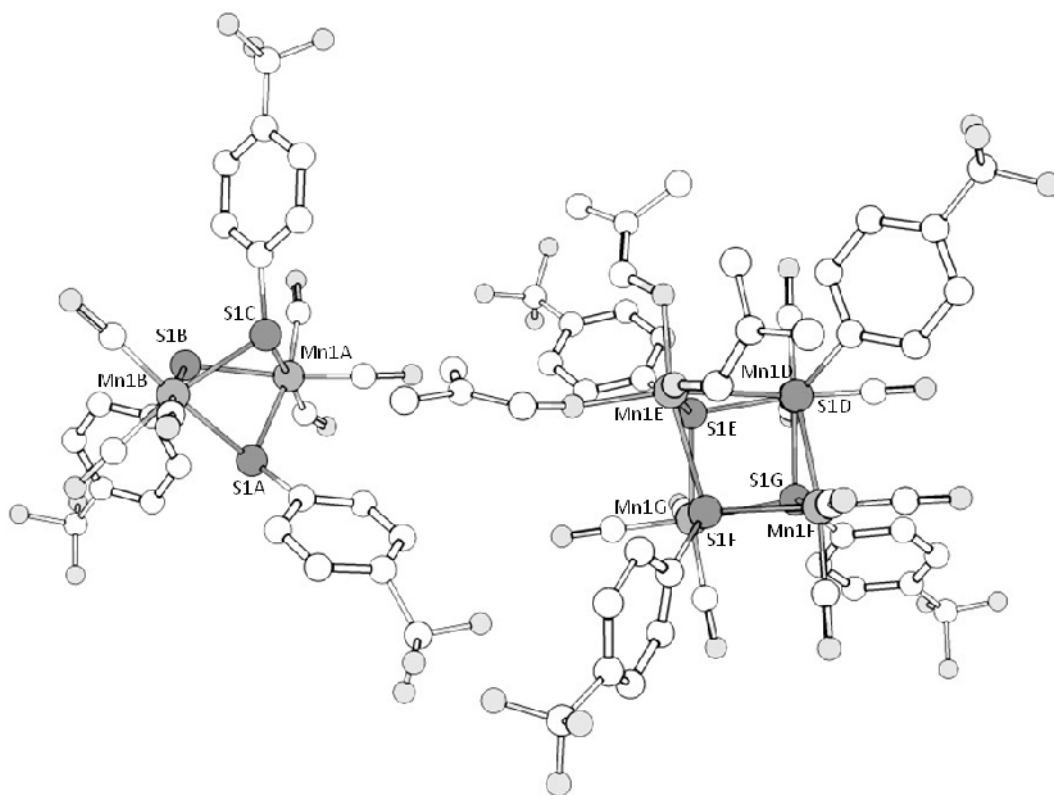


Figure 25: View of the molecular structure of complex $[\text{Mn}_2(\text{CO})_6(\mu\text{-SC}_6\text{H}_4\text{-4-CF}_3)_3][\text{Mn}_4(\text{DMF})_3(\text{CO})_9(\mu\text{-SC}_6\text{H}_4\text{-4-CF}_3)_4]$ (**13**). Hydrogen atoms are omitted for clarity. The atoms are drawn with arbitrary radii.

Table 14. Selected bond lengths and angles of $[\text{Mn}_2(\text{CO})_6(\mu\text{-SC}_6\text{H}_4\text{-4-CF}_3)_3][\text{Mn}_4(\text{DMF})_3(\text{CO})_9(\mu\text{-SC}_6\text{H}_4\text{-4-CF}_3)_4]$ (**13**)

Cation $[\text{Mn}_4(\text{DMF})_3(\text{CO})_9(\mu\text{-SC}_6\text{H}_4\text{-4-CF}_3)_4]^+$ in 13			
Bond lengths [Å]			
Mn1D-S1D	2.400(1)	Mn1F-S1E	2.400(1)
Mn1D-S1E	2.404(1)	Mn1F-S1F	2.382(1)
Mn1D-S1G	2.396(1)	Mn1F-S1G	2.364(1)
Mn1D-C8D	1.790(6)	Mn1F-C8F	1.806(5)
Mn1D-C9D	1.806(6)	Mn1F-C9F	1.828(5)
Mn1D-C10D	1.797(6)	Mn1F-C10F	1.798(5)
C8D-O1D	1.143(8)	C8F-O1F	1.148(6)
C9D-O2D	1.142(7)	C9F-O2F	1.134(6)
C10D-O3D	1.143(7)	C10F-O3F	1.147(6)
Mn1E-S1D	2.669(2)	Mn1G-S1D	2.396(1)
Mn1E-S1E	2.708(1)	Mn1G-S1F	2.399(1)
Mn1E-S1F	2.674(1)	Mn1G-S1G	2.376(1)
Mn1E-O2E	2.075(5)	Mn1G-C8G	1.813(5)
Mn1E-O3E	2.099(4)	Mn1G-C9G	1.821(5)
Mn1E-O1E	2.099(5)	Mn1G-C10G	1.810(5)
O2E-C11E	1.241(11)	C8G-O1G	1.148(7)
O3E-C14E	1.266(7)	C9G-O2G	1.138(6)
O1E-C8E	1.160(12)	C10G-O3G	1.146(6)
Angles [°]			
S1D-Mn1-S1E	81.34(4)	S1E-Mn1F-S1F	82.26(4)
S1D-Mn1D-S1G	77.10(4)	S1E-Mn1F-S1G	80.88(4)
S1E-Mn1D-S1G	80.15(4)	S1F-Mn1F-S1G	79.77(4)
C9D-Mn1D-S1G	94.5(2)	S1E-Mn1F-C8F	96.11(17)
S1D-Mn1D-C9D	90.9(2)	C8F-Mn1F-C10F	89.9(2)
S1D-Mn1D-C8D	97.5(3)	C9F-Mn1F-C10F	92.3(2)
C10D-Mn1D-S1G	97.1(2)	C9F-Mn1F-S1G	90.09(15)
C8D-Mn1D-S1E	93.1(2)	C10F-Mn1F-S1G	92.79(15)
C9D-Mn1D-C10D	90.8(3)	S1E-Mn1F-C10F	89.34(15)
S1D-Mn1D-C10D	174.1(2)	S1E-Mn1F-C9F	170.89(15)
C8D-Mn1D-S1G	171.8(2)	S1F-Mn1F-C10F	169.53(15)
C9D-Mn1D-S1E	171.3(2)	C8F-Mn1F-S1G	175.92(17)
S1D-Mn1E-S1E	71.22(4)	S1D-Mn1G-S1F	81.49(5)
S1D-Mn1E-S1F	71.69(4)	S1D-Mn1G-S1G	77.57(4)
S1E-Mn1E-S1F	71.51(4)	S1F-Mn1G-S1G	79.20(4)
S1D-Mn1E-O1E	97.18(16)	S1F-Mn1G-C9G	88.12(15)
O1E-Mn1E-S1F	96.22(17)	C8G-Mn1G-C10G	92.7(2)
O3E-Mn1E-O1E	93.9(2)	C9G-Mn1G-C10G	90.3(2)
O2E-Mn1E-O3E	98.33(19)	S1G-Mn1G-C8G	91.49(16)
S1E-Mn1E-O2E	96.18(17)	S1G-Mn1G-C9G	98.78(16)

S1D-Mn1E-O2E	97.82(16)	C8G-Mn1G-C9G	92.8(2)
S1D-Mn1E-O3E	159.56(12)	S1G-Mn1G-C10G	169.82(17)
S1E-Mn1E-O1E	165.05(13)	S1D-Mn1G-C9G	169.45(16)
O2E-Mn1E-S1F	165.70(18)	S1F-Mn1G-C8G	170.67(17)
Mn1D-S1D-Mn1E	102.68(5)	Mn1E-S1F-Mn1F	102.73(5)
Mn1D-S1D-Mn1G	101.70(5)	Mn1E-S1F-Mn1G	101.10(5)
Mn1E-S1D-Mn1G	101.33(5)	Mn1F-S1F-Mn1G	99.12(5)
Mn1D-S1E-Mn1E	101.47(5)	Mn1D-S1G-Mn1F	99.05(5)
Mn1D-S1E-Mn1F	97.85(5)	Mn1D-S1G-Mn1G	102.42(5)
Mn1E-S1E-Mn1F	101.28(5)	Mn1F-S1G-Mn1G	100.27(4)
Anion [Mn₂(CO)₆(μ-SC₆H₄-4-CF₃)₃] of 13			
Bond lengths [Å]			
Mn1A-S1A	2.379(2)	Mn1B-S1A	2.376(2)
Mn1A-S1B	2.395(2)	Mn1B-S1B	2.397(2)
Mn1A-S1C	2.397(2)	Mn1B-S1C	2.378(2)
Mn1A-C8A	1.779(7)	Mn1B-C8B	1.763(8)
Mn1A-C9A	1.802(6)	Mn1B-C9B	1.778(8)
Mn1A-C10A	1.796(6)	Mn1B-C10B	1.750(9)
C8A-O1A	1.148(8)	C8B-O1B	1.168(12)
C9A-O2A	1.146(8)	C9B-O2B	1.200(13)
C10A-O3A	1.146(7)	C10B-O3B	1.080(12)
Angles [°]			
S1A-Mn1A-S1B	82.07(6)	S1A-Mn1B-S1B	82.09(6)
S1A-Mn1A-S1C	77.72(6)	S1A-Mn1B-S1C	78.15(6)
S1B-Mn1A-S1C	78.54(5)	S1B-Mn1B-S1C	78.87(6)
C9A-Mn1A-S1B	95.1(2)	C10B-Mn1B-S1C	93.8(3)
C10A-Mn1A-S1B	90.8(2)	C8B-Mn1B-S1C	102.1(3)
S1A-Mn1A-C10A	100.3(2)	S1A-Mn1B-C8B	88.3(5)
S1A-Mn1A-C8A	91.8(3)	S1A-Mn1B-C9B	98.4(4)
C8A-Mn1A-S1C	99.7(2)	S1B-Mn1B-C9B	88.5(3)
C8A-Mn1A-C9A	90.8(4)	C8B-Mn1B-C9B	90.1(4)
C9A-Mn1A-C10A	90.8(3)	C9B-Mn1A-C10B	90.1(4)
S1A-Mn1A-C9A	168.5(2)	S1A-Mn1B-C10B	171.3(3)
C8A-Mn1A-S1B	173.8(3)	S1B-Mn1B-C8B	170.0(4)
C10A-Mn1A-S1C	169.3(2)	C9B-Mn1B-S1C	167.2(3)
Mn1A-S1A-Mn1B	85.07(6)	Mn1A-S1C-Mn1B	84.66(5)
Mn1A-S1B-Mn1B	84.26(5)		

2.2.3 Substitution reactions between $[\text{BrMn}(\text{CO})_5]$ and thiols

Tetranuclear manganese(I) complexes were synthesized with different thiophenolate ligands utilizing the synthetic strategy, similar to the one described by W. Hieber *et al.* [64]. The complexes $[\text{Mn}(\text{CO})_3(\mu\text{-SC}_6\text{H}_4\text{-4-CH}_3)]_4$ (**9**), $[\text{Mn}(\text{CO})_3(\mu\text{-SC}_6\text{H}_5)]_4$ (**14**), $[\text{Mn}(\text{CO})_3(\mu\text{-SC}_6\text{H}_4\text{-4-OCH}_3)]_4$ (**15**), $[\text{Mn}(\text{CO})_3(\mu\text{-SC}_6\text{H}_4\text{-4-Cl})]_4$ (**16**) were obtained by this approach.

2.2.3.1 Synthesis and characterization of $[\text{Mn}(\text{CO})_3(\mu\text{-SC}_6\text{H}_4\text{-4-R})]_4$ with R = H, CH₃, OMe, Cl

The thermal reaction of $[\text{BrMn}(\text{CO})_5]$ in combination with the appropriate thiol in methanol at 50°C was used by W. Hieber *et al.* for the syntheses of the dinuclear complex $[\text{Mn}(\text{CO})_4(\mu\text{-SC}_6\text{H}_5)]_2$ [64] and later D.S. Choi *et al.* described that the dinuclear compound can be converted into the tetranuclear complex by vigorously heating in THF [54]. Accordingly, a higher temperature in the related reaction W. Hieber *et al.* should favor the formation of tetranuclear complex. Based on the modification of this reaction four tetranuclear manganese(I) complexes with the general formula $[\text{Mn}(\text{CO})_3(\mu\text{-SC}_6\text{H}_5\text{-4-R})]_4$ with R = H, CH₃, OMe and Cl were synthesized as pure microcrystalline powders in high yields of 67.3 up to 95% (see figure 26).

The thiolate-bridged manganese clusters $[\text{Mn}(\text{CO})_3\text{SR}]_4$ with a central Mn_4S_4 heterocubane cage are already known and were prepared by a number of different routes [54, 64, 65, 68, 80, 83-85]. However, only very few crystallographic structure determinations have been performed on tetranuclear species. As noted in the salt metathesis reactions (section 2.2.2), two tetranuclear structures $[\text{Mn}(\text{CO})_3(\mu\text{-SC}_6\text{H}_4\text{-4-CH}_3)]_4$ (**9**) and $[\text{Mn}(\text{CO})_3(\mu\text{-SC}_6\text{H}_4\text{-4-CF}_3)]_4$ (**12**) were obtained as mixtures with the corresponding dinuclear complexes. In contrast, substitution reactions between $[\text{BrMn}(\text{CO})_5]$ and thiols in refluxing methanol appear to be a straightforward route for the synthesis of the tetranuclear species. The products were obtained as dark orange fine microcrystals after cooling of the reactions mixtures.

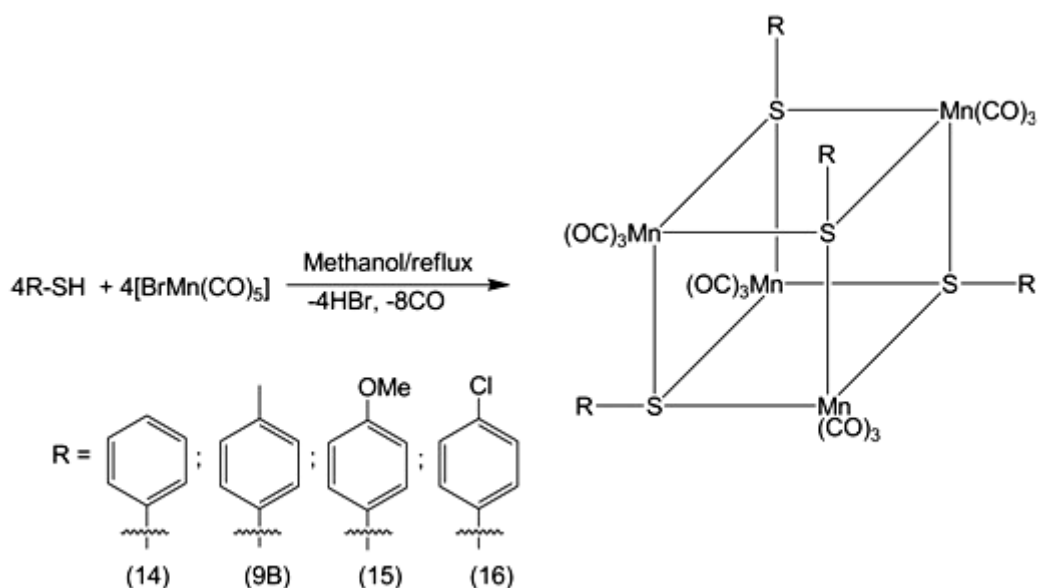


Figure 26: Synthesis of manganese carbonyl complexes $[\text{Mn}(\text{CO})_3(\mu\text{-SC}_6\text{H}_4\text{-4-R})]_4$.

All complexes were characterized by IR, ^1H NMR and ^{13}C NMR spectroscopy, as well as mass spectrometry and elemental analysis. Suitable crystals for X-Ray crystallographic analysis of **9** were obtained via slow cooling of the reaction mixture.

The reaction of thiophenol with $[\text{BrMn}(\text{CO})_5]$ in equimolar amounts under reflux in methanol led to the formation of the tetranuclear manganese complex $[\text{Mn}(\text{CO})_3(\mu\text{-SC}_6\text{H}_5)]_4$ (**14**). The structure for this complex was previously crystallographically determined by Choi D.S *et al.* and Onaka S *et al.* [54, 61].

The IR spectrum of **14** showed two $\nu_{\text{C-O}}$ stretching vibrations at 2010 and 1943 cm^{-1} as strong bands for the symmetric and asymmetric carbonyl stretching modes. This result is consistent with the fact that in the structure all $\{\text{Mn}(\text{CO})_3\}$ units are in equivalent environments with C_3 [74]. Also as expected, complexes **9**, **15** and **16** showed two strong bands in very similar ranges (**9**: 2012, 1920 cm^{-1} ; **15**: 2015, 1921 cm^{-1} ; **16**: 2020, 1930 cm^{-1}). Additionally, all spectra exhibited a very weak band at about 2080-2070 cm^{-1} indicating that the dinuclear species mentioned in the previous section, which show the same stretching vibrations, are present as minor impurities. This observation is not surprising since the dinuclear complexes are intermediates during the formation of the tetranuclear compounds.

In the ^1H NMR experiments all spectra showed exclusively the resonances corresponding to the tetranuclear complexes. The *ortho* protons of the thiophenolate ligands in all complexes exhibit the resonances in the region between 8.0 and 8.2 ppm, while the protons in *meta* positions showed different chemical shifts depending on the type of substitution in *para* position of the aromatic ring (See table 15).

Table 15. ^1H NMR data for the aromatic ring protons of $[\text{Mn}(\text{CO})_3(\mu\text{-SC}_6\text{H}_4\text{-4-R})_4]$ ($[\text{D}_8]\text{THF}$, 400 MHz, ppm).

Complex	R	<i>meta</i> protons	<i>ortho</i> protons
14	H	7.58	8.17
9	CH_3	7.36	8.00
15	O- CH_3	7.14	8.05
16	Cl	7.65	8.10

In the ^{13}C NMR spectra of the complexes, a single small broad resonance for the carbonyl ligands was found between 220 and 221 ppm for each derivative. The EI mass spectra showed the molecular ions of **14** and **9** at m/z (%) = 992 (10) and 1048 (10), respectively. However, their relative intensities were very low. In contrast, for complexes **15** and **16** the molecular ion signals could not be detected under identical conditions. The fragmentation patterns of all compounds involve a stepwise loss of carbonyl groups similar to that previously observed in the dinuclear complexes to give the ion peaks $[\text{Mn}_4(\text{SR})_4(\text{CO})_{12-n}]^+$ ($n = 1-12$) and finally $\text{Mn}_4(\text{SR})_4$ (see experimental section).

2.2.3.2 Molecular structure of $[\text{Mn}(\text{CO})_3(\mu\text{-SC}_6\text{H}_4\text{-4-CH}_3)]_4$ (**9B**)

$[\text{Mn}(\text{CO})_3(\mu\text{-SC}_6\text{H}_4\text{-4-CH}_3)]_4$ (**9B**)

In subsection 2.2.2.2, crystals of **9** and co-crystallized $[\text{Mn}(\text{CO})_4(\mu\text{-SC}_6\text{H}_4\text{-4-CH}_3)]_2$ (**5**) were used to determine the molecular structures of the complexes. Following the synthetic route outlined in section 2.2.3, it was now possible to obtain single crystals which contained only the tetranuclear manganese complex. Under these conditions, **9** crystallized in the orthorhombic space

group $Pna2_1$. In order to allow a differentiation between the molecular structures obtained from different crystals, this newly obtained structure will be labeled **9B**. The molecular structure of **9B** as well as the atom numbering scheme are illustrated in figure 27. Selected bond lengths and angles are summarized in table 16.

As expected, the molecular structure of **9B** is almost identical to the one described in subsection 2.2.2.2 with very similar bond lengths and angles. The Mn-S distances range from 2.377 to 2.406 Å. Furthermore, the Mn-C lengths were found between 1.804 and 1.822 Å. Moreover, all these distances were in agreement with the structural data previously exposed for **9** and the results obtained from the analogous $[\text{Mn}(\text{CO})_3(\mu\text{-SC}_6\text{H}_4\text{-4-CF}_3)]_4$ (**12**). Four shorter intramolecular Mn \cdots Mn separations in the range of 3.637 to 3.668 Å and two slightly elongated ones of 3.697 and 3.703 Å were found in **9B**. In all heterocubane subunits (**9**, **9B** and **12**), the S-Mn-S angles were similarly averaged to about 78.5°. Additionally, the Mn-S-Mn angles were averaged to about 100°. The other angles between *cis*-orientated ligands at the hexa-coordinate manganese centers range from 90.12 to 97.57°, indicating a distorted octahedral coordination geometry that can also be described by the *trans* S-Mn-C angles ranging from 168.77 to 174.65°.

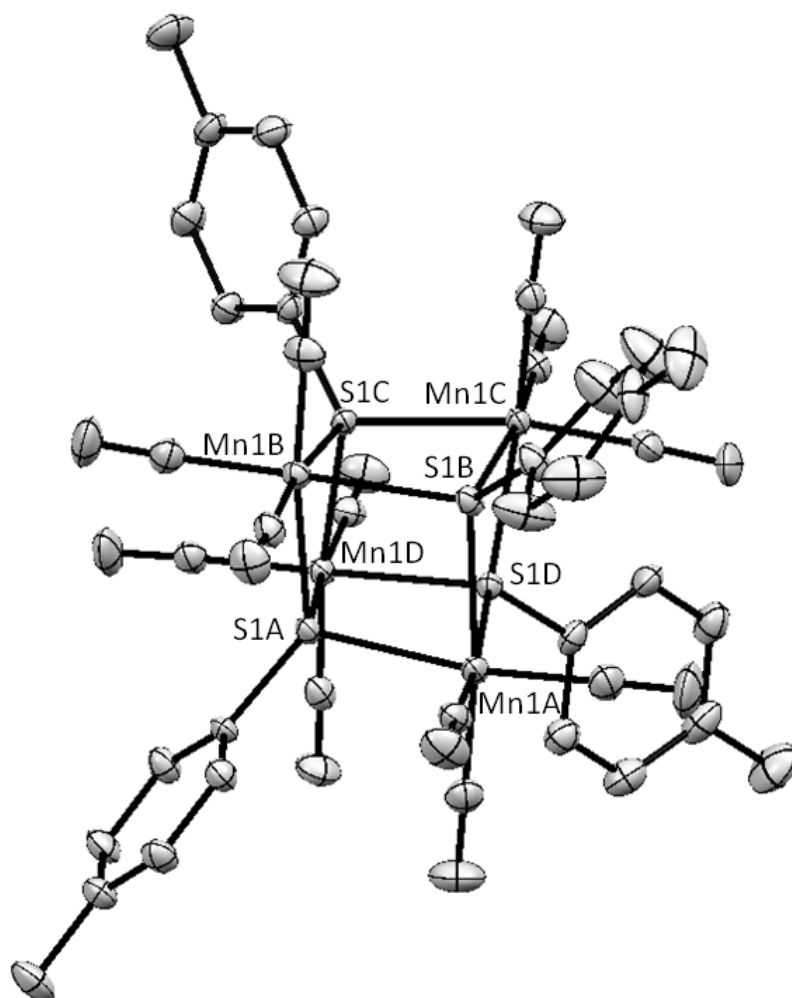


Figure 27: Molecular structure of $[\text{Mn}(\text{CO})_3(\mu\text{-SC}_6\text{H}_4\text{-4-CH}_3)]_4$ (**9B**). Thermal ellipsoids are drawn at the 50% probability level. Hydrogen atoms are omitted for clarity.

Table 16. Selected bond lengths and angles of [Mn(CO)₃(μ-SC₆H₄-4-CH₃)₂]₂ **9B**

Bond lengths [Å]			
Mn1A-S1A	2.392(1)	Mn1C-S1C	2.386(1)
Mn1A-S1B	2.382(1)	Mn1C-S1D	2.377(1)
Mn1A-S1D	2.394(1)	Mn1C-S1B	2.383(1)
Mn1A-C8A	1.815(3)	Mn1C-C8C	1.811(2)
Mn1A-C9A	1.804(2)	Mn1C-C9C	1.817(2)
Mn1A-C10A	1.821(2)	Mn1C-C10C	1.816(2)
C8A-O1A	1.132(3)	C8C-O1C	1.145(3)
C9A-O2A	1.145(3)	C9C-O2C	1.143(3)
C10A-O3A	1.142(3)	C10C-O3C	1.141(3)
Mn1B-S1B	2.395(6)	Mn1D-S1C	2.383(1)
Mn1B-S1C	2.383(1)	Mn1D-S1D	2.383(1)
Mn1B-S1A	2.406(1)	Mn1D-S1A	2.392(1)
Mn1B-C8B	1.810(3)	Mn1D-C8D	1.816(2)
Mn1B-C9B	1.822(2)	Mn1D-C9D	1.814(2)
Mn1B-C10B	1.811(2)	Mn1D-C10D	1.816(2)
C8B-O1B	1.149(3)	C8D-O1D	1.147(3)
C9B-O2B	1.137(3)	C9D-O2D	1.144(3)
C10B-O3B	1.151(3)	C10D-O3D	1.139(3)
Angles [°]			
S1A-Mn1A-S1B	79.41(2)	S1B-Mn1C-S1C	77.55(2)
S1A-Mn1A-S1D	77.90(2)	S1B-Mn1C-S1D	78.80(2)
S1B-Mn1A-S1D	78.47(2)	S1C-Mn1C-S1D	79.12(2)
C8A-Mn1A-S1D	94.19(8)	C9C-Mn1C-S1D	91.80(7)
C10A-Mn1A-S1D	97.96(8)	S1B-Mn1C-C9C	94.42(8)
S1A-Mn1A-C10A	93.42(8)	S1B-Mn1C-C10C	96.86(7)
S1A-Mn1A-C9A	97.17(8)	S1C-Mn1C-C10C	96.95(7)
C9A-Mn1A-S1B	93.93(8)	S1C-Mn1C-C8C	93.62(7)
C8A-Mn1A-S1B	94.60(9)	C8C-Mn1C-S1D	96.23(8)
C8A-Mn1A-C9A	90.12(11)	C9C-Mn1C-S1D	91.80(7)
S1A-Mn1A-C8A	170.84(8)	S1B-Mn1C-C8C	170.50(8)
C9A-Mn1A-S1D	171.54(8)	S1C-Mn1C-C9C	168.83(7)
C10A-Mn1A-S1B	172.49(8)	C10C-Mn1C-S1D	174.65(7)
S1A-Mn1B-S1B	78.89(2)	S1A-Mn1D-S1C	78.81(2)
S1A-Mn1B-S1C	78.54(2)	S1A-Mn1D-S1D	78.11(2)
S1B-Mn1B-S1C	77.37(2)	S1C-Mn1D-S1D	79.03(2)
S1B-Mn1B-C10B	97.57(7)	S1C-Mn1D-C10D	93.16(7)
C9B-Mn1B-C10B	92.29(10)	C9D-Mn1D-C10D	92.27(10)
C8B-Mn1B-C9B	91.39(12)	C8D-Mn1D-C9D	91.20(10)
C8B-Mn1B-S1C	95.77(7)	S1A-Mn1D-C8D	95.80(7)
S1A-Mn1B-C10B	94.87(8)	C8D-Mn1D-C10D	91.45(10)

C9B-Mn1B-S1C	92.27(8)	S1D-Mn1D-C8D	93.22(7)
S1A-Mn1B-C8B	171.60(8)	S1A-Mn1D-C10D	170.09(7)
S1B-Mn1B-C9B	168.77(8)	S1C-Mn1D-C8D	171.29(7)
C10B-Mn1B-S1C	172.30(8)	S1D-Mn1D-C9D	171.58(8)
Mn1A-S1A-Mn1B	99.19(2)	Mn1B-S1C-Mn1C	101.90(2)
Mn1A-S1A-Mn1D	101.19(2)	Mn1B-S1C-Mn1D	100.64(2)
Mn1B-S1A-Mn1D	99.73(2)	Mn1C-S1C-Mn1D	99.40(2)
Mn1A-S1B-Mn1B	99.78(2)	Mn1A-S1D-Mn1C	100.13(2)
Mn1A-S1B-Mn1C	100.28(2)	Mn1A-S1D-Mn1D	101.40(2)
Mn1B-S1B-Mn1C	101.62(2)	Mn1C-S1D-Mn1D	99.66(2)

2.2.3.3 Molecular structure of $[\text{Mn}_6(\text{CO})_{18}(\mu\text{-SC}_6\text{H}_4\text{-4-Cl})_8\{\text{Mn}_2(\mu\text{-Br})_2(\text{THF})\}]$ (**17**)

During the synthesis of $[\text{Mn}(\text{CO})_3(\mu\text{-C}_6\text{H}_4\text{-4-Cl})]_4$ (**16**) (section 2.2.3.1), a few crystals of a second complex were isolated in presence of trace amounts of THF. X-Ray diffraction experiments revealed that this novel product with the overall formula $[\text{Mn}_6(\text{CO})_{18}(\mu\text{-SC}_6\text{H}_4\text{-4-Cl})_8\{\text{Mn}_2(\mu\text{-Br})_2(\text{THF})\}]$ (**17**) is a mixed-valence compound, containing manganese in different oxidation states of +I and +II. Compound **17** is formally derived from two $[\text{Mn}(\text{CO})_3(\mu\text{-C}_6\text{H}_4\text{-4-Cl})]_4$ (**16**) units by oxidation with HBr. However, no reduced species like hydrogen were detected. Therefore the mechanism of the formation of **17** is not clear. Complex **17** crystallizes in the monoclinic space group $C2/c$. The molecular structure and labeling scheme of **17** is depicted in figure 28. Selected bond lengths and angles are summarized in table 17.

In complex **17** the six manganese ions in oxidation state +I, Mn2, Mn3, Mn4, Mn2A, Mn3A and Mn4A, display an octahedral ligand arrangement. Each of these manganese ions is bound to three terminal carbonyl ligands and three

bridging thiolate ligands. Three of these manganese(I) ions together with one manganese(II) ion (Mn1 or Mn1A) form a thiolate bridged heterocubane substructure. The resulting two heterocubanes are linked by additional bromo bridges between these manganese(II) ions. A disorder of the THF ligand additionally coordinated to Mn1 and of one bromide anion was observed in the investigated crystal, resulting in a pseudo-symmetry which makes the two manganese(II) centers Mn1 and Mn1A crystallographically equivalent. However, from a chemical point of view they aren't as the resolution of the disorder revealed. While one of these ions is surrounded by three bridging thiolate ligands, two bridging bromide ions and a THF ligand in a distorted octahedral fashion, the other manganese(II) ion is only penta-coordinated due to the absence of a THF ligand for sterical reasons. Unfortunately, this disorder limits a detailed discussion of bond lengths and angles around Mn1 and Mn1A to those within the heterocubane fragment.

As expected, in complex **17** the average value of the Mn(II)-S bond lengths, Mn1-S1A, Mn1-SC and Mn1-S1D of 2.613 Å was significantly longer than those to the Mn2, Mn3 and Mn4 ions indicating the high spin d^5 state of the manganese(II) center. The average S-Mn-S bond angle is 74.65° and *trans* S-Mn-C angles vary from 160.60 to 171.76 due to a significantly distorted octahedral coordination sphere. The intramolecular Mn···Mn distances in **17** are composed from three long separations 3.764-3.896 Å which belong to Mn(I)···Mn(II) contacts and these are shorter than those observed previously in the compound $[\text{Mn}_4(\text{DMF})_3(\text{CO})_9(\mu\text{-SC}_6\text{H}_4\text{-4-CF}_3)_4] [\text{Mn}_2(\text{CO})_6(\mu\text{-SC}_6\text{H}_4\text{-4-CF}_3)_3]$ (**13**). The three shorter separations refer to the Mn(I)···Mn(I) with values

between 3.650 and 3.675 Å and were similar to those in the complexes **9**, **12** and **13**. The Mn(I)-S bond lengths vary from 2.368 to 2.412 Å. The average distances between the manganese(I) center and the carbon atom of the carbon monoxide ligand of 1.812 Å is in accordance with the values observed in the tetranuclear complexes **9** and **12** as well as in the cation of **13**. The S-Mn-S angles in each manganese(I) center of complex **17** is similarly averaged to about 80.26° while the Mn-S-Mn angles are observed relatively obtuse with an average value of 100.09°. Furthermore, the other angles within all coordination manganese(I) centers range from 89.31 to 96.93°, indicating distorted octahedral coordination environments as also indicated by the *trans* S-Mn-C angles varying from 168.3 to 173.40°.

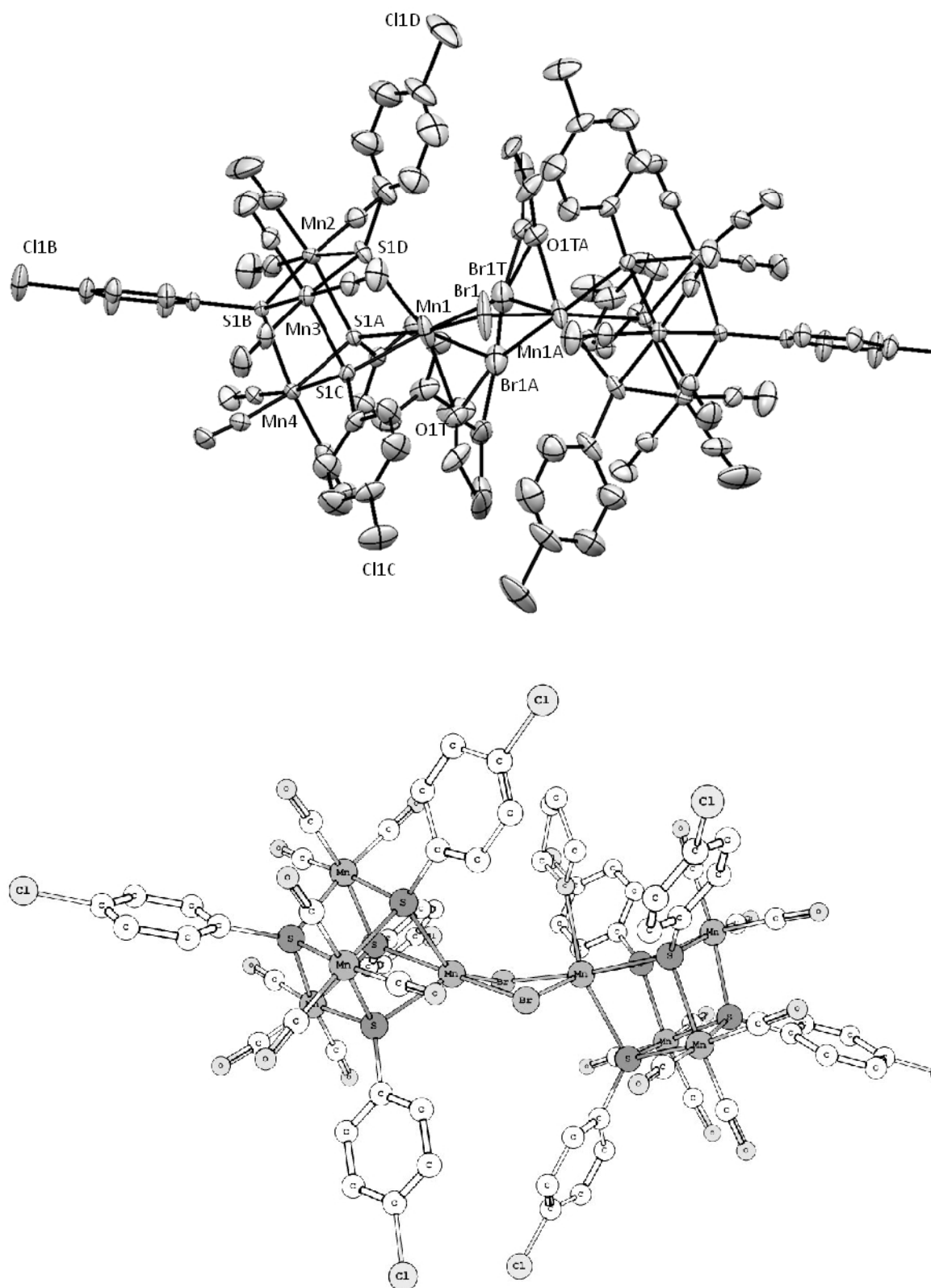


Figure 28: View of the molecular structure of $[\text{Mn}_6(\text{CO})_{18}(\mu\text{-SC}_6\text{H}_4\text{-4-Cl})_8\{\text{Mn}_2(\mu\text{-Br})_2(\text{THF})\}]$ (17). The disordering of the structure is depicted. Thermal ellipsoids are drawn at the 50% probability level. Hydrogen atoms are omitted for clarity (top). Representation of the molecular structure with resolved disorder (bottom).

Table 17 Selected bond lengths and angles of $[\text{Mn}_6(\text{CO})_{18}(\mu\text{-SC}_6\text{H}_4\text{-4-Cl})_6\{\text{Mn}_2(\mu\text{-Br})_2(\text{THF})_2\}]$ (**17**)

Bond lengths [Å]			
Mn1-Br1	2.600(1)	Mn3-S1B	2.380(1)
Mn1-Br1T	2.602(2)	Mn3-C7C	1.811(6)
Mn1-S1C	2.579(1)	Mn3-C8C	1.810(6)
Mn1-S1A	2.620(1)	Mn3-C9C	1.808(6)
Mn1-S1D	2.642(2)	C7C-O1C	1.142(7)
Mn1-O1T	2.411(8)	C8C-O2C	1.149(7)
Mn2-S1A	2.401(1)	C9C-O3C	1.138(7)
Mn2-S1D	2.385(2)	Mn4-S1C	2.399(1)
Mn2-S1B	2.384(1)	Mn4-S1A	2.395(1)
Mn2-C7B	1.819(7)	Mn4-S1B	2.368(1)
Mn2-C8B	1.809(6)	Mn4-C7D	1.803(8)
Mn2-C9B	1.812(6)	Mn4-C8D	1.813(5)
C7B-O1B	1.144(8)	Mn4-C9D	1.823(5)
C8B-O2B	1.142(7)	C7D-O1D	1.147(7)
C9B-O3B	1.147(7)	C8D-O2D	1.141(7)
Mn3-S1C	2.406(1)	C9D-O3D	1.139(7)
Mn3-S1D	2.412(2)		
Angles [°]			
Br1T-Mn1-Br1	92.61(5)	Br1-Mn1-BrT	87.24(4)
Mn1-Br1-Mn1A	84.28(5)	Mn1-Br1T-Mn1A	89.26(6)
Br1T-Mn1-S1D	96.99(5)	S1C-Mn3-S1D	84.82(5)
S1A-Mn1-S1D	73.13(4)	S1C-Mn3-S1B	78.96(4)
S1C-Mn1-S1A	73.86(4)	S1D-Mn3-S1B	78.78(5)
S1D-Mn1-S1C	76.97(5)	S1B-Mn3-C9C	94.34(17)
Br1-Mn1-S1C	99.85(4)	C7C-Mn3-C9C	91.8(3)
Br1-Mn1-O1T	98.47(2)	C7C-Mn3-C8C	90.9(3)
O1T-Mn1-Br1T	86.00(2)	S1D-Mn3-C8C	92.60(18)
Br1-Mn1-Br1T	87.24(4)	C8C-Mn3-C9C	89.8(2)
Br1-Mn1-S1A	169.13(6)	S1C-Mn3-C9C	173.20(18)
S1C-Mn1-Br1T	171.76(6)	S1D-Mn3-C7C	172.3(2)
S1D-Mn1-O1T	160.6(2)	S1B-Mn3-C8C	170.72(18)
S1A-Mn2-S1D	81.84(5)	S1C-Mn4-S1A	81.31(4)
S1A-Mn2-S1B	78.83(4)	S1C-Mn4-S1B	79.33(4)
S1D-Mn2-S1B	79.23(5)	S1A-Mn4-S1B	79.26(4)
S1A-Mn2-C8B-	91.96(18)	S1A-Mn4-C7D	90.46(17)
S1A-Mn2-C9B	96.93(18)	C7D-Mn4-C8D	89.8(2)
C8B-Mn2-C9B	89.31(2)	C8D-Mn4-C9D	93.9(2)
S1B-Mn2-C7B	89.6(2)	S1C-Mn4-C9D	93.22(18)
C7B-Mn2-C9B	94.4(3)	C7D-Mn4-C9D	92.0(2)
S1D-Mn2-C8B	173.40(19)	S1A-Mn4-C8D	169.46(17)
S1B-Mn2-C9B	172.1(2)	S1C-Mn4-C7D	170.73(16)
S1A-Mn2-C7B	168.3(2)	S1B-Mn4-C9D	171.91(18)

Mn1-S1A-Mn2	101.69(5)	Mn1-S1C-Mn3	98.03(5)
Mn1-S1A-Mn4	100.82(5)	Mn1-S1C-Mn4	101.90(5)
Mn2-S1A-Mn4	99.10(5)	Mn3-S1C-Mn4	99.45(5)
Mn2-S1B-Mn3	100.94(5)	Mn1-S1D-Mn2	101.49(5)
Mn2-S1B-Mn4	100.35(5)	Mn1-S1D-Mn3	96.18(5)
Mn3-S1B-Mn4	101.08(8)	Mn2-S1D-Mn3	100.01(5)

2.2.4 CO release properties of manganese based complexes and comparison with CORM-1

The first step to investigate the CO release properties of these complexes was the evaluation of some preconditions for CORMs, such as their air-stability and their solubility in aqueous DMSO, a solvent that is commonly used for drug delivery.

The isolated complexes were air-stable for long periods of time in the solid state (when kept in the dark). In DMSO, 16 to 18 μ M solutions of the dinuclear complexes can be prepared. Nevertheless, 10-15 minutes were required to thoroughly solubilize 20 mg of complex in 2 mL of DMSO (complex **6** requires twice as much time). After 5 h the color of the solution changed from yellow to orange and it was possible to observe CO liberation through small bubbles.

^1H NMR spectra revealed the gradual formation of paramagnetic species by broadening of the resonances (see figure 29). On the basis of these observations it is suggested that these complexes in DMSO are stable for only a few hours without inert atmosphere. Similarly, solutions were prepared with the tetranuclear complexes. We note that dissolution of complexes **9**, **14** and **15** occurred relatively fast, contrarily to complex **16**, which was only partially soluble. The solution remained unchanged for 5 h at 25°C. However, the final

Previous studies on **CORM-1** showed that irradiation with cold light ($\lambda > 400$ nm) cause the release of CO as evidenced by a myoglobin assay [8]. Usually, homoleptic metal carbonyl compounds exhibit poor solubility in protic solvents and require a high-power light source to achieve photolysis.

We also aimed to determine whether thiolate groups will cause a shift in the spectroscopic and structural parameters of the resulting carbonyl complexes and, as ultimate consequence, onto CO release. A comparison of the obtained data is summarized in Table 18. **CORM-1** shows three CO stretching vibrations in the IR spectrum at 2043, 2012 and 1980 cm^{-1} while complexes **4-7** exhibit four active vibrations. Hence, the lower energy (longer wavelength) CO stretching modes will involve those CO ligands with the short Mn-C bonds (1.812-1.822 Å). In contrast, the lower wavelength stretching modes correspond to CO ligands which are trans-positioned to each other resulting in shortened C-O and elongated Mn-C_(COtrans) bonds.

Table 18. Stretching modes $\nu(\text{CO})$ [cm^{-1}] and bond distances [Å] of the dinuclear complexes **4**, **5**, **6**, **7** and **CORM 1**

	4	5	6	7	CORM-1
$\nu(\text{CO})$	2072	2075	2072	2083	2043
	1996	1992	1995	1991	2012
	1981	1982	1986	1979	1980
	1945	1959	1942	1955	----
Mn-C	1.812 ^[54]	1.821	1.822	1.817	1.811 ^[86]
Mn-C _(COtrans)	1.869 ^[54]	1.872	1.871	1.873	1.856 ^[86]

CO release in complexes **4**, **5** and **7** was quantified in a myoglobin (Mb) assay for photo-CORMs. Normally, in this assay the conversion of myoglobin to the

corresponding myoglobin-carbon monoxid complex (MbCO) is monitored via UV/VIS measurement in the region between 500 and 600 nm. However, since the manganese complexes show absorption in this region and hence interfere with the signals of myoglobin and the myoglobin-carbon monoxid complex, it was found more reliable to monitor the CO release via the myoglobin bands in the region between 380 and 460 nm. CO uptake causes a shift of the Soret band at 435 nm to 424 nm, caused by myoglobin-carbon monoxid complex (MbCO) formation under the experimental conditions [87]. Iron(II)-based CORMs, e.g. $[\text{Fe}(\text{CO})(\text{NC-Me})(\text{H}_2\text{NCH}_2\text{CH}_2\text{PPh}_2)_2] [\text{BF}_4]_2$ (CORM-P1) and $[\text{Fe}(\text{CO})(\text{NC-Me})(\text{H}_2\text{NC}_6\text{H}_4\text{-2-PPh}_2)_2] [\text{BF}_4]_2$ (CORM-P2), have also been monitored in the higher energy band, since CORM-P2 also absorbs between 500 and 600 nm [50]. The determination of CO release under these conditions has also the advantage that it does not require high concentrations of the complex, therefore being an ideal scenario for compounds with relatively low solubility in DMSO, such as the case of **CORM-1** and complexes **4**, **5** and **7**.

Relevant discrepancies have been found in the apparent CO release rate of compounds $[\text{Ru}(\text{CO})_3\text{Cl}_2]$ (CORM-2) and $[\text{Ru}(\text{CO})_3\text{Cl}(\text{glycinate})]$ (CORM-3). This is basically due to the reducing agent sodium dithionite ($\text{Na}_2\text{S}_2\text{O}_4$), which is responsible for rapid CO release from these Ru-based CORMs in the myoglobin assay [88]. Based on this previous study, it is necessary to assess whether the presence of $\text{Na}_2\text{S}_2\text{O}_4$ already facilitates the CO release, triggered via redox process or ligand substitution reactions.

The photo-induced release of CO from compounds **CORM-1**, **4**, **5** and **7** was investigated at 5 μM by through the myoglobin assay. The complexes were irradiated for 5 minutes in a buffer solution, which contained approx. 0.1% of $\text{Na}_2\text{S}_2\text{O}_4$ and a 10 μM solution of myoglobin. As shown in figure 31, the release of CO from **CORM-1** caused a shift of the 435 nm band to 424 nm. In accordance to previous studies **CORM-1** shows no CO release in the dark [8]. The amount of MbCO was estimated from the change of the absorbance at 424 nm ($A_{max} = 1.442$, 9.25 μM MbCO). Additionally, the results showed that CO release in **CORM-1** is not dithionite-dependent. For comparison a spectrum of myoglobin saturated with CO gas was measured.

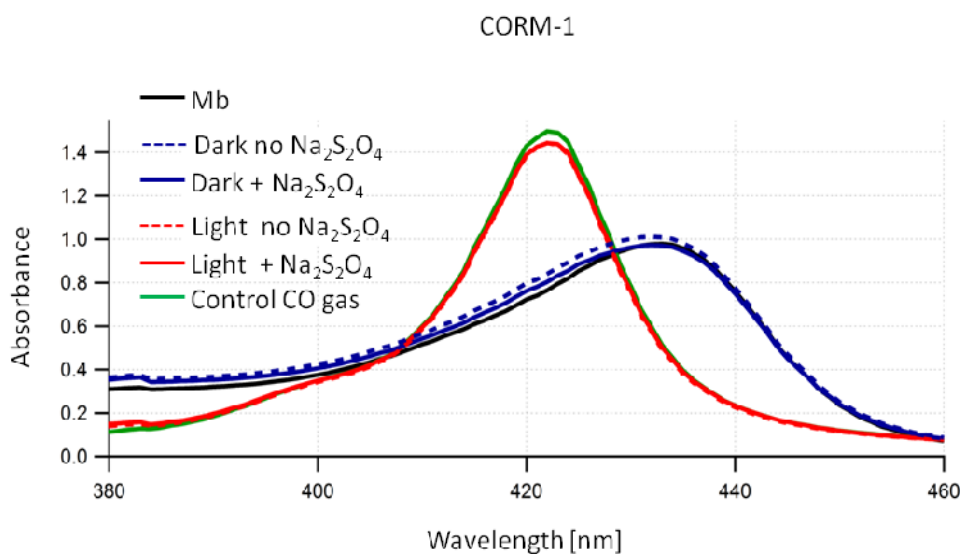


Figure 31: Absorption spectrum in the range of 380-460 nm for solutions of 5 μM of **CORM-1** and 10 μM deoxymyoglobin upon 5 min irradiation.

The spectra of complexes **4**, **5** and **7** are shown in figure 32. Despite the structural variations of these complexes, they were also active photo-CORMs like **CORM-1**.

For quantitative purposes, the absorbances at the position of the Soret bands of the MbCO product were also recorded and consequently the concentration of the product (MbCO) was calculated. The analysis of UV-Vis spectra (figure 32) of complexes **4**, **5** and **7** reveals that upon irradiation carbon monoxide was released in all cases and the MbCO concentrations were found between 9.5 and 10 μM . However, due to the presence of dithionite an important difference was noted in complex **7** and a slow, CO release is also observed under dark conditions.

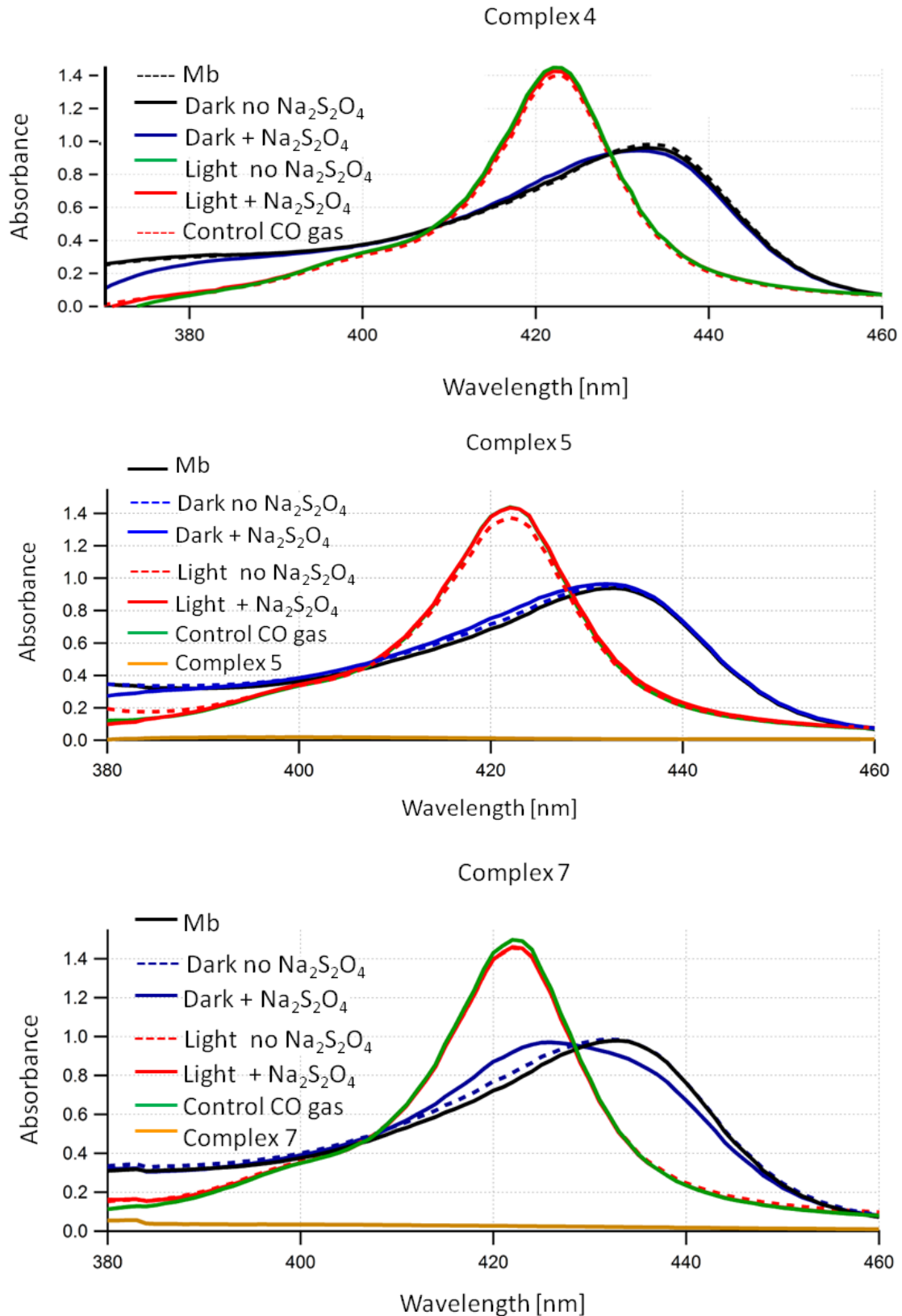


Figure 32: Absorption spectra demonstrating the conversion of deoxy-myoglobin (Mb, start spectrum) to carbon monoxide myoglobin (MbCO) for complexes 4, 5, 7 upon light irradiation, also monitoring the influence of sodium dithionite.

3 Summary and Outlook

This thesis comprises the targeted synthesis and characterization of ruthenium and manganese carbonyl complexes. Additionally, some of the complexes obtained, were analyzed with respect to their CO release properties as photo-CORMs in a myoglobin-based assay. According to the metal center this thesis can be divided into two parts, ruthenium-based carbonyl complexes and manganese-based carbonyl complexes.

Ruthenium-based carbonyl complexes: The mononuclear ruthenium(II) complexes $[\text{Ru}(\text{CO})_2(\text{H}_2\text{NC}_2\text{H}_4\text{S})_2]$ (**1**) and $[\text{Ru}(\text{CO})_2(\text{SC}_6\text{H}_4\text{NH}_2)_2]$ (**2**) were prepared from deprotonation of cysteamine and 2-aminothiophenol, respectively, with $[\text{Ru}_3(\text{CO})_{12}]$. They crystallized from donor solvents such as tetrahydrofuran and dimethylformamide as adducts with these bases bound by hydrogen bridges to the amino group.

In order to synthesize the dinuclear ruthenium(II) complex $[\text{Ru}_2(\text{CO})_5(\text{adamantyl-APE})]$ (**3**), it was necessary to perform first the synthesis of the novel Schiff-base ligand 2-pyridyl-methyl-N-adamantylimine (**1-**

adamantyl-Pyca). Afterwards, complex **3** was successfully obtained by oxidation of $[\text{Ru}_3(\text{CO})_{12}]$ from the addition of two C-C linked **1-adamantyl-Pyca** unit. This C-C coupling reaction takes place at the C atom of the imine moiety. Finally, the product was recrystallized from THF or CH_2Cl_2 as an adduct. It is important to highlight that significant intermolecular contacts occur only between the dinuclear complex and CH_2Cl_2 molecules. Structural analysis by crystallographic studies at a single crystal of the complex reveal that only one enantiomeric pair (*(R,R)* and *(S,S)*) of diastereomers is formed, whereas the meso-form is absent

Although the compounds **1** and **2** contain very similar coordination environments with respect to the homologous iron(II) derivatives, $[\text{Fe}(\text{CO})_2(\text{H}_2\text{NC}_2\text{H}_4\text{S})_2]$ (**CORM-S1**) and $[\text{Fe}(\text{CO})_2(\text{SC}_6\text{H}_4\text{NH}_2)_2]$ (**CORM-S2**), it was not possible to release CO from them with visible light due to the fact that the metal-centered electron transitions move to higher energies on going from Fe to Ru. In the case of the dinuclear ruthenium complex **3**, which has five carbonyl ligands, it was also not possible to observe light-induced loss of CO, and therefore, the three ruthenium complexes cannot be employed as light-triggered CORMs. For this reason, we focused our research on Manganese-based carbonyl complexes.

Manganese-based carbonyl complexes: Dinuclear manganese(I) complexes $[\text{Mn}(\text{CO})_4(\mu\text{-SC}_6\text{H}_4\text{-4-R})_2]$ (R= H (**4**), CH_3 (**5**), OCH_3 (**6**), Cl (**7**)) were obtained by photochemical reaction of $[\text{Mn}_2(\text{CO})_{10}]$ with diaryl disulfides. The structural analysis of all complexes reveal a planar Mn_2S_2 core with the aryl thiolate

groups attached to the μ -S atoms adopting *trans*-annular *anti* positions (see figure 33). Four carbonyl ligands are further bound at each manganese center. It is through this conformation that two carbonyl ligands are located *trans* to each other at the manganese centers with longer Mn-C bond lengths with respect to the Mn-C distances *trans* to the bridging thiolate groups. The reason is basically due to stronger π -back bonding to the carbonyl ligands which are in *trans* position to the sulfur atoms. Besides, a different dinuclear complex of the type $[\text{Mn}(\text{CO})_3(\text{SC}_6\text{H}_3\text{CH}_3\text{-}o\text{-SC}_6\text{H}_4\text{Me})_2]$ (**8**) was obtained through self-assembly process presumably by a radical mechanism.

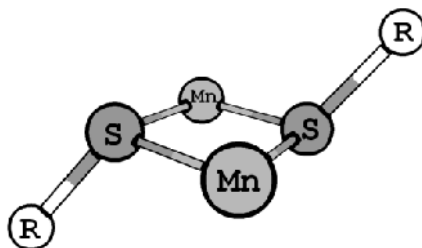


Figure 33: Schematic representation of the dinuclear core unit in the manganese complexes.

As a continuation of the approach utilized in the previous manganese complexes series with an arrangement of bridging aryl thiolates, salt metathesis reactions were used for the synthesis of the dinuclear complexes $[\text{Mn}(\text{CO})_4(\mu\text{-SC}_6\text{H}_4\text{-}4\text{-R})]_2$ (R= CH_3 (**5**), CF_3 (**11**)). Unfortunately, these complexes formed as a mixture with the tetranuclear complexes $[\text{Mn}(\text{CO})_3(\mu\text{-SC}_6\text{H}_4\text{-}4\text{-R})]_4$ (R= CH_3 (**9**) and CF_3 (**12**)). Moreover, the novel trinuclear $[\text{Mn}(\text{CO})_4(\mu\text{-SC}_6\text{H}_2\text{-}2,4,6\text{-CH}_3)]_3$ complex **10** was identified as the only product in the solid state however, complex **10** degraded in solution. The solvent-separated ion pair $[\text{Mn}_2(\text{CO})_6(\mu\text{-SC}_6\text{H}_4\text{-}4\text{-CF}_3)]_3[\text{Mn}(\text{CO})_3(\mu\text{-SC}_6\text{H}_4\text{-}4\text{-CF}_3)]$ (**13**), which formed in trace amount was crystallographically characterized. Nevertheless, the selective interaction with solvents that act as Lewis bases, such as dimethylformamide, makes the

complex **13** a very interesting example to observe the structural effects of such a single site oxidation on structural parameters of tetranuclear complexes.

Substitution reactions between $[\text{BrMn}(\text{CO})_5]$ and thiols by vigorous heating in methanol are a simple route for the synthesis of the tetranuclear species $[\text{Mn}(\text{CO})_3(\mu\text{-SC}_6\text{H}_4\text{-4-R})]_4$ (R = H (**14**), CH₃ (**9**), OMe (**15**), Cl (**16**)). All tetranuclear complexes were isolated as pure products allowing this extensive characterization. The IR spectra of the tetranuclear complexes exhibit two carbonyl stretching modes. Furthermore, in the ¹³C NMR spectra, the chemical shifts of the carbonyl ligands are found as single small broad resonances between 220 and 221 ppm. These results demonstrate the high symmetry of the complexes. In addition, the Mn-C bond lengths of **9** are found in the narrow range between 1.804 and 1.822 Å because all carbonyl ligands are located in *trans* positions to the corresponding sulfur atoms.

The formation of the complex $[\text{Mn}_6(\text{CO})_{18}(\mu\text{-SC}_6\text{H}_4\text{-4-Cl})_8\{\text{Mn}_2(\mu\text{-Br})_2(\text{THF})\}]$ (**17**) was observed during the synthesis of $[\text{Mn}(\text{CO})_3(\mu\text{-C}_6\text{H}_4\text{-4-Cl})]_4$ (**16**) as a by-product. This novel compound **17** showed an interesting molecular structure derived from two $[\text{Mn}(\text{CO})_3(\mu\text{-C}_6\text{H}_4\text{-4-Cl})]_4$ (**16**) units, containing manganese in two different oxidation states, Mn(I) and Mn(II).

The complexes $[\text{Mn}(\text{CO})_4(\mu\text{-SC}_6\text{H}_5)]_2$ (**4**) and $[\text{Mn}(\text{CO})_4(\mu\text{-SC}_6\text{H}_4\text{-4-CH}_3)]_2$ (**5**) act as CORMs that are stable in the dark and release CO upon irradiation with visible light. In contrast, complex $[\text{Mn}(\text{CO})_4(\mu\text{-SC}_6\text{H}_4\text{-4-Cl})]_2$ (**7**), despite being stable in the dark, the presence of dithionite facilitates the release of CO in this compound.

In near future, the dinuclear manganese(I) could serve as broad reference points since varying the substituents on the ring with the introduction of side chains can modify the physicochemical and pharmacokinetic properties. This would allow to adapt CORMs to relevant therapeutic applications. An emerging field is immobilization of photolabile transition metal carbonyls on solid matrices, such as films, particles, gels, dendrimers and fibers [89, 90] which represent an interesting strategy for such CO delivery in complexes with low solubility.

In our study, we did not attempt to collect pharmacokinetic and toxicological data. However, this will be required prior to clinical application.

4 Zusammenfassung und Aussichten

Diese Dissertation umfasst die gezielte Synthese und Charakterisierung von Ruthenium- und Mangancarbonylkomplexen. Einige der erhaltenen Komplexe wurden zusätzlich hinsichtlich ihrer CO Freisetzungseigenschaften als photo-CORMs in einem Myoglobin-Assay analysiert. Gemäß des Metallzentrums gliedert sich die Arbeit in zwei Teile: Ruthenium-basierte Carbonylkomplexe und Mangan-basierte Carbonylkomplexe.

Ruthenium-basierte Carbonylkomplexe: Die mononukleären Ruthenium(II)-Komplexe $[\text{Ru}(\text{CO})_2(\text{H}_2\text{NC}_2\text{H}_4\text{S})_2]$ (**1**) und $[\text{Ru}(\text{CO})_2(\text{SC}_6\text{H}_4\text{NH}_2)_2]$ (**2**) wurden durch die Deprotonierung von Cysteamin beziehungsweise 2-Aminothiophenol mit $[\text{Ru}_3(\text{CO})_{12}]$ hergestellt. Sie kristallisierten mit Spender-Lösungsmitteln wie Tetrahydrofuran und Dimethylformamid welche über Wasserstoffbrücken an die Aminogruppe als Addukte gebunden werden.

Zur Synthese des zweikernigen Ruthenium(II)-Komplex $[\text{Ru}_2(\text{CO})_5(\text{adamantyl-APE})]$ (**3**), war es notwendig, zuerst die Synthese des neuen Schiffbase-Liganden 2-

pyridyl-methyl-N-adamantylimine (**1-adamantyl-Pyca**) durchzuführen. Danach konnte der Komplex **3** durch Oxidation von $[\text{Ru}_3(\text{CO})_{12}]$ erfolgreich durch Addition von zwei C-C verbundenen **1-adamantyl-Pyca** Einheiten erhalten werden. Diese C-C-Kopplung erfolgt am C-Atom der Imineinheit. Schließlich wurde das Produkt aus THF oder CH_2Cl_2 als Addukt umkristallisiert. Dabei ist es wichtig herauszustellen, dass die signifikanten, intermolekulare Bindungen nur zwischen dem zweikernigen Komplex und CH_2Cl_2 -Molekülen bestehen. Die Kristallstrukturanalyse dieses Komplexes zeigte, dass nur ein Enantiomerenpaar ((*R,R*) and (*S,S*)) von Diastereomeren gebildet wird, während die meso-Form nicht vorhanden ist.

Obwohl die Verbindungen **1** und **2** bezüglich der homologen Eisen(II)-Derivate $[\text{Fe}(\text{CO})_2(\text{H}_2\text{NC}_2\text{H}_4\text{S})_2]$ (**CORM-S1**) und $[\text{Fe}(\text{CO})_2(\text{SC}_6\text{H}_4\text{NH}_2)_2]$ (**CORM-S2**) sehr ähnliche Koordinationsumgebungen aufweisen, war die Freisetzung von CO mit sichtbarem Licht nicht möglich, da sich die Metall-zentrierten Elektronenübergänge von Fe zu Ru zu höheren Energien verschieben. Im Falle des zweikernigen Rutheniumkomplexes **3**, welcher fünf Carbonylliganden besitzt, war es ebenfalls nicht möglich, die Licht-induzierte Freisetzung von CO zu beobachten und deshalb können die drei Rutheniumkomplexe nicht als Licht-induzierte CORMs eingesetzt werden. Auf dieser Grundlage haben wir den Fokus unserer Forschung auf Mangan-basierte Carbonylkomplexe gelegt.

Mangan-basierte Carbonylkomplexe: Die zweikernigen Mangan(I)-Komplexe $[\text{Mn}(\text{CO})_4(\mu\text{-SC}_6\text{H}_4\text{-4-R})_2]$ (R= H (**4**), CH_3 (**5**), OCH_3 (**6**), Cl (**7**)) wurden durch photochemische Reaktion von $[\text{Mn}_2(\text{CO})_{10}]$ mit Diaryldisulfiden erhalten. Die

strukturelle Analyse aller Komplexe zeigt einen planaren Mn_2S_2 Kern mit den Arylthiolatgruppen in *trans*-annularer anti Position an den μ -S-Atomen des Rings (siehe Abbildung 33). Weiterhin sind vier Carbonylliganden an jedem Mangan Zentrum gebunden. Durch diese Konformation befinden sich zwei Carbonylgruppen in *trans*-Position am Manganzentrum zueinander welche eine längere Mn-C-Bindung aufweisen im Vergleich zu denjenigen in *trans*-Position zu den verbrückenden Thiolatgruppen. Der Grund dafür liegt im Wesentlichen auf der stärkeren π -Bindung zu den Carbonyl-Liganden, die sich in *trans*-Stellung zu den Schwefel-Atomen befinden. Außerdem wurde ein anderer zweikerniger Komplex des Typs $[\text{Mn}(\text{CO})_3(\text{SC}_6\text{H}_3\text{CH}_3\text{-}o\text{-SC}_6\text{H}_4\text{Me})_2$ (**8**) durch Selbstorganisation erhalten, welcher vermutlich radikalisch entsteht.

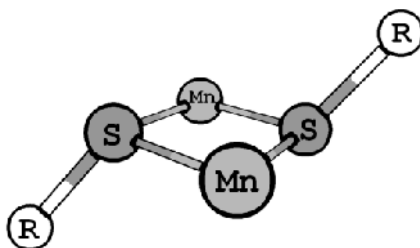


Figure 33: Schematische Darstellung der zweikernigen Kern-Einheit der Mangan-Komplexe.

Als Fortsetzung des vorherigen Ansatzes zur Herstellung von Mangan-Komplexen mit einer Brücken-Arylthiolat Anordnung, wurde die Salzmetathese für die Synthese zweikerniger $[\text{Mn}(\text{CO})_4(\mu\text{-SC}_6\text{H}_4\text{-}4\text{-R})]_2$ ($\text{R} = \text{CH}_3$ (**5**), CF_3 (**11**)) Komplexe verwendet. Leider formten sich diese Komplexe als Gemisch mit dem tetranuklearen Komplex $[\text{Mn}(\text{CO})_3(\mu\text{-SC}_6\text{H}_4\text{-}4\text{-R})]_4$ ($\text{R} = \text{CH}_3$ (**9**) und CF_3 (**12**)).

Darüber hinaus konnte der neue trinukleare $[\text{Mn}(\text{CO})_4(\mu\text{-SC}_6\text{H}_2\text{-2,4,6-CH}_3)]_3$ Komplex **10** als einziges Produkt im festen Zustand identifiziert werden, welcher sich jedoch in Lösung zersetzt. Das solvatgetrennte Ionenpaar $[\text{Mn}_2(\text{CO})_6(\mu\text{-SC}_6\text{H}_4\text{-4-CF}_3)_3][\text{Mn}(\text{CO})_3(\mu\text{-SC}_6\text{H}_4\text{-4-CF}_3)]$ (**13**), welches in Spuren gebildet wurde, konnte kristallographisch charakterisiert werden. Dennoch macht die selektive Wechselwirkung mit Lösungsmitteln, welche als Lewis-Basen wirken, wie beispielsweise Dimethylformamid, den Komplex **13** zu einem sehr interessanten Beispiel, um strukturelle Effekte einer solchen Single-Site-Oxidation auf strukturelle Parameter von tetranuklearen Komplexen zu beobachten.

Ein einfacher Weg zur Synthese von tetranuklearen Komplexen der Art $[\text{Mn}(\text{CO})_3(\mu\text{-SC}_6\text{H}_4\text{-4-R})_4]$ ($\text{R} = \text{H}$ (**14**), CH_3 (**9**), OMe (**15**), Cl (**16**)) sind Substitutionsreaktionen zwischen $[\text{BrMn}(\text{CO})_5]$ und Thiolen durch kräftiges Erhitzen in Methanol. Alle tetranuklearen Komplexe wurden als reine Produkte isoliert, was eine umfangreiche Charakterisierung erlaubt. Die IR-Spektren der tetranuklearen Komplexe zeigen zwei Carbonyl-Valenzschwingungen. Weiterhin konnten in den ^{13}C -NMR-Spektren die chemischen Verschiebungen der Carbonyl-Liganden bei Resonanzen zwischen 220 und 221 ppm gefunden werden. Diese Ergebnisse belegen die hohe Symmetrie der Komplexe. Darüber hinaus werden die Mn-C-Bindungen von **9** im engen Bereich zwischen 1.804 und 1.822 Å gefunden, weil sich alle Carbonylgruppen in trans-Stellung zu den entsprechenden S-Atomen befinden.

Die Bildung des Komplexes $[\text{Mn}_6(\text{CO})_{18}(\mu\text{-SC}_6\text{H}_4\text{-4-Cl})_8\{\text{Mn}_2(\mu\text{-Br})_2(\text{THF})\}]$ (**17**) wurde als Nebenprodukt während der Synthese von $[\text{Mn}(\text{CO})_3(\mu\text{-C}_6\text{H}_4\text{-4-Cl})]_4$ (**16**) beobachtet. Diese neue Verbindung **17** zeigte eine interessante Molekülstruktur, welche sich von zwei $[\text{Mn}(\text{CO})_3(\mu\text{-C}_6\text{H}_4\text{-4-Cl})]_4$ (**16**) Einheiten ableitet, welche Mangan in zwei verschiedenen Oxidationsstufen Mn (I) und Mn (II) enthält.

Die Komplexe $[\text{Mn}(\text{CO})_4(\mu\text{-SC}_6\text{H}_5)]_2$ (**4**) and $[\text{Mn}(\text{CO})_4(\mu\text{-SC}_6\text{H}_4\text{-4-CH}_3)]_2$ (**5**) fungieren als CORMs, die im Dunkeln stabil sind und bei Bestrahlung mit sichtbarem Licht CO freisetzen. Im Gegensatz dazu steht der im Dunkeln stabile $[\text{Mn}(\text{CO})_4(\mu\text{-SC}_6\text{H}_4\text{-4-Cl})]_2$ (**7**) Komplex, bei dem die Anwesenheit von Natrium-Dithionit die Freisetzung von CO erleichtert.

In naher Zukunft könnten zweikernige Mangan (I) Komplexe als Bezugspunkte dienen. Durch die Variation der Substituenten am Ring und die Einführung von Seitenketten können physikalisch-chemischen und pharmakokinetischen Eigenschaften modifiziert werden. Dies würde es erlauben, CORMs für relevante therapeutische Anwendungen anzupassen. Ein aufstrebendes Gebiet ist die Immobilisierung photolabiler Übergangsmetall-Carbonylverbindungen auf festen Oberflächen, wie Filme, Partikel, Gele, Dendrimere und Fasern [89, 90], welche eine interessante Strategie für CO Abgabe in Komplexen mit geringer Löslichkeit darstellt.

Das Ziel der vorliegenden Studien war es nicht, pharmakokinetische und toxikologische Daten zu sammeln. Dies wird jedoch vor der klinischen Anwendung erforderlich werden.

5 Experimental

5.1 Physical measurements

Melting points and decomposition points were measured in sealed capillaries, using a Stuart SMP3 melting point apparatus.

Elemental analyses (C, H, N) were performed in the Institute of Organic Chemistry and Macromolecular Chemistry with a LECO CHNS-932

IR spectra were measured on a Perkin Elmer System 2000 on samples prepared as Nujol mulls between KBr windows or neat between KBr windows and on a Bruker EQUINOX 55/FRA106/S, with Golden Gate ATR unit for pure samples.

^1H , ^{13}C , ^{19}F , $^1\text{H} \{^1\text{H}\}$ COSY, and $^1\text{H} \{^{13}\text{C}\}$ HSQC NMR experiments were carried out on Bruker AVANCE 200 and 400 spectrometers. Chemical shifts are reported in parts per million. The residual signals of $[\text{D}_8]\text{THF}$ (^1H NMR, δ 1.72, 3.58; ^{13}C NMR, δ 25.31, 67.21) were used as the internal standard.

FAB and DEI mass spectra were measured on a Finnigan MAT SSQ 710 and on a Finnigan MAT95XL for ESI mass spectra.

UV/Vis spectra of the myoglobin assay were recorded with an Ultrospec 1100pro spectrophotometer (Amersham Biosciences) and on an analytik Jena Specord S600.

5.2 Crystal structure determinations

Single crystals were selected while covered with mother liquor and perfluorinated oil under a polarizing microscope and fixed on fine glass fibers. The crystallographic data was collected on a Nonius Kappa CCD diffractometer using graphite-monochromated Mo-K α radiation ($\lambda = 71.073$ pm). A summary of crystallographic and structure refinement data is given in appendix A.1. Data were corrected for Lorentz and polarization effects, but not for absorption effects [91–93]. The structures were solved by direct methods with SHELXS-97 and refined by full-matrix least-squares techniques against F_o^2 using SHELXL-97 [94]. The program XP (SIEMENS Analytical X-ray Instruments, Inc.) was used for structure representations.

5.3 Syntheses

All manipulations were carried under an inert atmosphere (argon or nitrogen) using standard Schlenk techniques except the ligands for compound **3** and **7**. The solvents were purified and /or dried by standard techniques prior to use. [D₈]THF was dried over sodium, [D₇]DMF and [D₆]DMSO were dried with molecular sieves. The ligands 1-adamantyl-Pyca, bis(*p*-chlorophenyl) disulfide as well as the potassium thiophenolates were synthesized following published procedures. All other chemicals and solvents are commercially available and

were used as received without further purification, unless stated differently. Photoreactions were performed with light using a LED NSCU033AT Nichia unit.

5.3.1 Syntheses of ruthenium complexes

[Ru(SC₂H₄NH₂)₂(CO)₂] (1)

A solution of [Ru₃(CO)₁₂] (645 mg, 1.03 mmol) and cysteamine (463 mg, 7.4 mmol) in THF (20 mL) was vigorously stirred and heated to reflux for 3 h. During this time the crude product was obtained as yellow powder which was collected by filtration, dried in vacuum (678 mg, 2.19 mmol, 72%) and finally recrystallized from a saturated THF solution at 6 °C. The crystals contain THF. Decomposition above 240 °C (without melting). ¹H NMR (200 MHz, [D₇] DMF): δ = 2.53 (m, *J*=4.8 Hz, 4H), 2.89 (m, *J*=3.9 Hz, 4H), 3.21 (m, *J*=5.3 Hz, 4H), 3.85 (br, NH₂, 4H), 5.00 (m, NH₂, 2 H) ppm. ¹³C NMR (400 MHz, [D₇] DMF): δ = 30.3, 52.23, 201.3 ppm. MS (FAB), *m/z* (%): 310 [M + H]⁺ (80), 282 [M + H – CO]⁺ (60), 254 [M + H – 2CO]⁺ (75). IR (nujol) ν(CO): 2023 (s), 1950 (m) cm⁻¹. Elemental analysis of THF-free complex (C₆H₁₂N₂S₂O₂Ru, 309.07 g mol⁻¹): calcd. C 23.31, H 3.91, N 9.06, S 20.75; found C 23.00, H 3.81, N 8.68, S 20.79.

[Ru(CO)₂(SC₆H₄-2-NH₂)₂] (2)

The complex was prepared starting from 146 mg of [Ru₃(CO)₁₂] (0.228 mmol) and 270 mg of 2-aminothiophenol (1.94 mmol) in 20 mL of heptane (mixture of isomers). The suspension was refluxed for 3 h and then filtered. The filter cake

was dried yielding 260 mg of an orange solid (0.64 mmol, 94%). Crystals of **2** suitable for X-ray diffraction experiments were obtained by layering a saturated DMF solution with diethyl ether at room temperature. The crystals contain THF. Decomposition above 145 °C (without melting). ¹H NMR (600 MHz, [D₆]DMSO): δ = 5.75 [d, *J*=12.9 Hz, 2H], 6.78 [t, *J*=7.44 Hz, 2H], 6.83 [d, *J*=13.0 Hz, 2H], 6.90 [t, *J*=7.5 Hz, 2H], 7.06 [d, *J*=7.80 Hz, 2H], 7.27 [d, *J*=7.80 Hz, 2H] ppm. ¹³C NMR (600 MHz, [D₆]DMSO): δ = 120.46, 125.35, 125.73, 128.55, 142.12, 146.76, 189.26 ppm. MS (ESI), *m/z* (%): 405 (80) [M]⁺, 377 (100) [M-CO]⁺, 349 (55) [M-2CO]⁺. IR (nujol) ν(CO): 2044 (vs), 1989 (s) cm⁻¹. Elemental analysis of DMF-free complex (C₁₄H₁₂N₂O₂S₂Ru, 405 g mol⁻¹) calcd.: C 41.48, H 2.96, N 6.91, S 15.80; found: C 40.69, H 2.88, N 6.72, S 15.69.

[Ru₂(CO)₅(adamantyl-APE)] (3)

A solution of 1-adamantylamine (733 mg, 5 mmol) in dichloromethane was added dropwise to stirred pyridine-2-carbaldehyde (530 mg, 5 mmol). Sodium sulfate was added to remove the water produced in the reaction. After 3h of stirring at ambient temperature the resulting mixture was filtered, washed three times with 5 mL of dichloromethane and finally dried in vacuum yielding 824 mg (3.43. mmol, 62%) of a pale yellow solid. Melting point: 48.8°C ¹H NMR (200 MHz, CD₂Cl₂): δ = 1.70 - 1.80 [m, 12H], 2.10 [s, 3H], 7.30 [d, *J*= 4.8 Hz 1H], 7.70 [m *J*=8.0 Hz, 1H], 8.01 [d, *J*=7.9 Hz 1H], 8.3 [s, 1H], 8.60 [d, *J*=4.8 Hz 1H] ppm. ¹³C NMR (400 MHz, CD₂Cl₂): δ = 29.7, 36.4, 42.8, 57.8, 120, 124, 136, 149, 156 ppm. MS (EI), *m/z* (%): 240 (70) [M]⁺. IR (KBr, cm⁻¹): 3364 (w),

3267 (w), 3133 (vw), 3054 (m), 3009 (m), 2988 (m), 2678 (w), 2657 (w), 2571 (w), 2427 (vw), 1991 (w), 1889 (w), 1732 (vw), 1654 (m), 1641 (s), 1614 (w), 1588 (s), 1567 (s), 1452 (s), 1436 (s), 1353 (m), 1342 (m), 1307 (s), 1293 (m), 1259 (m), 1229 (m), 1185 (w), 1043 (m), 993 (s), 986 (m), 969 (w), 956 (w), 927 (m), 919 (m), 1102 (m), 1091 (m), 1084 (s), 1043 (m), 993 (s), 986 (m), 969 (w), 956 (vw), 927 (m), 919 (m), 881 (w), 864 (m), 813 (m), 775 (s), 740 (s), 674 (m), 621 (m), 563 (m), 525 (m), 490 (w), 460 (m). Elemental analysis ($C_{16}H_{20}N_2$, $240.34 \text{ g mol}^{-1}$) calcd.: C 80.0, H 8.3, N 11.6; found: C 79.87, H 8.58, N 11.67.

Under inert atmosphere to a stirred solution of the ligand (180 mg, 0.75 mmol) in toluene (20 mL) a suspension of 158 mg (0.25 mmol) of $[Ru_3(CO)_{12}]$ in toluene (20 mL) was added. The mixture was stirred for 5 min. The solution was heated at 120°C for 3 h. The solvent was evaporated under vacuum to dryness, leaving 124 mg (0.156 mmol, 39.8%) the product as a red powder. Crystals suitable for X-ray crystallography, were obtained by recrystallization from a hot saturated THF or dichloromethane solution during storage in the freezer at -20°C . Decomposition above 185°C (without melting). ^1H NMR (400 MHz, $[D_8]\text{THF}$): $\delta = 1.29 - 1.89$ [m, (broad), 30H], 4.17 [s, 4H], 7.33 [t, $J=7.4$ Hz, 2H], 7.62 [d, $J=7.8$ Hz, 1H], 7.85 [m, $J=8.2$ Hz, 2H], 8.4 [d, $J=5.0$ Hz, 2H]. ^{13}C NMR (400 MHz, $[D_8]\text{THF}$): $\delta = 31.5, 37.2, 58.7, 72.7, 121, 124, 139.5, 151.2, 167.2, 202.4, 203.6$. MS (ESI), m/z (%): 824 (25) $[M + 3H]^+$, 796 (100) 712 (5%) $[M + 2H - 4CO]^+$, 685 (5%) $[M + 2H - 5CO]^+$. IR (nujol) $\nu(\text{CO})$: 2011 (s), 1976 (s), 1913, 1911, 1682 (s) cm^{-1} . Elemental analysis ($C_{37}H_{40}O_5N_4Ru_2 \cdot 2\text{THF}$, 967 g mol^{-1}) calcd.: C 55.89, H 5.84, N 5.79; found: C 57.60, H 5.20, N 5.98.

5.3.2 Synthesis of manganese complexes

Method A: Oxidation of $[\text{Mn}_2(\text{CO})_{10}]$ by organic disulfides

$[\text{Mn}(\text{CO})_4(\mu\text{-SC}_6\text{H}_5)]_2$ (**4**)

A suspension of $[\text{Mn}_2(\text{CO})_{10}]$ (584 mg, 1.5 mmol) and diphenyl disulfide (1005 mg, 4.6 mmol) in 40 mL of heptane (mixture of isomers) was stirred until a clear solution formed. Then the solution was irradiated for 1 h. An orange solid precipitated. The crude product of the reaction was filtered. The filtrate was collected, concentrated in vacuum and stored at $-18\text{ }^\circ\text{C}$ yielding 490 mg (0.887 mmol, 59.2%) of orange crystal, Decomposition above $87.5\text{ }^\circ\text{C}$ (without melting). ^1H NMR (400 MHz/ $[\text{D}_8]$ THF): $\delta = 7.23$ [m, (broad), 2H, *p*-CH], 7.31 [m, (broad) 4H, *m*-CH], 7.63 [d, $J = 7.38$ Hz, 4H, *o*-CH]. ^{13}C (400 MHz/ $[\text{D}_8]$ THF): 127.4, 129.6, 133.2, 133.5, 137.0, 213.4, 214.8. MS (EI), *m/z* (%): 552 (10) $[\text{M}]^+$, 468 (10) $[\text{M} - 3\text{CO}]^+$, 440 (30) $[\text{M} - 4\text{CO}]^+$, 412 (25) $[\text{M} - 5\text{CO}]$, 356 (5) $[\text{M} - 7\text{CO}]$, 328 (100) $[\text{M} - 8\text{CO}]$. IR (heptane): $\nu(\text{CO})$: 2072 (m), 1995 (m), 1980 (s), 1935 (s) cm^{-1} . Elemental analysis ($\text{C}_{20}\text{H}_{10}\text{S}_2\text{O}_8\text{Mn}_2$, 552 g mol^{-1}): calcd. C 43.47, H 1.8, S 11.58; found C 44.12, H 1.87, S 12.05.

$[\text{Mn}(\text{CO})_4(\mu\text{-SC}_6\text{H}_4\text{-4-Me})]_2$ (**5**)

The synthesis of **5** is analogous to the one of complex **4** via the reaction of $[\text{Mn}_2(\text{CO})_{10}]$ (370 mg, 0.948 mmol), with di-*p*-tolylidyl disulfide (1168.8 mg, 4.7 mmol) in 50 mL heptanes (mixture of isomers). Then the solution was irradiated for 3 h and a yellow solid precipitated. After the suspension was filtered

(Caution: the solid is very unstable), the filtrate was collected and stored at -18°C giving a mixture of crystalline products. Furthermore, pure complex **5** was obtained by reduction of the mother liquor to dryness and subsequent washing of the residue with *n*-hexane. An orange powder (150 mg, 0.26 mmol, 27.2%) of $[\text{Mn}(\text{CO})_4(\text{SC}_6\text{H}_4\text{-}p\text{-Me})_2]$ (**5**) was isolated. ^1H NMR: (400MHz/ $[\text{D}_8]$ THF): δ = 2.30 [s, 6H, CH_3 tolyl], 7.13 [AA' part of an AA'BB' spin system, 4H, *m*-CH], 7.52 [BB' part, 4H, *o*-CH]. ^{13}C NMR (400 MHz/ $[\text{D}_8]$ THF): 20.9, 130.5, 133.2, 133.3, 137.6, 213.6, 215. MS (EI), *m/z* (%): 580 (5) $[\text{M}-2\text{H}]^+$, 523 (10) $[\text{M}-2\text{H}-2\text{CO}]^+$, 496 (5) $[\text{M}-2\text{H}-3\text{CO}]^+$, 468 (20) $[\text{M}-2\text{H}-4\text{CO}]^+$, 440 (10) $[\text{M}-2\text{H}-5\text{CO}]^+$, 356 (100) $[\text{M}-2\text{H}-8\text{CO}]^+$. IR (pure), $\nu(\text{CO})$: 2080 (w), 2026 (m), 1992 (m), 1944 (m) cm^{-1} . Elemental analysis ($\text{C}_{22}\text{H}_{16}\text{S}_2\text{O}_8\text{Mn}_2$, 582 g mol^{-1}): calcd. C 45.53, H 2.42, S 11.05; found C 45.82, H 2.65, S 10.08. As secondary products $[\text{Mn}(\text{CO})_3(\text{SC}_6\text{H}_3\text{Me-}o\text{-SC}_6\text{H}_4\text{Me})_2]$ (**8**) and $[\text{Mn}(\text{CO})_3(\text{SC}_6\text{H}_4\text{-}4\text{-Me})_4]$ (**9**) have been identified. The compound $[\text{Mn}(\text{CO})_3(\text{SC}_6\text{H}_3\text{Me-}o\text{-SC}_6\text{H}_4\text{Me})_2]$ crystallized directly in the filtrate of the reaction at -18°C; X-ray diffraction studies have defined the molecular structure of this compound. ^1H NMR: (400 MHz/ $[\text{D}_8]$ THF): 2.32, 2.36, 7.29, 7.43 and 7.49 ppm.

$[\text{Mn}(\text{CO})_4(\mu\text{-SC}_6\text{H}_4\text{-}4\text{-OMe})_2]$ (6**)**

The reaction was carried starting from 500 mg (1.28 mmol) of $[\text{Mn}_2(\text{CO})_{10}]$, and 1080 mg (3.8 mmol) of di-*p*-methoxyphenyl disulfide in 30 mL heptane. The mixture was stirred for 5 min. which leads to a dissolution of the starting materials resulting in a yellow solution. Subsequently, the solution was then irradiated for 1h and a yellow solid was precipitate which was removed by

filtration (Caution: the solid is very unstable). The filtrate was collected and stored at 6 °C, yielding 240 mg (0.39 mmol, 30.6%) of red crystals. Decomposition above 93°C (without melting). ¹H NMR: (400 MHz/[D₈]THF): 3.76 [s, 6H, OCH₃], 6.89 [d, *J*= 5.16 Hz AA' part of an AA'BB' spin system, 4H, *m*-CH], 7.55 [BB' part, 4H, *o*-CH]. ¹³C NMR (400 MHz/[D₈]THF): 55.32, 115.26, 126.33, 134.26, 159.98, 213.3, 215.08. MS (EI), *m/z* (%): 500 (10) [M - 4CO], 472 (5) [-5CO], 390 (50) [M - 8CO]. IR (nujol), ν (CO): 2072 (m), 1995 (m), 1986 (m) 1942 (m) Elemental analysis (C₂₂H₁₄O₁₀S₂Mn₂ 612 g mol⁻¹): calcd. C 43.15 H 2.30 S 10.47; found C 43.41, H 3.32, S 8.72.

[Mn(CO)₄(SC₆H₄-4-Cl)]₂ (7)

The ligand bis(*p*-chlorophenyl) disulfide was prepared starting from 418 mg (2.89 mmol) of *p*-Chlorophenylthiol in 2.5 mL of DMF and 293 mg of Et₃N (2.89 mmol). The reaction mixture was stirred at 40 °C for 5 min in an ultrasonic bath Sonorex Super Digital-DK 102, ultrasonic frequency 35 KHz. The product was extracted with Et₂O/H₂O (1:3); the solvent was removed under vacuum till a dry residue remained. Yield: 381 mg (1.32 mmol, 91.7 %) Decomposition above 90°C (without melting). ¹H NMR: (400 MHz/CDCl₃): 7.25 [AA' part of an AA'BB' spin system, 4H, *m*-CH,], 7.38 [BB' part, 4H, *o*-CH]. ¹³C NMR (400 MHz/[D₈]CDCl₃): 129.3, 129.35, 133.6, 135.15. MS (EI), *m/z* (%): 286 (50) [M]⁺, 143 (100) [M - C₆H₄ClS]⁺. Elemental analysis (C₁₂H₈S₂Cl₂ 286 g mol⁻¹): calcd. C 50.18, H 2.80, S 22.32; found C 50.14, H 3.02, S 22.32.

To a solution of the ligand bis(*p*-chlorophenyl) disulfide (617 mg, 2.15 mmol) in 15 mL heptane was added a stirred solution of $[\text{Mn}_2(\text{CO})_{10}]$ (210 mg, 0.53 mmol) in 15 mL heptanes, resulting a yellow solution which was irradiated for 2 h leading to a yellow solid precipitate. The suspension was filtered and an orange filtrate collected. Afterwards the filtrate was stored at -18°C . After one week afforded orange crystals suitable for X-ray crystallography. Yield: 163 mg (0.26 mmol, 49%). Decomposition above 90°C (without melting). ^1H NMR: (400 MHz/ $[\text{D}_8]$ THF): 7.36 [AA' part of an AA'BB' spin system, 4H, *m*-CH], 7.6 [BB' part, 4H, *o*-CH]. ^{13}C NMR (400 MHz/ $[\text{D}_8]$ THF): 129.7, 133.5, 134.5, 135.8, 212.9, 214.4. MS (EI), *m/z* (%): 536 (5) $[\text{M}-3\text{CO}]^+$, 508 (20) $[\text{M}-4\text{CO}]^+$, 480 (15) $[\text{M}-5\text{CO}]^+$, 395 (100) $[\text{M}-8\text{CO}]$. IR (heptane) $\nu(\text{CO})$: 2083 (s), (s), 1991 (s), 1979 (m), 1955 (s). Elemental analysis: ($\text{C}_{20}\text{H}_8\text{Cl}_2\text{O}_8\text{S}_2\text{Mn}_2$, 621 g mol $^{-1}$): calcd. C 38.67, H 1.29, S 10.32; found C 39.24, H 1.37, S 10.45

$[\text{Mn}(\text{CO})_3(\text{SC}_6\text{H}_3\text{Me-}o\text{-SC}_6\text{H}_4\text{Me})]_2$ (8)

(See synthesis of 5)

Method B: Salt metathesis reactions of $[\text{BrMn}(\text{CO})_5]$ with potassium thiophenolates

$[\text{Mn}(\text{CO})_3(\mu\text{-SC}_6\text{H}_4\text{-4-Me})]_4$ (9) and $[\text{Mn}(\text{CO})_4(\mu\text{-SC}_6\text{H}_4\text{-4-Me})]_2$ (5)

A solution of $\text{HSC}_6\text{H}_4\text{-}p\text{-CH}_3$ (343 mg, 2.76 mmol) and $[\text{KN}(\text{Si}(\text{CH}_3)_3)_2]$ (550 mg, 2.76 mmol) in 30 mL of toluene was stirred at room temperature for 6 h to give a white precipitate (435 mg, 2.68 mmol 97%) of potassium 4-methylphenylthiolate. Decomposition above 180.6°C (without melting). ^1H NMR: (200 MHz/ $[\text{D}_7]$ DMF): 2.05 [s, 3H CH_3]; 6.48 [AA' part of an AA'BB'

spin system, 2H, *m*-CH]; 7.12 [BB' part, 2H, *o*-CH]. ^{13}C NMR (200 MHz / $[\text{D}_7]\text{DMF}$): 20.7; 124.4; 127.6; 133.8; 157.4.

To a suspension of 95 mg (0.59 mmol) of potassium *p*-methylphenylthiolate in 20 mL of THF, 163 mg (0.59 mmol) of $[\text{BrMn}(\text{CO})_5]$ was added. The mixture was stirred at room temperature for 18 h to give an orange solution containing a white solid (KBr), which was collected. All volatiles were removed under vacuum and the dry residue was recrystallized from 10 mL of *n*-hexane at 5°C leading to two crystal structures, the dinuclear complex $[\text{Mn}(\text{CO})_4(\text{SC}_6\text{H}_4\text{-}p\text{-CH}_3)]_2$ (**5**). ^1H NMR: (400 MHz/ $[\text{D}_8]\text{THF}$): 2.30 [s, 6H CH₃], 7.14 [AA' part of an AA'BB' spin system, 4H, *m*-CH], 7.51 [BB' part, 4H, *o*-CH]. ^{13}C NMR (400 MHz/ $[\text{D}_8]\text{THF}$): 20.7, 130.3, 133, 133.1, 137.4, 213.3, 214.9. IR (pure) $\nu(\text{CO})$: 2077 (w), 1991 (m), 1957 (m), 1940 (m). The tetranuclear complex $[\text{Mn}(\text{CO})_3(\text{SC}_6\text{H}_4\text{-}p\text{-CH}_3)]_4$ (**9**): ^1H NMR: (400 MHz/ $[\text{D}_8]\text{THF}$): 2.38 [s, 12H CH₃], 7.37 [AA' part of an AA'BB' spin system, 8H, *m*-CH], 8.02 [BB' part, 8H, *o*-CH] ^{13}C NMR (400 MHz/ $[\text{D}_8]\text{THF}$): 20.9, 130, 131.1, 131.8, 140, 221.

$[(\text{CO})_4\text{Mn}(\mu\text{-SC}_6\text{H}_2\text{2,4,6-CH}_3)]_3$ (10**)**

298 mg (1.50 mmol) of potassium bis(trimethylsilyl)amide and 300 mg (1.97 mmol) of 2,4,6-trimethylphenylthiol in 20 mL of toluene were stirred at room temperature for 2 h to give a white precipitate. Decomposition above 224,8 °C (without melting). ^1H NMR (400MHz/ $[\text{D}_8]\text{THF}$): δ = 2.09 [s, 3H]; 2.36 [s, 6H]; 6.64 [s, 2H]. ^{13}C (400 MHz/ $[\text{D}_8]\text{THF}$): δ = 18.9, 20.8, 126, 127.4, 130.3 138.8 150. Subsequently 80 mg (0.42 mmol) of product and 130 mg (0.47 mmol) of

[BrMn(CO)₅] were suspended in 20 mL of THF and stirred at room temperature for 24 h. A orange solution formed, containing a white solid (KBr), which was removed by filtration. The filtrate was distilled under vacuum to drynes and the orange residue was recrystallized from 5 mL of *n*-hexane at 5 °C yielding 45 mg (0.047 mmol, 30%) of red crystals. Decomposition above 105 °C ¹H NMR: (400MHz/[D₈]THF) showed three different signal groups due to instability in solution: δ = {A = 2.16 [s]; 2.52 [s] 6.82 [s]}; {B = 2.19 [s]; 2.84[s]; 6.92 [s]}; {C = 2.28 [s]; 2.79 [s]; 6.89 [s]}. ¹³C NMR (400 MHz/[D₈]THF): δ = 21.4; 23.1; 129.1; 129.6 IR in Nujol ν(CO): 2080(m); 2001(s); 1970(m); 1952(m); 1922(w) cm⁻¹.

[Mn(CO)₄(μ-SC₆H₄-4-CF₃)₂ (11) and [Mn(CO)₃(μ-SC₆H₄ 4-CF₃)₄ (12)

672 mg (3.36mmol) of [KN(Si(CH₃)₃)₂] suspended in 25 mL of toluene was mixed with a solution of HSC₆H₄-*p*-CF₃ (600 mg, 2.76 mmol) in 5 mL of toluene. The resulting mixture was stirred at room temperature for 18 h to give a white precipitate of potassium *p*-trifluormethyl phenylthiolate. The ligand was filtered off, intensely washed with toluene, and finally dried in vacuum. Yield: 633 mg (2.93 mmol, 87%) ¹H NMR: (200 MHz/[D₈]THF): 6.88 [AA' part of an AA'BB' spin system, 2H, *m*-CH]; 7.32 [BB' part, 2H, *o*-CH]; ¹³C NMR (200 MHz/[D₈]THF): δ = 123.2; 123.3; 123.37; 123.4; 133.9.

A suspension of 188 mg (0.87 mmol) of potassium *p*-trifluormethylphenylthiolate in 30 mL of THF was added to 246 mg (0.87 mmol) of [BrMn(CO)₅]. The mixture was stirred at room temperature for 18 h to give an orange solution containing a white solid (KBr), which was removed by filtration. After removing the volatile components in vacuum the crude product

was obtained as orange powder. This was redissolved twice in *n*-hexane (5 mL) and stored at 6°C giving a mixture of two different crystalline products, the dinuclear complex **11**. ^1H NMR: (400 MHz/[D₈]THF): δ = 7.66 [AA' part of an AA'BB' spin system, 4H, *m*-CH], 7.81 [BB' part, 4H, *o*-CH]. ^{13}C NMR (400 MHz/[D₈]THF): δ = 126, 129, 130.2, 133.5, 143, 212.9, 214 IR (pure) $\nu(\text{CO})$: 2083 (w); 2023 (m), 1994 (s), 1936 (s) cm^{-1} . The tetranuclear complex **12** ^1H NMR (400 MHz/[D₈]THF): δ = 8.00 [AA' part of an AA'BB' spin system, 8H, *m*-CH]; 8.32 [BB' part, 8H, *o*-CH]. ^{13}C NMR (400 MHz/[D₈]THF): δ = 124.5; 127; 132; 134.3; 150; 220.

Method C: Substitution reactions between [BrMn(CO)₅] and thiols

[Mn(CO)₃(μ -SC₆H₅)₄] (14)

To a suspension of 300 mg (1.09 mmol) of [BrMn(CO)₅] in 25 mL of methanol, 120 mg (1.09 mmol) of HSC₆H₅ was added. The reaction mixture was stirred and heated under reflux for three hours; during this reaction time an orange suspension formed. The solid was collected and the filter cake dried in vacuum giving pure orange microcrystalline **14**. Yield: 270 mg (0.183 mmol, 67.25%) Decomposition above (without melting) 172,2°C ^1H NMR (400 MHz/[D₈]THF): δ = 7.48 [m, (broad), 4H, *p*-CH] 7.57 [m, (broad), 8H, *m*-CH], 8.16 [d, *J*= 7.08 Hz, 8H]. ^{13}C (400 MHz/[D₈]THF): δ = 129.6, 130.4, 131.8, 133.4, 220.9. MS (EI), *m/z* (%) 992 (10)[M]⁺, 908 (30) [M -3CO]⁺, 824 (10) [M -6CO]⁺, 796 (20) [M -7CO]⁺, 768 (30) [M -8CO]⁺, 740 (50) [M -9CO]⁺, 712 (15) [M -10CO]⁺, 656 (30) [M -12CO]⁺ IR (pure) $\nu(\text{CO})$: 2010 (s), 1943(s), cm^{-1} . Elemental analysis: (C₃₆H₂₀S₄O₁₂Mn₄ 992 g mol⁻¹): calcd. C 43.56, H 2.02, S 12.92, found. C 43.77, H 1.92, S 12.84.

[Mn(CO)₃(μ-SC₆H₄-4-Me)]₄ (9)

The ligand HSC₆H₄CH₃-*p* (130 mg, 1 mmol) was stirred in 10 mL of methanol followed by the addition of a solution of [BrMn(CO)₅] (207 mg, 0.75 mmol) in 20 mL methanol. The reaction mixture was vigorously stirred and heated at 80 °C (bath temperature) for 4 h. After cooling (r.t.), the solvent volume was reduced to about 5 mL, the product **3** precipitated immediately as an orange microcrystal. Yield 188 mg (0.180 mmol, 95%). Decomposition above 200 °C (without melting). ¹H NMR (400 MHz/[D₈]THF): 2.38 [s, 12H], 7.37 [AA' part of an AA'BB' spin system, 2H, *m*-CH], 8.02 [BB' part, 2H, *o*-CH]. ¹³C NMR (400 MHz/[D₈]THF): 20.9, 130, 131.1, 131.8, 140, 221. MS (EI), *m/z* (%): 1048 (10) [M]⁺, 964 (100) [M -3CO]⁺, 880 (5) [M -6CO], 852 (10) [M -7CO]⁺, 824 (40) [M -8CO]⁺, 796 (80) [M -9CO]⁺, 768 (20) [M -10CO]⁺, 712 (30) [M -12CO]⁺. IR (pure), ν(CO): 2012, 1920. Elemental analysis: (C₄₀H₂₈O₁₂S₄Mn₄ 1048 g mol⁻¹): calcd. C 45.81, H 2.69, S 12.23; found. C 44.92, H 2.46, S 10.73.

[Mn(CO)₃(μ-SC₆H₄-4-OMe)]₄ (15)

To a vigorously stirred suspension of [BrMn(CO)₅] (199 mg, 0.72 mmol) in 20 mL of methanol a solution of HSC₆H₄-*p*-OCH₃ (102 mg, 0.72 mmol) in 5 mL of methanol was added. The heated under reflux for three hours led the formation of orange microcrystalline product **15**. The solid was collected and dried in vacuum. Yield: 147 mg (0.128 mmol, 73%) Decomposition above 220 °C (without melting). ¹H NMR(400 MHz/[D₈]THF): δ = 3.85 [s, 12H], 7.13 [AA' part of an AA'BB' spin system, 8H, *m*-CH], 8.05 [d, , BB' part, 8H, *o*-CH]. ¹³C NMR (400 MHz/[D₈]THF): δ = 55.61, 116, 123, 133, 161, 221. MS (EI), *m/z* (%): 1028 (100) [M -3CO]⁺, 998 (10) [M -4CO]⁺, 944 (20) [M -6CO]⁺, 916 (25)

$[M - 7CO]^+$, 888 (30) $[M - 8CO]^+$, 860 (80) $[M - 9CO]^+$, 832 (25) $[M - 10CO]^+$, 776 (25) $[M - 12CO]^+$. IR (pure) $\nu(CO)$: 2015 (m), 1921(m). Elemental analysis: ($C_{40}H_{28}O_{16}S_4Mn_4$ 1112 g mol⁻¹): calcd. C 43.18, H 2.54, S 11.53; found. C 42.47, H 2.39, S 11.33

$[Mn(CO)_3(\mu-SC_6H_4-4-Cl)]_4$ (16)

375 mg (1.36 mmol) of $BrMn(CO)_5$ and 200 mg (1.38 mmol) of HSC_6H_4Cl-p in 25 mL methanol were stirred under reflux for three hours, during this reaction time an orange suspension was formed. The solid was collected and the filter cake dried in vacuum giving pure orange microcrystalline **16**. Yield 266 mg (0.235 mmol, 69.2%). Decomposition above 120 °C (without melting). ¹H NMR (400 MHz/[D₈]THF): δ = 7.6 [AA' part of an AA'BB' spin system, 2H, *m*-CH], 8.1 [BB' part, 2H, *o*-CH] ¹³C NMR (400 MHz/[D₈]THF): δ = 130.9, 131.8, 133.3, 136.2, 2, 220.7. MS (EI): *m/z* (%) 1046 (100) $[M - 3CO]^+$, 962 (5) $[M - 6CO]^+$, 935 (15) $[M - 7CO]^+$, 906 (30) $[M - 8CO]^+$, 794 (5) $[M - 12CO]^+$ IR (pure) $\nu(CO)$: 2017 (s), 1926 (vs). Elemental analysis: ($C_{36}H_{16}Cl_4O_{12}S_4Mn_4$ 1130 g mol⁻¹): calcd. C 38.25, H 1.43, S 11.35 found. C 36.55, H 1.22, S 10.82. By the oxidation of **16** with HBr during preparation and trace amounts of THF, it allowed the formation of a second product $[Mn_6(CO)_{18}(\mu-SC_6H_4-4-Cl)_8\{Mn_2(\mu-Br)_2(THF)\}]$ (**17**). X-ray diffraction studies have defined the molecular structure of the novel compound.

5.4 Quantification of CO release (Myoglobin assay)

CO release was measured spectrophotometrically based on absorbance changes upon conversion of deoxymyoglobin (Mb) to the myoglobine-CO complex (Mb-CO). A myoglobin solution (horse skeletal muscle myoglobin, Sigma) in phosphate buffered saline (PBS) was converted to deoxymyoglobin by addition of 0.1% sodium dithionite. Difference spectra for Mb with and without CORMs were measured in the range of 500-600 nm (Ru-complexes) or 380-460 (Mn-complexes). Spectra in the absence of CO and in CO-saturated solution were recorded to calculate the maximal absorbance difference, required to convert absorbance changes to relative CO release. The time course of CO release from CORMs was monitored by measuring the absorbance at 424 nm. To test the dependency of CO release from light, myoglobin, or dithionite, the solutions of the manganese complexes were preincubated for 5 min under different conditions. For illumination a cold light source (20 W halogen lamp, Osram GZX4) with a light guide was used yielding 2 W output power placed 2 cm above the cuvette.

Appendix

A.1 Crystallographic Details

Crystallographic data and structure refinement parameters for complex
[Ru(SC₂H₄NH₂)₂(CO)₂] (1)

Empirical formula	C ₆ H ₈ N ₂ O ₂ RuS ₂ ·C ₄ H ₈ O
Formula weight (g mol ⁻¹)	377.44
Crystal system	monoclinic
Space group	<i>P</i> 2 ₁ / <i>n</i>
<i>a</i> [Å]	16.5181(6)
<i>b</i> [Å]	9.7343(3)
<i>c</i> [Å]	20.1750(8)
α [°]	90.00
β [°]	111.248
γ [°]	90.00
<i>V</i> [Å ³]	3023.46(19)
<i>Z</i>	8
Crystal size [mm]	0.05 x 0.05 x 0.02
<i>D</i> _{calcd} [g cm ⁻³]	1.658
μ [cm ⁻¹]	13.14
θ range of data collection [°]	2.36 < θ < 27.54
measured reflections	17299
unique reflections/ <i>R</i> _{int}	6854/0.0588
goodness-of-fit on <i>F</i> ²	1.117
<i>R</i> indices (all data) ^[a]	<i>R</i> ₁ = 0.0795, <i>wR</i> ₂ = 0.1172
final <i>R</i> indices (<i>I</i> > 2 σ (<i>I</i>)) ^[a]	<i>R</i> ₁ = 0.0559, <i>wR</i> ₂ = 0.1061

[a] $R_1 = (\sum||F_o| - |F_c||)/\sum|F_o|$; $wR_2 = \{\sum[w(F_o^2 - F_c^2)^2]\}^{1/2}$

Crystallographic data and structure refinement parameters for complex
 [Ru(CO)₂(SC₆H₄-2-NH₂)₂] (**2**)

Empirical formula	C ₁₄ H ₁₂ N ₂ O ₂ RuS ₂ ·2C ₃ H ₇ NO
Formula weight (g mol ⁻¹)	551.64
Crystal system	monoclinic
Space group	<i>P</i> 2 ₁ / <i>n</i>
<i>a</i> [Å]	5.6470(1)
<i>b</i> [Å]	20.4208(3)
<i>c</i> [Å]	22.3020(3)
α [°]	90.00
β [°]	90.743
γ [°]	90.00
<i>V</i> [Å ³]	2571.57(7)
<i>Z</i>	4
Crystal size [mm]	0.05 x 0.03 x 0.03
<i>D</i> _{calcd} [g cm ⁻³]	1.519
μ [mm ⁻¹]	0.809
θ range of data collection [°]	2.92 < θ < 27.47
measured reflections	13093
unique reflections/ <i>R</i> _{int}	5584/0.0256
goodness-of-fit on <i>F</i> ²	1.152
<i>R</i> indices (all data) ^[a]	<i>R</i> ₁ = 0.0659, <i>wR</i> ₂ = 0.1183
final <i>R</i> indices (<i>I</i> > 2 σ (<i>I</i>)) ^[a]	<i>R</i> ₁ = 0.0571, <i>wR</i> ₂ = 0.1135

$$[a] R_1 = (\sum||F_o| - |F_c||)/\sum|F_o|; wR_2 = \{\sum[w(F_o^2 - F_c^2)^2]\}^{1/2}$$

Crystallographic data and structure refinement parameters for complex
 [Ru₂(CO)₅(adamantyl-APE)] (**3**)

Empirical formula	C ₄₀ H ₄₇ N ₄ O ₆ Ru ₂
Formula weight (g mol ⁻¹)	881.96
Crystal system	orthorhombic
Space group	<i>Pnma</i>
<i>a</i> [Å]	17.4863(7)
<i>b</i> [Å]	18.0512(8)
<i>c</i> [Å]	11.7497(4)
α [°]	90.00
β [°]	90.00
γ [°]	90.00
<i>V</i> [Å ³]	3708.8(3)
<i>Z</i>	4
Crystal size [mm]	0.04 x 0.04 x 0.04
<i>D</i> _{calcd} [g cm ⁻³]	1.580
μ [cm ⁻¹]	8.67
θ range of data collection [°]	3.08 < θ < 27.50
measured reflections	22747
unique reflections/ <i>R</i> _{int}	4374/0.0864
goodness-of-fit on <i>F</i> ²	1.056
<i>R</i> indices (all data) ^[a]	<i>R</i> ₁ = 0.0995, <i>wR</i> ₂ = 0.1971
final <i>R</i> indices (<i>I</i> > 2 σ (<i>I</i>)) ^[a]	<i>R</i> ₁ = 0.0637, <i>wR</i> ₂ = 0.1725

$$[a] R_1 = (\sum||F_o| - |F_c||)/\sum|F_o|; wR_2 = \{\sum[w(F_o^2 - F_c^2)^2]\}^{1/2}$$

Crystallographic data and structure refinement parameters for complex
 [Ru₂(CO)₅(adamantyl-APE)] (**3B**)

Empirical formula	C _{39.25} H _{44.50} Cl _{4.50} N ₄ O ₅ Ru ₂
Formula weight (g mol ⁻¹)	1013.95
Crystal system	monoclinic
Space group	<i>P</i> 2 ₁ / <i>c</i>
<i>a</i> [Å]	17.3317(4)
<i>b</i> [Å]	26.2217(4)
<i>c</i> [Å]	19.7974(6)
α [°]	90.00
β [°]	100.1140
γ [°]	90.00
<i>V</i> [Å ³]	8857.4(4)
<i>Z</i>	8
Crystal size [mm]	0.04 x 0.04 x 0.03
<i>D</i> _{calcd} [g cm ⁻³]	1.521
μ [cm ⁻¹]	9.98
θ range of data collection [°]	2.22 < θ < 27.46
measured reflections	55231
unique reflections/ <i>R</i> _{int}	20171/0.1072
goodness-of-fit on <i>F</i> ²	1.046
<i>R</i> indices (all data) ^[a]	<i>R</i> ₁ = 0.1630, <i>wR</i> ₂ = 0.2613
final <i>R</i> indices (<i>I</i> > 2 σ (<i>I</i>)) ^[a]	<i>R</i> ₁ = 0.0827, <i>wR</i> ₂ = 0.2191

$$[a] R_1 = (\sum||F_o| - |F_c||)/\sum|F_o|; wR_2 = \{\sum[w(F_o^2 - F_c^2)^2]\}^{1/2}$$

Crystallographic data and structure refinement parameters for complex
 $[\text{Mn}(\text{CO})_4(\mu\text{-SC}_6\text{H}_5)]_2$ (**4**)

Empirical formula	$\text{C}_{20}\text{H}_{10}\text{Mn}_2\text{O}_8\text{S}_2$
Formula weight (g mol^{-1})	552.28
Crystal system	triclinic
Space group	$P\bar{1}$
a [\AA]	7.6194(15)
b [\AA]	17.821(4)
c [\AA]	18.031(4)
α [$^\circ$]	61.35(3)
β [$^\circ$]	89.77(3)
γ [$^\circ$]	78.61(3)
V [\AA^3]	2094.7(7)
Z	4
Crystal size [mm]	0.05 x 0.05 x 0.05
D_{calcd} [g cm^{-3}]	1.751
μ [cm^{-1}]	14.51
θ range of data collection [$^\circ$]	$1.33 < \theta < 27.48$
measured reflections	14676
unique reflections/ R_{int}	8898/0.3051
goodness-of-fit on F^2	1.112
R indices (all data) ^[a]	$R_1 = 0.1964, wR_2 = 0.4680$
final R indices ($I > 2\sigma(I)$) ^[a]	$R_1 = 0.0827, wR_2 = 0.2191$

$$[\text{a}] R_1 = (\sum||F_o| - |F_c||)/\sum|F_o|; wR_2 = \{\sum[w(F_o^2 - F_c^2)^2]\}^{1/2}$$

Crystallographic data and structure refinement parameters for complex
 $[\text{Mn}(\text{CO})_4(\mu\text{-SC}_6\text{H}_4\text{-4-CH}_3)_2]$ (**5**)

Empirical formula	$\text{C}_{22}\text{H}_{14}\text{Mn}_2\text{O}_8\text{S}_2$
Formula weight (g mol^{-1})	580.33
Crystal system	triclinic
Space group	$P\bar{1}$
a [\AA]	9.6294(5)
b [\AA]	11.8965(6)
c [\AA]	12.0584(5)
α [$^\circ$]	116.375(2)
β [$^\circ$]	90.353(3)
γ [$^\circ$]	108.027(2)
V [\AA^3]	1159.97(10)
Z	2
Crystal size [mm]	0.06 x 0.05 x 0.04
D_{calcd} [g cm^{-3}]	1.662
μ [mm^{-1}]	1.315
θ range of data collection [$^\circ$]	$2.75 < \theta < 27.44$
measured reflections	7115
unique reflections/ R_{int}	5000/0.0247
goodness-of-fit on F^2	1.145
R indices (all data) ^[a]	$R_1 = 0.0559, wR_2 = 0.1016$
final R indices ($I > 2\sigma(I)$) ^[a]	$R_1 = 0.0449, wR_2 = 0.0965$

$$[\text{a}] R_1 = (\sum||F_o| - |F_c||)/\sum|F_o|; wR_2 = \{\sum[w(F_o^2 - F_c^2)^2]\}^{1/2}$$

Crystallographic data and structure refinement parameters for complex
 $[\text{Mn}(\text{CO})_4(\mu\text{-SC}_6\text{H}_4\text{-4-OMe})_2]$ (**6**)

Empirical formula	$\text{C}_{22}\text{H}_{14}\text{Mn}_2\text{O}_{10}\text{S}_2$
Formula weight (g mol^{-1})	612.33
Crystal system	monoclinic
Space group	$P2_1/c$
a [\AA]	10.5593(3)
b [\AA]	9.4284(3)
c [\AA]	12.5227(3)
α [$^\circ$]	90
β [$^\circ$]	102.598(2)
γ [$^\circ$]	90
V [\AA^3]	1216.71(6)
Z	2
Crystal size [mm]	0.06 x 0.05 x 0.02
D_{calcd} [g cm^{-3}]	1.671
μ [mm^{-1}]	1.264
θ range of data collection [$^\circ$]	$2.73 < \theta < 27.54$
measured reflections	7160
unique reflections/ R_{int}	2791/0.0291
goodness-of-fit on F^2	1.096
R indices (all data) ^[a]	$R_1 = 0.0323, wR_2 = 0.0654$
final R indices ($I > 2\sigma(I)$) ^[a]	$R_1 = 0.0279, wR_2 = 0.0635$

$$[\text{a}] R_1 = (\sum||F_o| - |F_c||)/\sum|F_o|; wR_2 = \{\sum[w(F_o^2 - F_c^2)^2]\}^{1/2}$$

Crystallographic data and structure refinement parameters for complex
 $[\text{Mn}(\text{CO})_4(\mu\text{-SC}_6\text{H}_4\text{-4-Cl})_2]$ (7)

Empirical formula	$\text{C}_{20}\text{H}_8\text{Cl}_2\text{Mn}_2\text{O}_8\text{S}_2$
Formula weight (g mol^{-1})	621.16
Crystal system	triclinic
Space group	$P\bar{1}$
a [Å]	8.2467(3)
b [Å]	8.8721(3)
c [Å]	9.5582(3)
α [°]	66.959(2)
β [°]	66.175(2)
γ [°]	65.853(1)
V [Å ³]	561.93(3)
Z	1
Crystal size [mm]	0.06 x 0.05 x 0.05
D_{calcd} [g cm^{-3}]	1.836
μ [mm^{-1}]	1.594
θ range of data collection [°]	$3.04 < \theta < 27.52$
measured reflections	3755
unique reflections/ R_{int}	2554/0.0150
goodness-of-fit on F^2	1.086
R indices (all data) ^[a]	$R_1 = 0.0260, wR_2 = 0.0594$
final R indices ($I > 2\sigma(I)$) ^[a]	$R_1 = 0.0246, wR_2 = 0.0579$

$$[\text{a}] R_1 = (\sum||F_o| - |F_c||)/\sum|F_o|; wR_2 = \{\sum[w(F_o^2 - F_c^2)^2]\}^{1/2}$$

Crystallographic data and structure refinement parameters for complex
 $[\text{Mn}(\text{CO})_3(\text{SC}_6\text{H}_3\text{Me-o-SC}_6\text{H}_4\text{Me})_2]$ (**8**)

Empirical formula	$\text{C}_{34}\text{H}_{26}\text{Mn}_2\text{O}_6\text{S}_4$
Formula weight (g mol^{-1})	768.67
Crystal system	monoclinic
Space group	$C/2c$
a [\AA]	23.9640(15)
b [\AA]	12.8427(8)
c [\AA]	13.5112(9)
α [$^\circ$]	90
β [$^\circ$]	110.910(4)
γ [$^\circ$]	90
V [\AA^3]	3884.4(4)
Z	4
Crystal size [mm]	0.06 x 0.05 x 0.05
D_{calcd} [g cm^{-3}]	1.314
μ [mm^{-1}]	0.903
θ range of data collection [$^\circ$]	$2.64 < \theta < 27.44$
measured reflections	11081
unique reflections/ R_{int}	4369/0.0542
goodness-of-fit on F^2	1.145
R indices (all data) ^[a]	$R_1 = 0.1052, wR_2 = 0.2194$
final R indices ($I > 2\sigma(I)$) ^[a]	$R_1 = 0.0742, wR_2 = 0.1994$

$$[\text{a}] R_1 = (\sum ||F_o| - |F_c||) / \sum |F_o|; wR_2 = \{\sum [w(F_o^2 - F_c^2)^2]\}^{1/2}$$

Crystallographic data and structure refinement parameters for complex
 $[\text{Mn}(\text{CO})_3(\mu\text{-SC}_6\text{H}_4\text{-4-CH}_3)]_4 \cdot [\text{Mn}(\text{CO})_4(\mu\text{-SC}_6\text{H}_4\text{-4-CH}_3)]_2$ (**9**)

Empirical formula	$\text{C}_{62}\text{H}_{42}\text{Cl}_2\text{Mn}_6\text{O}_{20}\text{S}_6$
Formula weight (g mol^{-1})	1628.96
Crystal system	monoclinic
Space group	$P2_1/c$
a [\AA]	12.2008(3)
b [\AA]	31.5255(7)
c [\AA]	18.3025(4)
α [$^\circ$]	90
β [$^\circ$]	106.572(1)
γ [$^\circ$]	90
V [\AA^3]	6747.4(3)
Z	4
Crystal size [mm]	0.05 x 0.05 x 0.04
D_{calcd} [g cm^{-3}]	1.604
μ [mm^{-1}]	1.346
θ range of data collection [$^\circ$]	$2.21 < \theta < 27.50$
measured reflections	38279
unique reflections/ R_{int}	15345/0.0963
goodness-of-fit on F^2	1.180
R indices (all data) ^[a]	$R_1 = 0.1314, wR_2 = 0.1620$
final R indices ($I > 2\sigma(I)$) ^[a]	$R_1 = 0.0902, wR_2 = 0.1505$

[a] $R_1 = (\sum||F_o| - |F_c||)/\sum|F_o|$; $wR_2 = \{\sum[w(F_o^2 - F_c^2)^2]\}^{1/2}$

Crystallographic data and structure refinement parameters for complex
 $[\text{Mn}(\text{CO})_3(\mu\text{-SC}_6\text{H}_4\text{-4-CH}_3)]_4 \cdot (\mathbf{9B})$

Empirical formula	$\text{C}_{40}\text{H}_{28}\text{Mn}_4\text{O}_{12}\text{S}_4$
Formula weight (g mol^{-1})	1048.62
Crystal system	orthorhombic
Space group	$Pna2_1$
a [\AA]	19.3656(2)
b [\AA]	15.9446(1)
c [\AA]	14.0502(1)
α [$^\circ$]	90
β [$^\circ$]	90
γ [$^\circ$]	90
V [\AA^3]	4338.37(6)
Z	4
Crystal size [mm]	0.06 x 0.05 x 0.05
D_{calcd} [g cm^{-3}]	1.605
μ [mm^{-1}]	1.390
θ range of data collection [$^\circ$]	$2.86 < \theta < 27.48$
measured reflections	24.515
unique reflections/ R_{int}	9708/0.0165
goodness-of-fit on F^2	1.039
R indices (all data) ^[a]	$R_1 = 0.0239, wR_2 = 0.0614$
final R indices ($I > 2\sigma(I)$) ^[a]	$R_1 = 0.0245, wR_2 = 0.0619$

[a] $R_1 = (\Sigma||F_o| - |F_c||)/\Sigma|F_o|$; $wR_2 = \{\Sigma[w(F_o^2 - F_c^2)^2]\}^{1/2}$

Crystallographic data and structure refinement parameters for complex
 $[\text{Mn}(\text{CO})_4(\mu\text{-SC}_6\text{H}_2\text{-2,4,6-CH}_3)_2]$ (**10**)

Empirical formula	$\text{C}_{39}\text{H}_{33}\text{Mn}_3\text{O}_{12}\text{S}_3$
Formula weight (g mol^{-1})	954.65
Crystal system	triclinic
Space group	$P\bar{1}$
a [\AA]	8.7224(2)
b [\AA]	14.5346(6)
c [\AA]	16.5814(6)
α [$^\circ$]	103.291(1)
β [$^\circ$]	91.005(2)
γ [$^\circ$]	98.173(2)
V [\AA^3]	2022.29(12)
Z	2
Crystal size [mm]	0.05 x 0.04 x 0.04
D_{calcd} [g cm^{-3}]	1.568
μ [mm^{-1}]	1.139
θ range of data collection [$^\circ$]	$2.36 < \theta < 27.52$
measured reflections	12266
unique reflections/ R_{int}	9033/0.0255
goodness-of-fit on F^2	1.146
R indices (all data) ^[a]	$R_1 = 0.0746, wR_2 = 0.1416$
final R indices ($I > 2\sigma(I)$) ^[a]	$R_1 = 0.0572, wR_2 = 0.1330$

$$[\text{a}] R_1 = (\Sigma||F_o| - |F_c||)/\Sigma|F_o|; wR_2 = \{\Sigma[w(F_o^2 - F_c^2)^2]\}^{1/2}$$

Crystallographic data and structure refinement parameters for complex
 $[\text{Mn}(\text{CO})_4(\mu\text{-SC}_6\text{H}_4\text{-4-CF}_3)]_2$ (**11**)

Empirical formula	$\text{C}_{22}\text{H}_8\text{Mn}_2\text{O}_8\text{S}_2$
Formula weight (g mol^{-1})	688.28
Crystal system	monoclinic
Space group	$P2_1/c$
a [\AA]	11.5033(3)
b [\AA]	6.3460(2)
c [\AA]	17.4457(3)
α [$^\circ$]	90
β [$^\circ$]	101.244(1)
γ [$^\circ$]	90
V [\AA^3]	1249.09(6)
Z	2
Crystal size [mm]	0.05 x 0.05 x 0.04
D_{calcd} [g cm^{-3}]	1.830
μ [mm^{-1}]	1.270
θ range of data collection [$^\circ$]	$3.42 < \theta < 27.46$
measured reflections	7171
unique reflections/ R_{int}	2840/0.0220
goodness-of-fit on F^2	1.037
R indices (all data) ^[a]	$R_1 = 0.0312, wR_2 = 0.0683$
final R indices ($I > 2\sigma(I)$) ^[a]	$R_1 = 0.0291, wR_2 = 0.0673$

[a] $R_1 = (\sum||F_o| - |F_c||)/\sum|F_o|$; $wR_2 = \{\sum[w(F_o^2 - F_c^2)^2]\}^{1/2}$

Crystallographic data and structure refinement parameters for complex
 $[\text{Mn}(\text{CO})_3(\mu\text{-SC}_6\text{H}_4\text{-4-CF}_3)]_4$ (**12**)

Empirical formula	$\text{C}_{40}\text{H}_{14}\text{F}_{12}\text{Mn}_4\text{O}_{12}\text{S}_4$
Formula weight (g mol^{-1})	1262.51
Crystal system	monoclinic
Space group	$C2/c$
a [\AA]	10.0188(3)
b [\AA]	20.0950(5)
c [\AA]	22.9661(6)
α [$^\circ$]	90
β [$^\circ$]	97.568(1)
γ [$^\circ$]	90
V [\AA^3]	4583.4(2)
Z	4
Crystal size [mm]	0.06 x 0.06 x 0.05
D_{calcd} [g cm^{-3}]	1.830
μ [mm^{-1}]	1.369
θ range of data collection [$^\circ$]	$3.07 < \theta < 27.55$
measured reflections	13457
unique reflections/ R_{int}	5151/0.0399
goodness-of-fit on F^2	1.110
R indices (all data) ^[a]	$R_1 = 0.0439$, $wR_2 = 0.0970$
final R indices ($I > 2\sigma(I)$) ^[a]	$R_1 = 0.0367$, $wR_2 = 0.0922$

[a] $R_1 = (\sum||F_o| - |F_c||)/\sum|F_o|$; $wR_2 = \{\sum[w(F_o^2 - F_c^2)^2]\}^{1/2}$

Crystallographic data and structure refinement parameters for complex $[\text{Mn}_2(\text{CO})_6(\mu\text{-SC}_6\text{H}_4\text{-4-CF}_3)_3][\text{Mn}_4(\text{DMF})_3(\text{CO})_9(\mu\text{-SC}_6\text{H}_4\text{-4-CF}_3)_4]$ (**13**)

Empirical formula	$\text{C}_{73}\text{H}_{49}\text{F}_{21}\text{Mn}_6\text{N}_3\text{O}_{18}\text{S}_7$
Formula weight (g mol^{-1})	2209.21
Crystal system	triclinic
Space group	$P\bar{1}$
a [\AA]	14.5972(3)
b [\AA]	16.7965(3)
c [\AA]	18.1274(3)
α [$^\circ$]	88.819(1)
β [$^\circ$]	89.635(1)
γ [$^\circ$]	80.177(1)
V [\AA^3]	4378.40(14)
Z	2
Crystal size [mm]	0.06 x 0.04 x 0.04
D_{calcd} [g cm^{-3}]	1.676
μ [mm^{-1}]	1.116
θ range of data collection [$^\circ$]	$3.04 < \theta < 27.50$
measured reflections	26883
unique reflections/ R_{int}	19495/0.0247
goodness-of-fit on F^2	1.015
R indices (all data) ^[a]	$R_1 = 0.1017, wR_2 = 0.1858$
final R indices ($I > 2\sigma(I)$) ^[a]	$R_1 = 0.0780, wR_2 = 0.1717$

$$[\text{a}] R_1 = (\sum||F_o| - |F_c||)/\sum|F_o|; wR_2 = \{\sum[w(F_o^2 - F_c^2)^2]\}^{1/2}$$

Crystallographic data and structure refinement parameters for
 complex $[\text{Mn}_6(\text{CO})_{18}(\mu\text{-SC}_6\text{H}_4\text{-4-Cl})_6\{\text{Mn}_2(\mu\text{-Br})_2(\text{THF})_2\}]$ (17)

Empirical formula	$\text{C}_{70}\text{H}_{41}\text{Br}_2\text{Cl}_8\text{Mn}_8\text{O}_{20}\text{S}_8$
Formula weight (g mol^{-1})	2341.45
Crystal system	monoclinic
Space group	$C2/c$
a [\AA]	19.2988(2)
b [\AA]	18.2968(2)
c [\AA]	28.8908(3)
α [$^\circ$]	90
β [$^\circ$]	102.462(1)
γ [$^\circ$]	90
V [\AA^3]	9961.17(18)
Z	4
Crystal size [mm]	0.06 x 0.06 x 0.06
D_{calcd} [g cm^{-3}]	1.561
μ [mm^{-1}]	2.221
θ range of data collection [$^\circ$]	$1.61 < \theta < 27.49$
measured reflections	11414
unique reflections/ R_{int}	11414/0.000
goodness-of-fit on F^2	1.030
R indices (all data) ^[a]	$R_1 = 0.0843, wR_2 = 0.2072$
final R indices ($I > 2\sigma(I)$) ^[a]	$R_1 = 0.0729, wR_2 = 0.1717$

$$[\text{a}] R_1 = (\sum||F_o| - |F_c||)/\sum|F_o|; wR_2 = \{\sum[w(F_o^2 - F_c^2)^2]\}^{1/2}$$

Bibliography

- [1] Piantadosi C.A. *Antioxid. Redox Sign.* **2002**, 4, 2, 259-270
- [2] Johnson R.T., Mann B.E., Clark J.E., Foresti R., Green C., Motterlini R. *Angew. Chem.* **2003**, 115, 3850-3858
- [3] Ryter S.W., Alam J., Choi A.M. *Physiol Rev.* **2006**, 86, 583-650
- [4] Ryter S.W., Otterbein L.E., Morse D., Choi A.M. *Mol. Cell. Biochem.* **2002**, 234/235, 249-263
- [5] Miyahara S., Takahashi H.J. *Biochem.* **1971**, 69, 231-233
- [6] Wu L., Wang R. *Pharmacol. Rev.* **2005**, 57, 585-630
- [7] Romão C.C., Blättler W.A., Seixas J.D., Bernardes G. J. L. *Chem. Soc. Rev.* **2012**, 41, 3571-3583
- [8] Motterlini R., Clark J.E., Foresti R., Sarathchandra P., Mann B.E., Green C.J. *Circ. Res.* **2002**, 90, e17-e24
- [9] Sawle P., Foresti R., Mann B.E., Johnson T.R., Green C.J. and Motterlini R. *Brit J. Pharmacol.* **2005**, 145, 800-810
- [10] Megías J., Busserolles J., Alcaraz J.M. *Brit J. Pharmacol.* **2007**, 150, 977-986
- [11] Li M.H., Cha Y.N., Surh Y.J. *Biochem. Bioph. Res. Comm.* **2006**, 342, 984-990
- [12] Allanson M. and Reeve V.E. *Cancer Immunol. Immun.* **2007**, 56, 1807-1815
- [13] Taille C., El-Benna J., Lanone S., Boczkowski J., Motterlini R. *J. Biol. Chem.* **2005**, 280, 27, 25350-25360
- [14] Srisook K., Han S.S., Choi H.S., Li M.H., Ueda H., Kim C., Cha Y.M. *Biochem. Pharmacol.* **2006**, 307-318
- [15] Józkwicz A. Huk I., Nigisch A., Weigel G., Dietrich W., Motterlini R., Dulak J. *Antioxid. Redox Sign.* **2003**, 5, 2, 155-162
- [16] Vera T., Henegar J.R. Drummond H.A., Rimoldi J.M., Stec D.E. *J Am Soc Nephrol.* **2005**, 16, 950-958,
- [17] Botros F.T., Navar L.G. *Am. J. Physiol. Heart. Circ. Physiol.* **2006**, 291, H2772-H2778

- [18] Deshane J., Chen S., Caballero S, Grochot-Przeczek A, Was H, Calzi S.L., Lach R., Hock T.D., Chen B, Hill-Kaptureczak N., Siegal G.P., Dulak J., Jozkowicz A., Grant M.B., Agarwal A. *J. exp. Med.* **2007**, 204, 3, 605-618
- [19] Clark, J.E., Naughton P., Shurey S., Green C.J., Johnson T.R., Mann B.E., Foresti R., Motterlini R. *Circ. Res.* **2003**, 93, E2-E8
- [20] Sandouka A., Fuller B.J., Mann B.E., Green C.J., Foresti R., Motterlini R. *Kidney Int.* **2006**, 69, 239-247
- [21] Guo Y., Stein A.B., Wu W.J., Tan W., Zhu X., Li Q.H., Dawn B., Motterlini R., Bolli R. *Am. J. Physiol. Heart. Circ. Physiol.* **2004**, 286, H1649-H1653
- [22] Musameh M.D., Fuller B.J., Mann B.E., Green C.J., Motterlini R. *Brit. J. Pharmacol.* **2006**, 149, 1104-1112
- [23] Bani-Hani M.G., Greenstein D., Mann B.E., Green C.J., Motterlini R. *J. Pharmacol. Exp. Ther.* **2006**, 318, 1315-1322
- [24] Urquhart P., Rosignoli G., Cooper D., Motterlini R., Perretti M. *J. Pharmacol. Exp. Ther.* **2007**, 321, 2, 656-662
- [25] Chlopicki S., Olszanecki R., Marcinkiewicz E., Lomnicka M., Motterlini R. *Cardiovasc. Res.* **2006**, 71, 393-401
- [26] Tayem Y., Johnson T.R., Mann B.E., Green C.J., Motterlini R. *Am. J. Physiol. Renal. Physiol.* **2006**, 290, F789-F794
- [27] Stein A.B., Guo Y., Tan W., Wu W.J., Zhu X., Li Q., Luo C., Dawn B., Johnson T.R., Motterlini R., Bolli R. *J Mol. Cell. Cardiol.* **2005**, 38, 127-134
- [28] Motterlini R., Sawle P., Bains S., Hammad J., Alberto R., Foresti R., Green C.J. *Faseb J.* **2005**, 19, 284-286
- [29] Parfenova H., Basuroy S., Bhattacharya S., Tcheranova D., Qu Y., Regan R.F., Leffler C.W. *Am. J. Physiol. Cell. Physiol.* **2005**, 290, C1399-C1410
- [30] Ryan M.J., Jernigan N.L., Drummond H.A., McLemore G.R. Jr., Rimoldi J.M., Poreddy S.R., Gadepalli R.S., Stec D.E. *Pharmacol. Res.* **2006**, 54, 24-29
- [31] Mann B.E. *Top. Organomet.Chem.* **2010**, 32, 247-285
- [32] Niesel J., Pinto A., Peindy N'Dongo H.W., Merz K, Ott I., Gustb R., Schatzschneider U. *Chem. Commun.* **2008**, 1798-1800
- [33] Kretschmer R., Gessner G., Görls H., Heinemann S.H., Westerhausen M. *J Inorg. Biochem.* **2011**, 105, 1, 6-9.
- [34] Schatzschneider U. *Inorg. Chim. Acta* **2011**, 374, 19-23
- [35] Pfeiffer H., Rojas A., Niesel J., Schatzschneider U. *Dalton Trans.* **2009**, 4292-4298

- [36] Dördelmann G., Pfeiffer H., Birkner A., Schatzschneider U. *Inorg. Chem.* **2011**, 50, 4362–4367
- [37] Rimmer R.D., Pierri A.E., Ford P.C. *Coordin. Chem. Rev.* **2012**, 256, 1509-1519
- [38] Schatzschneider U. *Eur. J. Inorg. Chem.* **2010**, 1451–1467
- [39] Takács J., Soós E., Nagy-Magos Z., Markó L., Gervasio G., Hoffmann T. *Inorg. Chim. Acta.* **1989**, 166, 39-46
- [40] Kingston J.V., Jamieson J.W.S, Wilkinson G. *J. Inorg. Nucl. Chem.* **1967**, 29, 133-138
- [41] Loret-Velásquez V.P., Jazzazi T.M.A., Malassa A., Görls H., Gessner G., Heinemann S.H., Westerhausen M. *Eur. J. Inorg. Chem.* **2012**, 1072-1078
- [42] Sellmann D., Reineke U. *J. Organomet. Chem.* **1986**, 310, 83-93
- [43] Bähr G., Thämlitz H. *Z. Anorg. Allg. Chem.* **1955**, 282, 3- 11
- [44] Bähr G., Döge H. *Z. Anorg. Allg. Chem.* **1957**, 292, 119-138
- [45] Massa W., Dehghanpour S., Jahani K. *Inorg. Chim. Acta.* **2009**, 362, 2872-2878
- [46] Polm L.H., Koten G., Elsevier C.J., Vrieze K. *J. Organometallic Chem.* **1986**, 304, 353-370
- [47] Polm L.H., Elsevier C.J., Koten G., Ernsting J.M., Stufkens D.J., Vrieze K. *Organometallics.* **1987**, 6, 1096-1104
- [48] Keijsper J., Polm L., Koten G., Vrieze K., Abbel G., Stam C. H. *Inorg. chem.* **1984**, 23, 2142-2148
- [49] Jackson C.S., Schmitt S., Dou Q.P., Kodanko J.J. *Inorg. Chem.* **2011**, 50, 5336-5338.
- [50] Jazzazi T.M.A., Görls H., Gessner G., Heinemann S., Westerhausen M. *J Organomet Chem.* **2013**, 733, 63-70
- [51] Lee K.W., Brown T.L. *Inorg. Chem.* **1987**, 26, 1852-1856
- [52] Wrighton M.S., Ginley D.S. *J. Am. Chem. Soc.* **1975**, 97, 8 2065-2072
- [53] Schaafsma Y., Bickel A.F., Kooyman E.C. *Tetrahedron* **1960**, 10, 76-80
- [54] Choi D.S., Hong S.H., Lee S.S., Chung Y.K. *J. Organomet. Chem.* **1999**, 579, 385-390
- [55] Chen J., Young Jr. V.G., Angelici R.J. *Organometallics.* **1996**, 15, 1, 325-331
- [56] Killops S.D., Knox E.A.R, Riding G.H., Welch A.J. *J.C.S. Chem. Comm.* **1978**, 486-488
- [57] García Ruano J.L., Parra A., Alemán J. *Green Chem.* **2008**, 10, 706-711
- [58] Flörke U., Egold H., Schwarze D. *Acta Cryst.* **2000**, C56, 184-186
- [59] Thiele G., Liehr G., Lindner E. *J. Organomet. Chem.* **1974**, 70, 427-435

- [60] Si Y., Hu M., Chen C. *C. R. Chimie*. **2008**, 11, 932-937
- [61] Onaka S., Katukawa Y. *J. Coord. Chem.* **1996**, 39, 135-146
- [62] Fenske D. Meyer J., Merzweiler K. *Z. Naturforsch. B chem.* **1987**, 42, 1207-1211
- [63] Treichel P.M., Morris J.H., Stone F.G.A. *J. Chem. Soc.* **1963**, 720-723
- [64] Hieber W., Schropp. *Z. Naturforsch. Teil B.* **1959**, 14, 460-461
- [65] Abel E.W., Crosse B.C. *J. Chem. Soc. A.* **1966**, 1141-1143
- [66] King R.B., Welcman N. *Inorg. Chem* **1969**, 8, 2540-2543
- [67] Chaudhuri M.K, Haas A., Wensky A. *J. Organomet. Chem.* **1976**, 116, 323-326
- [68] Johnson B.F.G., Pollick P.J., Williams I.G., Wojcicki A. *Inorg. Chem.* **1968**, 7, 831-834]
- [69] Ahmad M., Knox G.R., Preston F.J., Reed R.I. *Chem Commun.* **1967**, 138-139
- [70] Kückmann T.I., Schödel F., Sängler I., Bolte M., Wagner M., Lerner H.W. *Organometallics*. **2008**, 27, 3272-3278
- [71] Herberhold M., Milius W., Lui J. *Z. Naturforsch.* **2004**, 59b, 673-680
- [72] Reyes-Lezama M., Toscano R. A., Zuñiga-Villareal N. *J. Organomet. Chem.* **1996**, 517, 19-23
- [73] Edgar K., Johnson B.F.G., Lewis J., Williams G., Wilson J.M. *J. Chem. Soc. A.* **1967**, 379-382
- [74] Braterman P.S. *J. Chem. Soc. A.* **1968**, 2907-2909
- [75] Braterman P.S. *Chem. Commun.* **1988**, 91
- [76] Abel E.W., Hendra P.J., McLean R.A.N., Qurashi M.M. *Inorg. Chim. Acta.* **1969**, 3, 77-80
- [77] Arnett E.M., Wu C.Y., *J. Am. Chem. Soc.* **1960**, 82, 5661-5665.
- [78] Englich U., Ruhlandt-Senge K. *Coordin. Chem. Rev.* **2000**, 210, 135-179
- [79] Vahrenkamp H. *Chem. Ber.* **1970**, 103, 3580-3590
- [80] Osborne A.G., Stone F.G.A. *J. Chem. Soc. A.* **1966**, 1143-1146
- [81] Huang S.D., Lai C.P., Barnes C. *Angew. Chem. Int. Ed. Engl.* **1997**, 36, No17, 1854-1856
- [82] Sheng T., Dechert S., Hyla-Kryspin I., Winter R.F., Meyer F. *Inorg. Chem.* **2005**, 44, 3863-3874
- [83] Jenkins C.R., *J. Organomet. Chem.* **1968**, 15, 441-445
- [84] Abel E.W., Atkins A.M., Crosse B.C., Hutson G.V. *J. Chem. Soc. A.* **1968**, 687-689

-
- [85] Abel E.W., Farrow G., Towle I.D.H. *J. Chem. Soc. Dalton Trans.* **1979**, 71-73
- [86] Churchill M.R., Amoh K.N., Wasserman H.J. *Inorg. Chem.* **1981**, 20, 1609-1611
- [87] Gonzalez M.A., Yim M.A., Cheng S., Moyes A., Hobbs A.J., Mascharak P.K. *Inorg. Chem.* **2012**, 51, 601-608
- [88] McLean S., Mann B.E., Poole R.K. *Anal. Biochem.* **2012**, 427, 1, 36-40
- [89] Crespy D., Landfester K., Schubert U.S., Schiller A. *Chem Commun.* **2010**, 46, 6651-6662
- [90] Kunz P.C., Meyer H., Barthel J., Sollazzo S., Schmidt A.M., Janiak C. *Chem Commun.* **2013**, 49, 4896-4898
- [91] SMART COLLECT, Data Collection Software, Nonius B. V., Netherlands **1998**.
- [92] SMART, Software for the CCD Detektor System, version 5.05: Bruker AXS: Madison, WI **1998**.
- [93] Otwinowski Z., Minor W., In Carter C.W., Sweet R.M. (Editors) *Macromolecular Crystallography, Part A*, volume 276 of *Methods in Enzymology*, Academic Press, San Diego **1997** 307-326.
- [94] Sheldrick G. M., SHELXS97 and SHELXL97, University of Göttingen, Germany **1997**.

Selbständigkeitserklärung

Ich erkläre, dass ich die vorliegende Arbeit selbständig und unter Verwendung der angegebene Hilfsmittel, persönlichen Mitteilungen und Quelle angefertigt habe.

Jena, 17. 09. 2013

Vaneza Paola Lorett Velásquez

Curriculum Vitae

Name: Vaneza Paola Lorett Velásquez

Date of Birth 07.11.1982

Place of Birth Cartagena de Indias - Colombia

Nationality Colombian

2009-2013 Doctoral student (DAAD-Scholarship) and DFG Project 1738 in the “Institut für Anorganische und Analytische Chemie (IAAC)” (Institute of Inorganic and Analytic Chemistry)
Friedrich-Schiller-Universität Jena, Germany

2008 Researcher (ministerio de ciencia y técnica de Argentina FONCYT- Scholarship) in the “Instituto de Química Física de los Materiales, Medio Ambiente y Energía (INQUIMAE)” (Institute of Physical Chemistry of Materials, Environment and Energy)
Universidad de Buenos Aires (UBA), Argentina

2007-2009 Master in Comprehensive Pharmaceutical Care
Universidad de Barcelona

2001-2006 Bachelors Degree in Pharmaceutical Chemistry
Universidad de Cartagena, Colombia

Jena, 17.09. 13